



## Optimization of a "Bump-and-Hole" Approach to Allele-Selective BET Bromodomain Inhibition

Journal:	<i>Chemical Science</i>
Manuscript ID	SC-EDG-06-2017-002536.R1
Article Type:	Edge Article
Date Submitted by the Author:	n/a
Complete List of Authors:	<p>Runcie, Andrew; University of Dundee, Division of Biological Chemistry and Drug Discovery  Zengerle, Michael; University of Dundee, Division of Biological Chemistry and Drug Discovery  Chan, Kwok-Ho; University of Dundee, Division of Biological Chemistry and Drug Discovery  Testa, Andrea; University of Dundee, Division of Biological Chemistry and Drug Discovery  van Beurden, Lars; University of Dundee, Division of Biological Chemistry and Drug Discovery  Baud, Matthias; University of Dundee, Division of Biological Chemistry and Drug Discovery  Epemolu, Ola; University of Dundee, Division of Biological Chemistry and Drug Discovery  Ellis, Lucy; University of Dundee, Division of Biological Chemistry and Drug Discovery  Read, Kevin; University of Dundee, Division of Biological Chemistry and Drug Discovery  Coulthard, Victoria; Reach Separations Ltd  Brien, Alex; Reach Separations Ltd  Ciulli, Alessio; University of Dundee, Division of Biological Chemistry and Drug Discovery</p>

## Chemical Science – guidelines for referees

[www.rsc.org/chemicalscience](http://www.rsc.org/chemicalscience)



*Chemical Science* is the flagship journal from the Royal Society of Chemistry that publishes research of exceptional significance from across the chemical sciences. The Editorial Board are driving the journal with the ambition to be a top tier international general chemistry journal that rivals the very best in chemistry. We are aiming for an impact factor of over 10; this means that *Chemical Science* can only accept <10% of submitted manuscripts. You as an expert reviewer will greatly contribute to the high standards of the journal.

Accepted articles must report **original, very high quality** and **cutting-edge** work that will be of **exceptional general interest** to the journal's wide international readership.

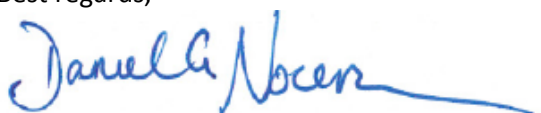
*Chemical Science* publishes one manuscript type for frontier and novel research: **Edge Article**.

An Edge Article should present a novel piece of scientific research in an exciting, succinct format. It has no page limits, enabling research findings to be introduced without the need for abridged discussions or perspectives. However, overtly lengthy introductions and discussion, extensive data, and excessive experimental details and non-experiment based conjecture should not be included. Experimental procedures and characterisation data should be placed in the [Electronic Supplementary Information \(ESI\)](#) where appropriate.

The Editor-in-Chief and the Editorial Board ask you to **recommend only the best work** for publication in *Chemical Science*. Routine and incremental work – however competently researched and reported – should not be recommended for publication.

Thank you very much for your assistance in evaluating this manuscript.

Best regards,

A handwritten signature in blue ink that reads 'Daniel G. Nocera'.

Daniel G. Nocera  
Editor-in-Chief, *Chemical Science*  
[chemicalscience-RSC@rsc.org](mailto:chemicalscience-RSC@rsc.org)

### General Guidance

Referees have the responsibility to treat the manuscript as confidential. Please be aware of our [Ethical Guidelines](#), which contain full information on the responsibilities of referees and authors, and our [Refereeing Procedure and Policy](#).

*When preparing your report, please:*

- Comment on the significance, originality, impact and scientific reliability of the work
- State clearly whether you would like to see the article accepted or rejected and give detailed comments (with references, as appropriate) that will help both the Editor to make a decision on the paper and the authors to improve it

*Please inform the Associate Editor if:*

- There is a conflict of interest
- There is a significant part of the work which you are not able to referee with confidence
- If the work, or a significant part of the work, has previously been published

Submit your report at <http://mc.manuscriptcentral.com/chemsci>



## ARTICLE

## Optimization of a “Bump-and-Hole” Approach to Allele-Selective BET Bromodomain Inhibition

Received 00th January 2017,  
Accepted 00th January 2017

DOI: 10.1039/x0xx00000x

www.rsc.org/

A. C. Runcie<sup>a†</sup>, M. Zengerle<sup>a†</sup>, K.-H. Chan<sup>a†</sup>, A. Testa<sup>a</sup>, L. van Beurden<sup>a</sup>, M. G. J. Baud<sup>a</sup>, O. Epemolu<sup>a</sup>, L. C. J. Ellis<sup>a</sup>, K. D. Read<sup>a</sup>, V. Coulthard<sup>b</sup>, A. Brien<sup>b</sup>, A. Ciulli<sup>a\*</sup>

Allele-specific chemical genetics enables selective inhibition within families of highly-conserved proteins. The four BET (bromodomain & extra-terminal domain) proteins – BRD2, BRD3, BRD4 and BRDT bind acetylated chromatin via their bromodomains and regulate processes such as cell proliferation and inflammation. BET bromodomains are of particular interest, as they are attractive therapeutic targets but existing inhibitors are pan-selective. We previously established a bump-&-hole system for the BET bromodomains, pairing a leucine/alanine mutation with an ethyl-derived analogue of an established benzodiazepine scaffold. Here we optimize upon this system with the introduction of a more conservative and less disruptive leucine/valine mutation. Extensive structure-activity-relationships of diverse benzodiazepine analogues guided the development of potent, mutant-selective inhibitors with desirable physicochemical properties. The active enantiomer of our best compound – 9-ME-1 – shows ~200 nM potency, >100-fold selectivity for the L/V mutant over wild-type and excellent DMPK properties. Through a variety of *in vitro* and cellular assays we validate the capabilities of our optimized system, and then utilize it to compare the relative importance of the first and second bromodomains to chromatin binding. These experiments confirm the primacy of the first bromodomain in all BET proteins, but also significant variation in the importance of the second bromodomain. We also show that, despite having a minor role in chromatin recognition, BRD4 BD2 is still essential for gene expression, likely through the recruitment of non-histone proteins. The disclosed inhibitor:mutant pair provides a powerful tool for future cellular and *in vivo* target validation studies.

### Introduction

Chemical probes are biologically-active small-molecules (typically inhibitors) that are used to investigate the importance and functions of proteins<sup>1-3</sup>. The use of chemical probes and observation of the resulting phenotypes in this fashion is known as chemical genetics. Although possessing various advantages to classical genetics (such as gene knockouts) chemical genetics require that any probes used have a well-defined mode of action and high-selectivity for their target proteins. In cases where target proteins are not structurally distinct enough for the development of selective probes more advanced techniques are needed.

The ‘bump-&-hole’ system is a way of engineering selective inhibition of structurally conserved proteins through the generation of orthogonal protein:ligand pairs<sup>4</sup>. In this system existing small-molecule inhibitors, showing high affinity and

desirable DMPK properties, are modified to include a steric ‘bump’ that weakens or abolishes binding to the target wild-type proteins. Simultaneously, a reciprocal mutation is introduced to the target, replacing a large amino acid residue with a smaller one to create a ‘hole’ that can accommodate the bumped ligand. Using this approach one can take a pan-selective inhibitor that binds multiple structurally-related proteins and generate a bumped ligand that will only inhibit a target protein that has been mutated to contain a ‘hole’. This system allows the specific inhibition of multiple proteins without the costly design of multiple target-specific chemical probes, and takes advantage of existing chemical tools to bypass the discovery of a high-quality chemical scaffold. Such engineered selectivity has successfully been applied to protein kinases and ATP-competitive inhibitors<sup>5</sup> and FKBP-targeting chemical dimerizers<sup>6, 7</sup>. The bump-&-hole approach has not previously been applied to any inhibitor of epigenetic proteins, but the use of mutant enzymes and modified co-factors has been used on a number of epigenetic enzymes for target identification<sup>1, 4, 8, 9</sup>.

In previous work we have explored the potential for establishing a bump-&-hole system targeting the bromodomains of the BET (bromo and extra-terminal) protein family<sup>10, 11</sup>. These four human proteins – BRD2, BRD3, BRD4 and BRDT – each contain two tandem bromodomains that bind acetylated lysine residues in histone tails, leading to the

<sup>a</sup> Division of Biological Chemistry and Drug Discovery, School of Life Sciences, University of Dundee, Dundee, Scotland, UK.

<sup>b</sup> Reach Separations Ltd, BioCity Nottingham, Nottingham.

† These authors contributed equally.

\* Corresponding author, e-mail: a.ciulli@dundee.ac.uk

Electronic Supplementary Information (ESI) available: Supplemental results (Figures S1-10 and tables S1-S13). Crystallography data collection and refinement statistics. Experimental section. Detailed compound synthesis and characterisation. Supplemental references. See DOI: 10.1039/x0xx00000x

recruitment of multi-protein complexes to chromatin<sup>12, 13</sup>. Through this function the BET proteins play a significant role in controlling transcription and regulating gene expression<sup>14-16</sup>. The BET proteins regulate proliferation, the cell-cycle and cell differentiation in a wide array of contexts and they have been associated with many disease states such as cancer, inflammation, HIV infection and neurological disorders<sup>17</sup>.

In the last decade many high-quality small-molecule inhibitors of BET bromodomains have been developed (Chart 1), both for therapeutic and research purposes<sup>18-22</sup>. The phenotypes generated by said inhibitors have been used to investigate the functions of BET proteins and their significance as therapeutic targets. This process has been limited by the pan-selective nature of the BET inhibitors, as they typically target all BET bromodomains with similar potency<sup>10</sup>, hence specific proteins/bromodomains cannot be associated to specific phenotypes<sup>1-3</sup>. Furthermore this pan-selectivity increases the possibility of side-effects limiting the usability of therapeutic BET inhibitors as all four BET proteins will be inhibited when only one may be disease-relevant<sup>23</sup>. Additionally it is becoming increasingly apparent that the phenotypes generated by non-BET bromodomain inhibitors is in part driven by low-level BRD4 inhibition<sup>24-27</sup>. Recently some advances have been made, as several inhibitors have been reported to be mildly selective for the 'second' bromodomains (BD2s)<sup>11, 28, 29</sup> or the 'first' bromodomains (BD1s)<sup>30</sup> of the BET proteins and one recently reported compound showed >10-fold selectivity for BRD4 BD1, through exploiting the differing dynamics of the ZA loop between different bromodomains<sup>31</sup>. The BET bromodomains have also been successfully targeted for degradation by bifunctional PROTAC (proteolysis targeting chimera) compounds, based on existing BET inhibitor scaffolds<sup>32-35</sup> and novel scaffolds<sup>36</sup>. In our research we discovered a series of PROTACs that are BRD4-selective through the exploitation of novel protein-protein interactions between BRD4 and the VHL ubiquitin E3 ligase<sup>37</sup>.

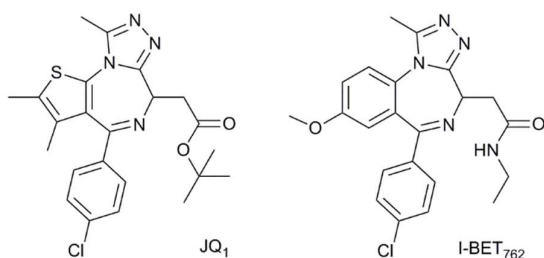


Chart 1. Benzodiazepine-based BET Inhibitors.

For our bump-&-hole project<sup>10</sup> we have previously identified a conserved leucine residue in the BET bromodomains binding site (L94 & L387 in BRD4) that can be substituted with an alanine, yielding relatively stable and functional bromodomain mutants. Compound ET – an I-BET762<sup>19</sup>/JQ1<sup>18</sup>-related benzodiazepine scaffold bearing an ethyl bump targets the L/A mutation with high-affinity and ~100-fold selectivity relative to wild-type (Figure 1A). We have since worked to optimize,

validate and implement this system. Although still capable of binding acetylated histone peptides the L/A mutants show a noticeable loss in binding affinity, and if not functional enough may compromise the viability of mutant cell-lines and animal models (Figure 1B). Additionally screening of additional chemical modifications may deliver optimized inhibitors that are more selective and have improved physiochemical properties (Figure 1C).

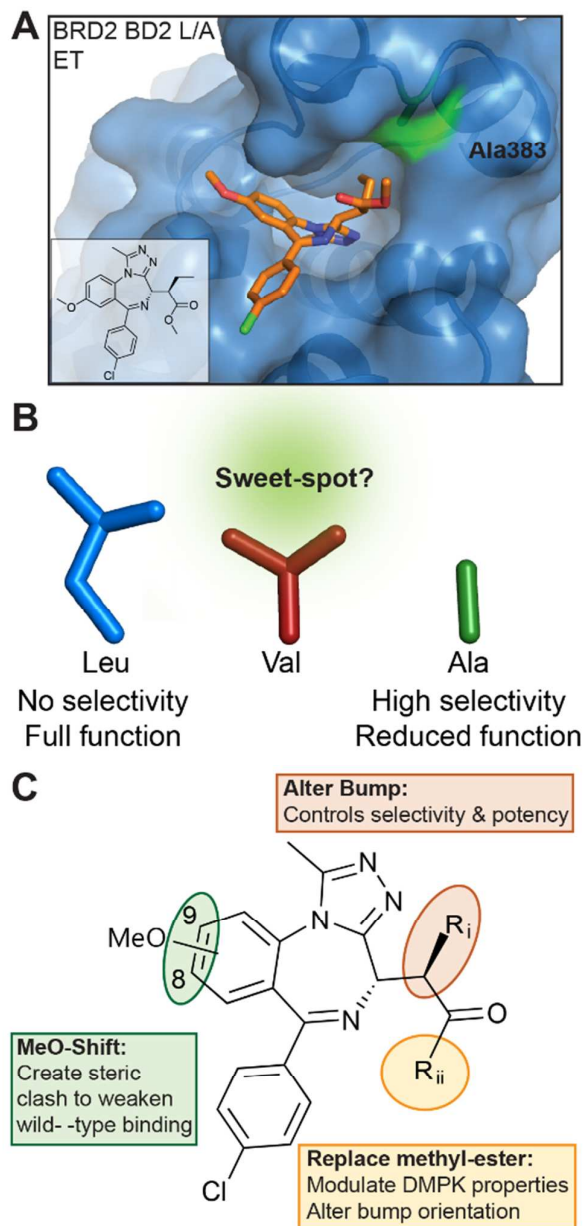


Figure 1. Bump-&-Hole System Optimization. A) Co-crystal structure of ET bound to BRD2 BD2 L383A (4QEW). B) Comparison of WT leucine and mutated residues. C) Scaffold of bumped compounds, with modification sites highlighted.

## Results

### An Optimised Leucine/Valine Mutation Displays High Structural & Functional Conservation

Here we explored the possibility of improving the bump-&-hole system through replacement of the previously described<sup>10</sup> and potentially problematic L/A mutation (L94 and L387 in BRD4) (Fig. S1). Through structural analysis of the bromodomain we hypothesized that a leucine/valine substitution (L/V) would be more conservative change than the previous L/A substitution, resulting in a smaller 'hole' but still allowing enough space to accommodate a bumped ligand. The mutant BET bromodomains were purified as single-bromodomain constructs, following site-directed mutagenesis, for *in vitro* characterization. This characterization focused on the ability of the bromodomains to bind and discriminate between acetylated histone peptides. We used differential scanning fluorimetry (DSF) to show that the BET bromodomain constructs were not destabilized by the L/V mutation (Table S1).

We next assessed how the L/V mutation impacted the ability of the bromodomains to bind acetylated histone peptides. We used isothermal titration calorimetry (ITC) to measure the affinity and thermodynamic parameters for di-acetylated H4K(5,8)ac and tetra-acetylated H4K(5,8,12,16)ac substrate peptides<sup>12</sup> binding to BET bromodomain constructs. The L/V mutation typically decreased the affinity of the peptide:bromodomain interaction by around two-fold (Table S2), which is close to experimental errors and a significant improvement over the L/A mutation which showed up to 10-fold decreases in affinity<sup>10</sup>. The supremacy of L/V over L/A was confirmed by titrations of H4K(5,8,12,16)ac against BRD2 BD1 and BRD4 BD1 L/A (Figure 2A). Analysis of the thermodynamic parameters of binding ( $\Delta H$ ,  $T\Delta S$ ,  $\Delta G$ ) suggested that the L/V mutation does not substantially impact the binding mode of these peptides. In contrast, changes in these parameters relative to wild-type were much greater for the L/A mutation, consistent with a more detrimental effect (Fig. S2).

The cellular function of the BET proteins is based not just on how strongly they bind histone peptides with specific epigenetic marks but also on what combinations of marks they recognize. To assess the impact of the L/V mutation on the binding profiles of the BET bromodomains we used bio-layer interferometry (BLI) to screen a library of acetylated histone peptides (Figure 2B). Both WT and L/V bromodomains showed a marked preference for a cluster of poly-acetylated H4

peptides, especially H4K(5,8)ac, H4K(5,8,12)ac and H4K(5,8,12,16)ac. The WT and L/V binding profiles for all BD1s were virtually identical; and overall the L/V mutation had a visibly smaller effect on peptide recognition than the L/A mutant<sup>10</sup>. No significant binding was observed for any non-H4 peptides (Fig. S3).

To better understand how the L/V mutation affects histone binding, the X-ray crystal structure of the apo form of BRD2 BD2 L383V was solved and compared to the previously solved structures of WT and L383A BRD2 BD2 (ref. <sup>10</sup>). Both the L/V and L/A mutants retain the overall structure of WT BRD2 BD2. The conformation of the ZA loop in the L/V mutant structure superposes very well with that of the WT (so-called "open" conformation), which differs from that observed in the L/A mutant, which is in a closed conformation (Figure 2C). Notably however, the L/A mutant when ligand-bound had instead an open ZA loop (ref. <sup>10</sup>, Fig. S4). Re-orienting the ZA loop during binding might be contributing to the varying affinities observed between WT and mutant bromodomains for acetylated histone peptides. However, differences in crystallization space group and consequently crystal packing around the ZA loop amongst the various crystal structures might also contribute to the different conformations observed for the ZA loop.

To assess the functionality of the L/V mutants in a cellular environment we used a cellular fluorescence recovery after photobleaching (FRAP) assay to monitor the interaction between full-length BET proteins (GFP-tagged) and chromatin inside cells. Inhibition by ligands or deleterious mutations would reduce the proportion of GFP-tagged BET proteins bound to chromatin, increasing the rate of fluorescence recovery and decreasing the measured recovery time ( $t_{1/2}$ )<sup>38</sup>. Mutant forms of BRD4 were compared in this assay and the L/V mutation was shown to have a much smaller impact on chromatin binding than the L/A mutation (Figure 2D), in line with our *in vitro* data with histone peptides. Similar results were obtained for the L/V mutants of BRD2, BRD3 and BRDT (Fig. S5). Both our biophysical and cellular data show that the L/V mutation is a major improvement over the L/A mutation, and has a minor effect on the structure of the BET bromodomains and their substrate binding properties

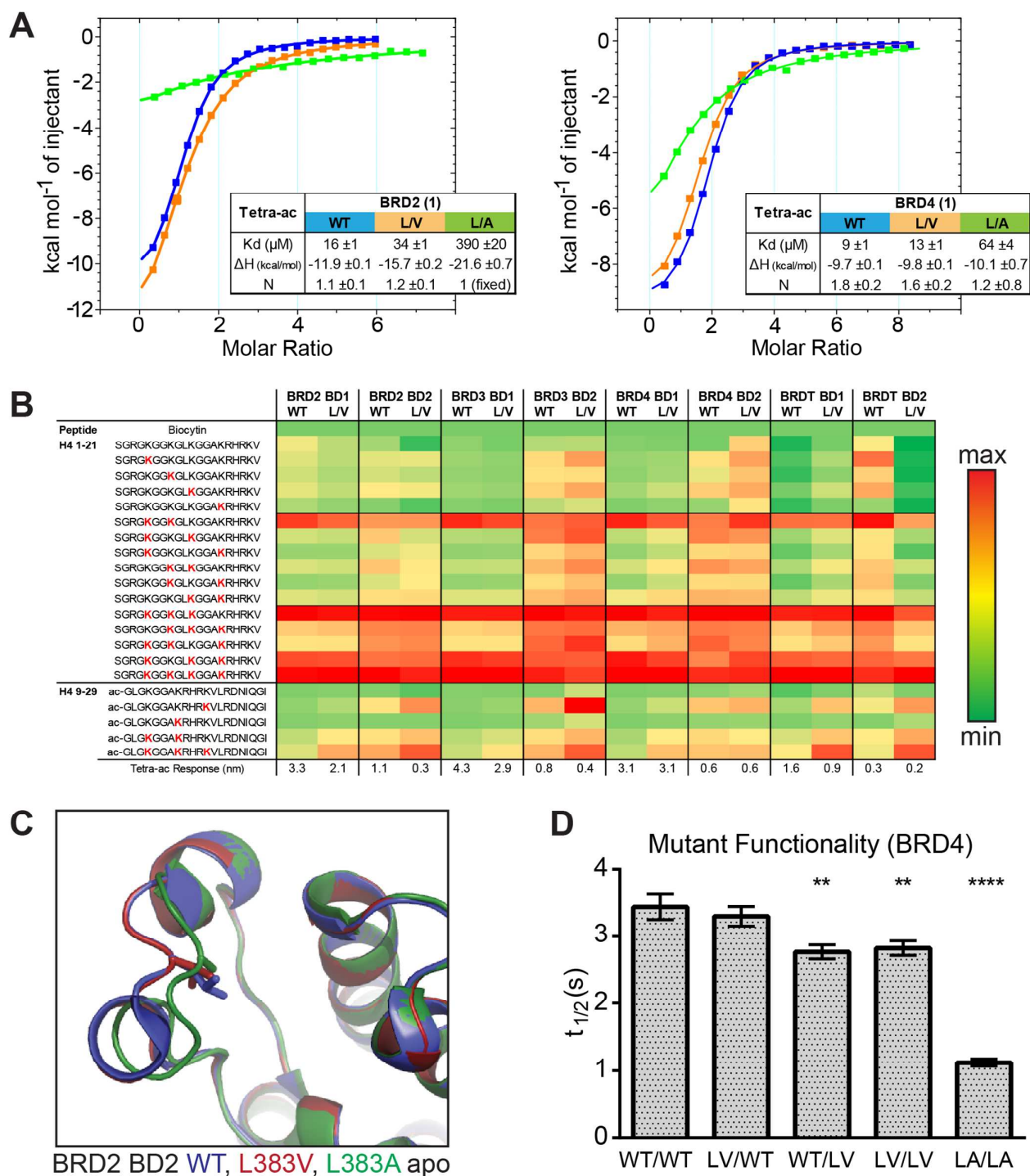


**Figure 2.** L/V Mutant Characterization. A) ITC titrations of tetra-acetylated H4 peptide into BET bromodomains. B) Binding profiles of WT and L/V bromodomains for acetylated H4 peptides, derived from BLI screen. Responses normalized to strongest response of each construct, and color-coded. Red 'K' in peptide sequence denotes lysine acetylation. C) Alignment of BRD2 BD2 WT (2D2V), L/V and L/A (4QEU) apo structures, with leucine/valine/alanine highlighted. D) Recovery times of GFP-labelled BRD4 constructs following 0.5s laser bleach event, at 2  $\mu\text{M}$  SAHA and 0.03% DMSO. Each bar is mean and SE of ~50 U2OS cells tested over two separate experiments.

### Chemical Modifications for Selective Probing of the L/V Bromodomains

In addition to optimizing the 'biology' of the bump-&-hole system (the mutation) we were interested in optimizing the 'chemistry' through the design of chemical probes superior in terms of binding selectivity, potency and DMPK properties.

First, to cover a range of bump sizes, we included primary alkyl methyl, ethyl and propyl as well as allyl 'bump' modifications. As the L/V mutation is more subtle than the previous L/A and is expected to generate a smaller 'hole', we decided not to include more sterically-demanding modifications.

Second, we explored the possibility of modifying the core scaffold with the aim to weaken binding to wild-type protein, potentially more so than against the mutant. Previous SAR studies on I-BET762 analogues described a number of chemical modifications to the benzodiazepine scaffold that resulted in weaker binding affinities to the WT BET bromodomains<sup>39</sup>. One such modification, the shifting of the methoxy group from the 8' to the 9' position on the fused-phenyl ring, was deemed attractive as it reduced the BRD4 pIC<sub>50</sub> by 0.5 log units and resulting analogues would retain very similar physicochemical properties to the parent compounds. We hypothesized that such a "Methoxy-shift" could enhance selectivity if the resulting steric clash was better accommodated by the mutated binding site compared to the WT protein.

Finally, we placed our attention to the flexible side chain on which the alkyl bump is located. Our 'first generation' compounds ME and ET both possess a methylester group at this position. Co-crystal structures showed the methylester side chain of ME and ET bound to the L/A mutant moved significantly compared to the bound conformation of the corresponding ethyl-amide group in I-BET762 bound to the WT protein<sup>10</sup>. Such freedom to rotate could allow the bumped compound to accommodate itself in the WT binding pocket, leading to the residual affinity observed for ME and ET against WT. In contrast, 'locking' this side-chain in place would be expected to further weaken WT binding. We therefore decided to replace the methyl-ester side-group first with an amide, as in I-BET762, which would lock the side-group in place through a hydrogen bond from the amide NH to the ASN140 residue<sup>19, 39</sup>. In addition, we decided to include a *tert*-butyl ester group, as in JQ1, as this could form favourable hydrophobic interactions, and its bulky nature may limit the flexibility of the side-chain. The ethyl-amide and *tert*-butyl ester side-groups

were also deemed as attractive ways to fine-tune the ADMET and physicochemical properties of our chemical probes.

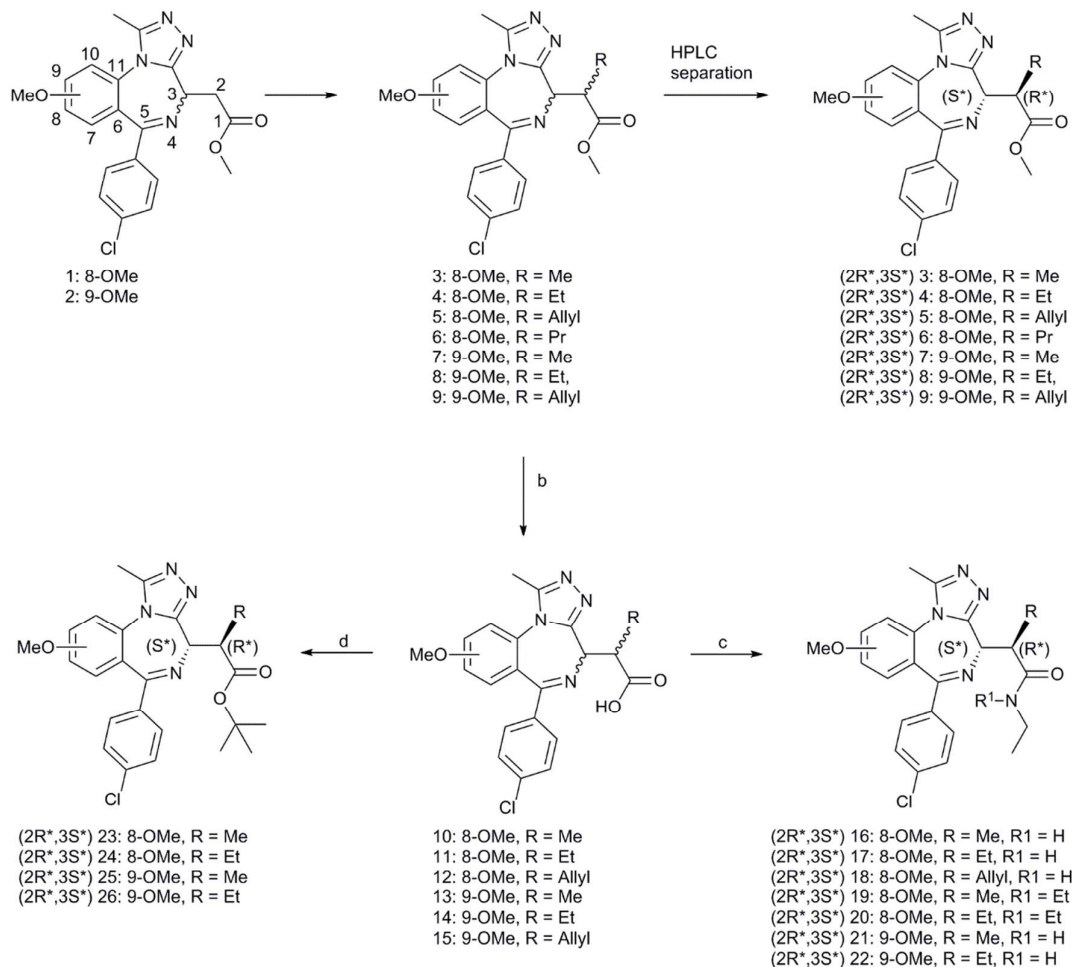
Our L/V-selective 'bumped' compounds are derived from analogues of the known BET bromodomain probe, and clinical trial candidate, I-BET762. The synthesis and SAR of this 1,4-benzodiazepine scaffold is well described in the literature<sup>39</sup>, allowing easy access to our scaffold I-BET-OMe (**1**) and its analogue incorporating the methoxy shift (9-IBET-OMe) (**2**). The key stage of the synthesis of all our bumped compounds was the addition of the sterically demanding alkyl 'bump' on the  $\alpha$ -carbon. Potassium hexamethyldisilazane (KHMDS) was used to deprotonate in the  $\alpha$ -position to the acetic acid methyl ester, to generate the desired enolate intermediate<sup>11</sup>. These intermediates were then reacted with the appropriate alkyl iodides to form the desired  $\alpha$ -alkylated derivatives (**3-11**) as diastereoisomeric mixtures.

From previous work<sup>10</sup>, the biologically active product presents a 2*R*\*,3*S*\* relative stereochemistry; however the diastereomeric mixture was at times inconveniently biased towards the inactive 2*S*\*3*S*\* diastereomer, which could be formed at an excess of up to 25-fold. When this occurred the diastereomeric mixtures were epimerized using sodium methoxide in anhydrous methanol under microwave irradiation.

Once the bumped group was installed, aqueous sodium hydroxide was used to hydrolyze the methyl-ester group to and obtain the free carboxylic acids (**10-15**). Ethyl and di-ethyl amide groups (**16-22**) were introduced using standard peptide coupling conditions, using 1-[Bis(dimethylamino)methylene]-1*H*-1,2,3-triazolo[4,5-*b*]pyridinium 3-oxid hexafluorophosphate (HATU) as the coupling reagent and *N,N*-diisopropylethylamine (DIPEA) as the amine base. *Tert*-butyl esters (**23-26**) were obtained from the carboxylic acids using *tert*-butyl trichloroacetimidate and boron-trifluoride as a catalyst.

All compounds were synthesized as diastereomeric mixtures. Reverse phase HPLC was then used to obtain pure samples of the 2*R*\*,3*S*\* diastereoisomer as a racemate, which was expected to contain the active compound, based on our previous work<sup>10</sup>. Individual enantiomers were not separated at this stage of the project and unless explicitly stated otherwise, ligand concentrations and measured K<sub>d</sub> and IC<sub>50</sub> values refer to the concentration of the active enantiomer, i.e. half the concentration of the racemate.

Scheme 1. Bumped Compound Synthesis



## Evaluation & SAR Trends of Bumped Compounds

### AlphaLISA & X-ray Crystallography

Our compounds were first evaluated in a robust and efficient competitive AlphaLISA assay (Table 1), which gave us broad SAR trends and allowed us to disqualify compounds lacking sufficient potency ( $L/V$   $pIC_{50} \geq 5.9$ ) or selectivity ( $\Delta pIC_{50} \geq 1.3$ ). This AlphaLISA assay measured the displacement from the bromodomain binding pocket of a biotinylated JQ1 probe<sup>40</sup> (Bio-JQ1) (Fig. S7), which we show to be a potent binder of both WT and L/V BET bromodomains (Fig. S8 & Table S3). As SAR trends were identified from the data, a series of compounds showing potential as chemical probes were co-crystallized with L/V BRD2 BD2 and the resulting crystal structures used to rationalize experimental observations.

Our scaffold compound **1** was as potent as I-BET762 & (+)JQ1 against WT bromodomains, which was unsurprising given their structural similarity. Meanwhile, ITC titrations with **1** provided  $K_d$  values of 150 nM and 290 nM for BRD4 BD1 WT and L/V, respectively. Due to the assay's high sensitivity we were able to detect very weak displacement by the inactive (-)JQ1 isomer at high concentrations. Several bumped compounds (e.g. **17-**

**22**) showed similarly low potency, which we interpret as them being unlikely to bind WT BET proteins at commonly used concentrations.

Many of our bumped compounds showed promise as potent and selective probes of L/V BET bromodomains. Methyl, ethyl and allyl bumps (**3-5**), the 9' methoxy group (**7-9**, **21**) and the ethyl-amide side-group (**16-18**, **21**) typically met our criteria. Overall this dataset shows the efficacy of the bump-&-hole approach, with only the propyl bump (**6**) and tert-butyl ester compounds (**23-26**) showing less than 10-fold selectivity. Moreover, a wide range of selectivity and potency was observed across the series, showing that the activity of bumped compounds can be fine-tuned with the right modifications.

As expected the addition of alkyl bumps weakened binding for WT bromodomains and is necessary for L/V selectivity. The smaller bumps increase potency for L/V bromodomains, as the bump and hole now form a new hydrophobic interaction. The effect of the bump on potency mostly results from its size, as shown by the highly potent **3** binding much more intimately within the L/V hole (Figure 3A). With larger bumps, however,



the rotational flexibility of the bump becomes important, with the semi-rigid **5** bump acting more like the equally flexible **4** bump than the **6** bump of similar length.

Shifting the methoxy group to the 9' position (**7-9**) did not cause large changes in the L/V potency of bumped compounds, despite its pronounced effect on the scaffold (**2**). The methoxy shift only clearly enhanced selectivity when paired with the methyl bump (**7**), where it also does not alter the compound binding orientation (Figure 3B).

The replacement of the methyl-ester with an amide group results in a pronounced reduction on WT binding affinities. Co-crystal structures (Figure 3C) confirm the formation of the expected hydrogen bond to Asn140. As this hydrogen bond locks the bump in an orientation facing the WT leucine residue it exacerbates the steric clash

The ethyl-amide side-group and its hydrogen bond does not reduce potency in non-bumped scaffolds, as can be seen with I-BET762 and **1**. Compounds featuring the di-ethyl amide side-group (**19, 20**) show greater WT potency and lower selectivity than ethyl-amide compounds.

An alternative methyl-ester replacement was the tert-butyl ester group (**23-26**), present in the BET inhibitor JQ1. This group had a very deleterious effect on selectivity, as it both increased WT potency and reduced L/V potency. Co-crystal structures (Figure 3D) of BRD2 BD2 L/V bound to **5** and **24** show that the tert-butyl group clashes with Leu381, reducing L/V potency. As this clash pushes the ligand away from the ZA loop it may relieve the bump/leucine steric clash and increase WT potency.

**Table 1.** SAR of Bumped Compounds

Compound	R <sub>i</sub>	R <sub>ii</sub>	MeO- Position <sup>a</sup>	AlphaLISA pIC <sub>50</sub> ±SD <sup>b</sup>			CLogP <sup>c</sup>	Plasma t <sub>1/2</sub> (min)	CL int (ml/min/g)	P <sub>e</sub> (nm/s)	ITC pK <sub>d</sub> ±SD <sup>d</sup>		
				WT	L/V	Δ					WT	L/V	Δ
(+) JQ1	H	O <sup>t</sup> Bu	-	6.6 ±0.1	6.5 ±0.1	-0.1 ±0.1	4.8	>180	7.5				
(-) JQ1	H	O <sup>t</sup> Bu	-	4.8 ±0.2	4.6 ±0.1	-0.2 ±0.2	4.8						
I-BET762	H	NHEt	8	6.5 ±0.2	6.5 ±0.3	0.0 ±0.3	2.8	>180	1.3	25			
<b>1</b>	H	OMe	8	6.6 ±0.2	6.6 ±0.3	0.0 ±0.2	3.3	54	<0.5	149	6.8	6.5	-0.3
<b>2</b>	H	OMe	9	5.8 ±0.2	5.9 ±0.2	0.1 ±0.1	3.3	67	1.7				
<b>3</b>	methyl	OMe	8	6.2 ±0.3	7.4 ±0.1	1.2 ±0.2	3.5	>180	0.7	185			
<b>4</b>	ethyl	OMe	8	5.0 ±0.1	6.8 ±0.2	1.7 ±0.2	3.9	>180	1.5	153	5.1 ±0.5	6.9 ±0.3	1.8 ±0.4
<b>5</b>	allyl	OMe	8	5.1 ±0.1	6.6 ±0.3	1.5 ±0.3	3.9	>180	6.7	127	5.1 ±0.4	6.6 ±0.2	1.5 ±0.5
<b>6</b>	propyl	OMe	8	4.5 ±0.2	5.0 ±0.1	0.6 ±0.2	4.3	>180	5.2				
<b>7</b>	methyl	OMe	9	5.4 ±0.2	6.8 ±0.2	1.4 ±0.2	3.5	>180	<0.5	158	4.5 ±0.2	6.6 ±0.3	2.0 ±0.4
<b>8</b>	ethyl	OMe	9	5.5 ±0.2	6.8 ±0.2	1.4 ±0.2	3.9	>180	4.1	155	<4.2	6.4 ±0.2	>2.2 ±0.2
<b>9</b>	allyl	OMe	9	4.4 ±0.1	5.7 ±0.2	1.3 ±0.2	3.9	>180	9.4	136			
<b>16</b>	methyl	NHEt	8	5.3 ±0.2	6.7 ±0.2	1.4 ±0.2	3.1	>180	1.2	26	5.6 ±0.3	6.9 ±0.2	1.3 ±0.3
<b>17</b>	ethyl	NHEt	8	4.4 ±0.1	5.9 ±0.3	1.5 ±0.2	3.5	>180	1.4	45	<4.2	6.0 ±0.2	>1.8 ±0.2
<b>18</b>	allyl	NHEt	8	4.3 ±0.1	5.9 ±0.2	1.5 ±0.1	3.5	>180	2.6	52			
<b>19</b>	methyl	N[Et] <sub>2</sub>	8	4.9 ±0.2	6.1 ±0.2	1.2 ±0.2	3.8	>180	>50				
<b>20</b>	ethyl	N[Et] <sub>2</sub>	8	4.6 ±0.1	5.8 ±0.2	1.2 ±0.2	4.1	>180	>50				
<b>21</b>	methyl	NHEt	9	4.7 ±0.3	6.0 ±0.2	1.3 ±0.2	3.1	>180	1.5	40	4.5 ±0.4	6.3 ±0.2	1.8 ±0.5
<b>22</b>	ethyl	NHEt	9	<4.0	5.2 ±0.2	>1.2	3.5	>180	2.1	59			
<b>23</b>	ethyl	O <sup>t</sup> Bu	8	5.3 ±0.1	6.0 ±0.2	0.7 ±0.1	4.8	>180	30.7				
<b>24</b>	allyl	O <sup>t</sup> Bu	8	5.3 ±0.1	6.2 ±0.2	0.9 ±0.2	4.9	>180	39.1				
<b>25</b>	ethyl	O <sup>t</sup> Bu	9	4.6 ±0.1	5.0 ±0.2	0.4 ±0.2	4.8	>180	31.0				
<b>26</b>	allyl	O <sup>t</sup> Bu	9	5.2 ±0.2	5.8 ±0.2	0.5 ±0.1	4.9	>180	39.4				

a) JQ1 compounds possess a thiophene ring with no methoxy group. b) Values are mean and standard deviation of all somatic bromodomains – BD1 and BD2 of BRD2, BRD3 and BRD4. c) CLogP calculated in StarDrop. d) Values are mean and standard deviation of all somatic bromodomains except for **1** which was titrated only against BRD4 BD1.

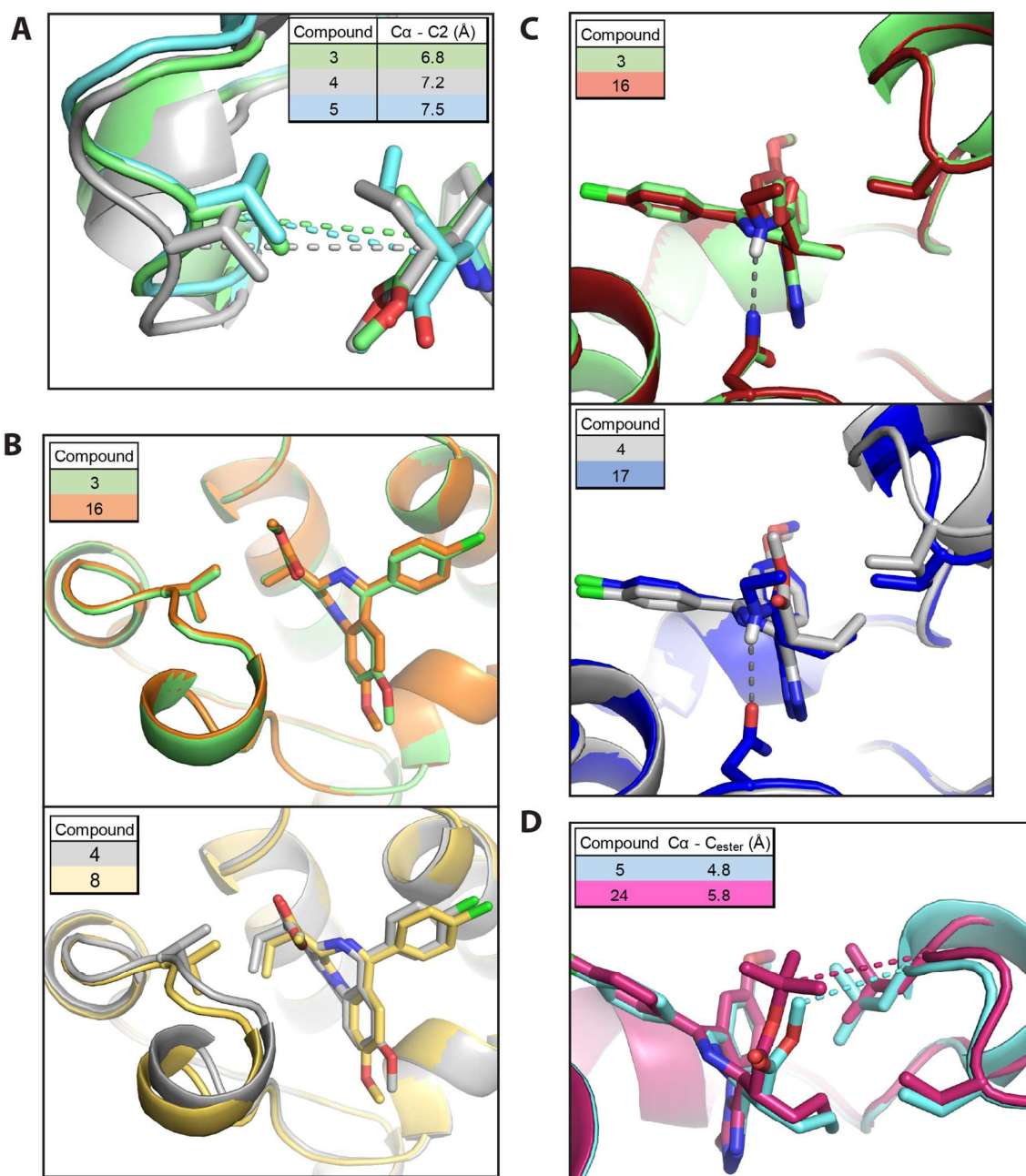


**Figure 3.** Compound Modifications & BRD:Ligand co-crystal structure. A) comparison of alkyl bumps; B) effect of methoxy shift; C) effect of ethyl-amide group; D) effect of tert-butyl ester. Structural alignments of different bumped-compounds co-crystallized with BRD2 BD2 L/V. Dark grey dashes represent hydrogen bonds. Other dashes show inter-atom distances of interest. C $\alpha$  = alpha carbon of valine or other residue. C2 = 2' carbon of compound. C<sub>ester</sub> = carbon following ester bond

### DMPK Triage

The AlphaLISA screen suggested several promising compounds showing high potency for L/V bromodomains and selectivity against WT. A secondary triage of the compounds, investigating their DMPK qualities, was conducted to eliminate potential candidates with poor PK properties that would later undermine their utility as chemical probes in cells and *in vivo*. To proceed beyond this triage compounds were required to show no breakdown in plasma, microsomal clearance rates

similar to existing BET probes and high apparent permeability (>10 nm/s).

Pleasingly, all bumped compounds were very stable in plasma (half-lives over 3 hours), while the scaffold compounds (**1,2**) had lower stability, likely due to esterase activity. This is consistent with the theory that the presence of an alkyl bump on the  $\alpha$ -carbon is important to increase the ester group stability, and suggested that replacement of the methyl-ester side-group was not necessary. Unlike in plasma, **1** and **2** were found to be very stable in liver microsomes, showing low

intrinsic clearance, which is an indicator of low CYP450 metabolism<sup>41</sup>. Compounds bearing the methoxy shift and ethyl-amide side-group showed very little clearance, while hydrophobic modifications (**6**, **23-26**) and the di-ethyl-amide side-group (**19,20**) produced unacceptably high (>10 ml/min/g) clearance rates.

Compounds that had passed previous selection criteria, and others still deemed of interest, were then tested in the *in vitro* PAMPA assay (Table 1), an artificial model of cell permeability. All tested compounds with a methyl-ester side-group (**1,3-9**) show extremely high permeability, with  $P_e$  values between 127 and 185 nm/s, whereas those compounds with the ethyl-amide side-group (**16-18,21,22**) show 25 to 59 nm/s. The PAMPA and microsomal clearance data confirms our hypothesis that compound DMPK properties could be tuned through side-group modifications while altering the position of the methoxy group has little impact on DMPK properties.

#### Full ITC Profiles

To finally determine the best bumped compound(s) a small number of compounds were titrated against all somatic BET bromodomains, WT and L/V, in ITC (Table 1). The following compounds met the selection criteria for both the AlphaLISA assay and DMPK triage and hence underwent ITC profiling: **4**, **5**, **7**, **8**, **16**, **17** and **21**. Results for specific bromodomains can be found in Table S6.

9-ME (**7**) and 9-ET (**8**) were clearly the most promising, with selectivity values around 100-fold, and their ITC profiles were replicated until reliable values of potency and selectivity could be generated. **7** is more potent against both L/V and WT bromodomains, while **8** shows greater overall selectivity (Table S6). **7** was used for the majority of our cellular experiments, as it was the most potent compound to show >100-fold selectivity and has slightly better DMPK properties.

The remaining compounds were not as promising, but are likely still usable as allele-selective inhibitors, and could be preferable in certain contexts. **4** and **16** show very high potency, while **17** was the only compound to show no detectable binding to any WT BET bromodomain

#### Validation of Bump-&-Hole system

The ability of the bump-&-hole system to target a single bromodomain, within one BET protein, was shown through ITC titrations of **4** against BRD2 constructs containing both bromodomains. Through measurements of the ligand:protein stoichiometry it was confirmed that **4** bound with a 2:1 stoichiometry when both bromodomains were mutated, and 1:1 stoichiometry to the single-bromodomain mutants. Furthermore negligible WT binding was observed. (Figure 4A).

To test the potency and selectivity of our bumped compounds in cells we used a fluorescence recovery after photobleaching (FRAP) assay, using U2OS cells over-expressing GFP-labelled full-length BET proteins<sup>38</sup>. While the BET proteins are active and bound to chromatin fluorescence recovery times can be several seconds long. However, if inhibited by compounds and freely diffusing in the nucleus we expect fluorescence to

recover much faster. The HDAC inhibitor suberoylanilide hydroxamic acid (SAHA) was used to increase the assay window by increasing chromatin acetylation and thus reducing the levels of 'free' GFP-BET protein (Fig. S10). Several compounds were tested against WT and L/V BRD4 (Fig 4B) and were shown to enter cells and displace full-length BET proteins from chromatin in an L/V-selective manner. **7** was confirmed to be potent and selective in cells, and this compound was hence used further.

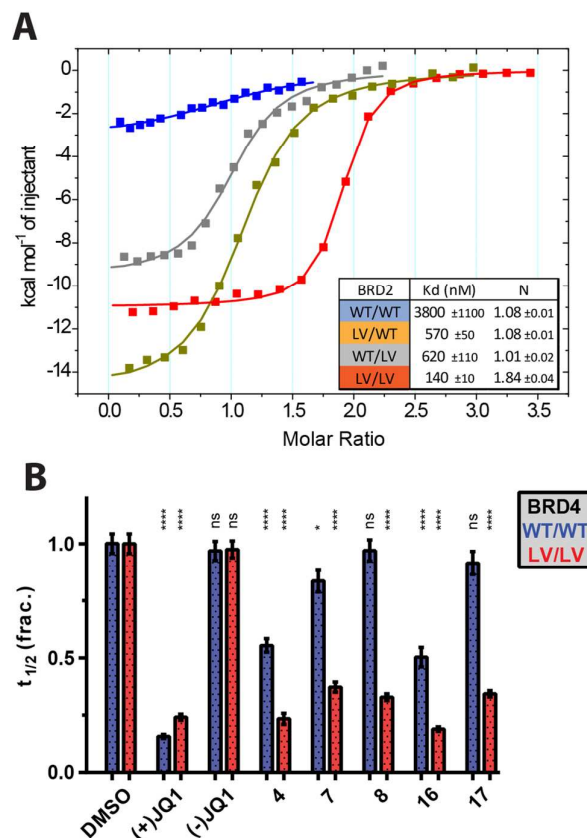


**Figure 4.** Bumped Compounds can Inhibit Single Bromodomains and are Effective in Cells. A) ITC titrations of **4** into BRD2 tandem constructs (containing both bromodomains). B) Effects of range of compounds on fluorescence recovery of GFP-labelled BRD4 constructs in U2OS cells, following 0.5s laser bleach event, at 1  $\mu$ M compound, 2  $\mu$ M SAHA and 0.03% DMSO.

#### Enantiomer Separation

At this point in the project, with the best compounds identified, it was decided to separate the two enantiomers from our racemic mixtures. A method for said separation was developed by Reach Separations Ltd. Racemic mixtures were dissolved to 20 mg/ml in ethanol and purified by HPLC, using a Lux A1 column (21.2 mm x 250 mm, 5  $\mu$ m) at ambient temperature and a flow rate of 21 ml/min. Samples were injected at a volume of 1 ml with 4:6 HEPT:EtOH (0.1% v/v NH<sub>3</sub>). A 42 mg sample of **7** at 96% purity could be separated into two clear peaks. The first peak to elute yielded 11 mg of compound (chemical purity of 94% and enantiomeric excess of 98), while the second peak yielded 9 mg, at 98% purity and enantiomeric excess of 97.

Separated enantiomers were next titrated against BRD4 BD1 in the AlphaLISA assay (Table S7). The compound in the first elution peak was more potent than the racemic mixture, and even more so than the compound eluted in the second peak (Figure 5A). We can assign the active enantiomer as **(2R,3S)-7**, and consequently the less active enantiomer as **(2S,3R)-7**. This assignment is based on analyses of the co-crystal structures. In all structures obtained, electron density around the chiral centres in question was well resolved (Fig. S6). All ligands could be fitted with high quality (ligand real space correlation coefficient  $\geq 0.87$  and real space R-value  $\leq 0.18$ ). Based on these analyses, we therefore conclude that the (2R,3S) enantiomer is the more active compound.

ITC titrations (Table S8) showed the (2S,3R) enantiomers of 7 and 8 to bind BRD4 BD1 L/V with high affinity and a 1:1 stoichiometry, while the racemic mixtures showed ~2-fold decreases in affinity and enthalpy and N values close to 2 (Fig 5B), consistent with only half the mixture binding the bromodomain. Finally no detectable binding was observed for the (2S,3R) enantiomers.

chose to exclusively use the active enantiomer going forward. ITC titrations (Fig. S11) showed **(2R,3S)-7** to be in general more potent and mutant-selective than the racemic mixture. The use of the purified active enantiomer overall boosts potency and selectivity and reducing the total compound concentration by half will provide other benefits (easier dosing, reduced compound metabolism). We therefore present 9-ME-1 (Figure 6) as our preferred bumped inhibitor, showing high potency, selectivity for L/V BET bromodomains and a strong DMPK profile. The (2S,3R) enantiomer – 9-ME-2 – can also be used as an inactive control

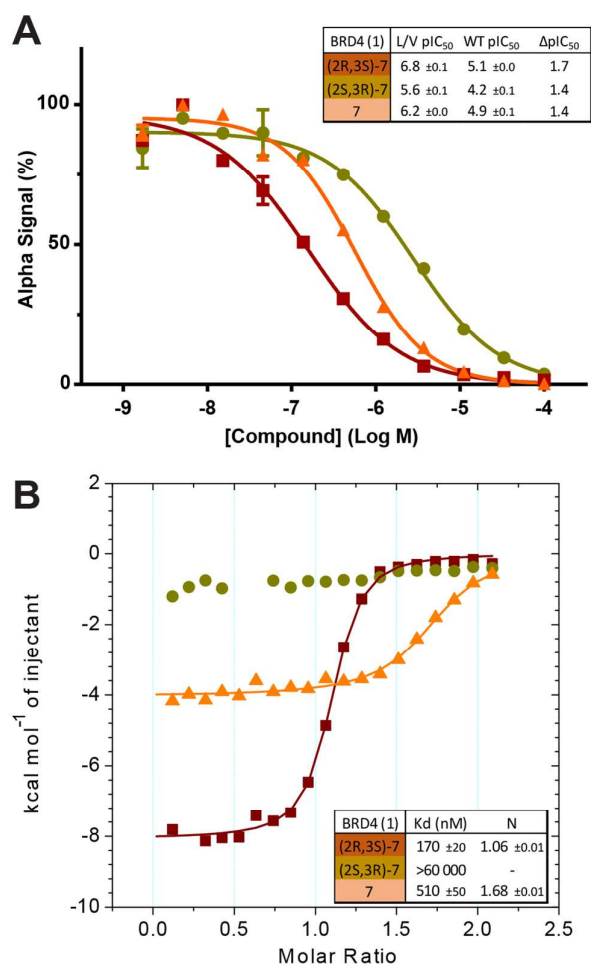


**Figure 5.** Enantiomer Characterization. Purified 7 enantiomers, and racemic mixture thereof, titrated against BRD4 BD1 L/V in competitive AlphaLISA assay (A) and ITC (B).

Although the inactivity of the second enantiomer means racemic mixtures can still be reliably used in experiments we

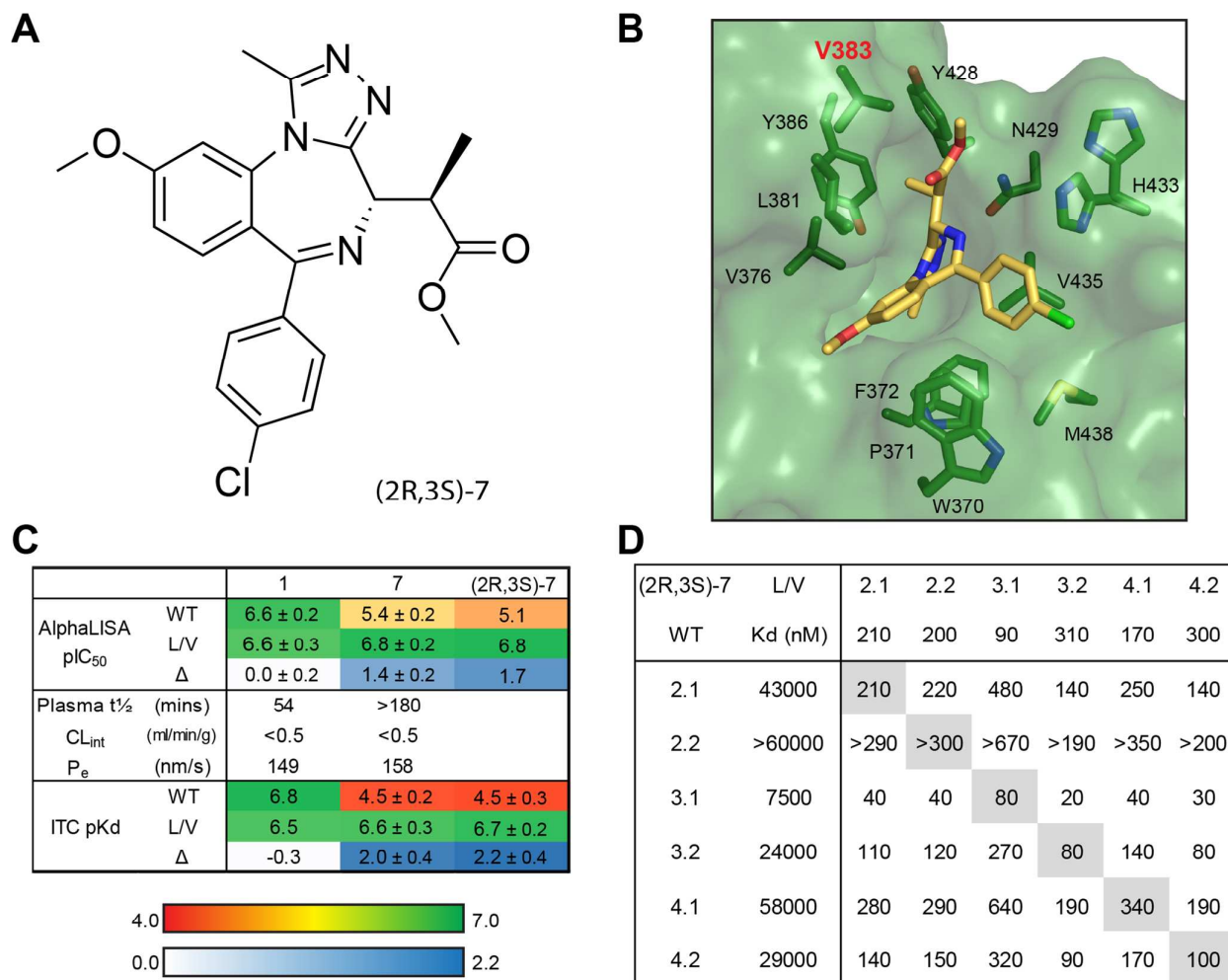


**Figure 6.** (2R,3S)-7: A Potent and Highly-Selective Bumped BET Inhibitor. A) Chemical structure of (2R,3S)-7. B) Co-crystal structure of (2R,3S)-7 bound to BRD2 BD2 L/V, with key residues highlighted. C) SAR of scaffold (1), 7 and (2R,3S)-7. (2R,3S)-7 AlphaLISA data and 1 ITC data from BRD4 BD1 only, other data is mean ± SD of titrations against all somatic BET bromodomains. D) Selectivity plot of (2R,3S)-7.

### WT Cytotoxicity

To confirm that our bumped compounds will not inhibit WT BET proteins at commonly used concentrations, nor alter the phenotypes of BET-sensitive cells we assayed the activity of our compounds on the viability of BET-dependent AML cell-lines MV4-11 and HL-60<sup>14</sup> (Fig. 7). Pleasingly, (2R,3S)-7 affected these cell-lines at a similar level to the 'inactive' (-)JQ1 control, and showed no cytotoxicity below 1 μM. This data supports the use of (2R,3S)-7 for allele-selective BET inhibition at commonly used concentrations (100 nM – 1 μM).

### Off-Target Screening

We have used several techniques to show that our bumped compounds are strongly selective for L/V BET bromodomain mutants. To show selectivity against non-BET WT bromodomains we employed the BROMOscan screen (DiscoverRX), testing 32 human bromodomains (Fig. S12). Using BROMOscan technology we first tested our scaffold (1) as a

positive control. Against BRD4 BD1 WT this gave a K<sub>d</sub> value of 15 nM and showed >90% inhibition above 100 nM. (2R,3S)-7 was screened at 1 μM and was found to bind non-BET bromodomains to a lesser degree than BET bromodomains. Some overlap was observed for SMARCA2, SMARCA4 and WDR9 BD2, an identified off-target of JQ1<sup>18</sup>.

To check for any unexpected off-target activity outside of the BET bromodomain subfamily we employed two high-quality screens. A screen of 50 representative human kinases showed no more than 20% inhibition at 1 μM (2R,3S)-7 (Table S9). A test of 55 receptors, transporters and ion channels (Table S10) showed 20% or less inhibition at 1 μM (2R,3S)-7, with the exception of the melatonin receptor MT1 which showed 77% inhibition. Undergoing the same screen, JQ1 also had previously shown off-target inhibition of MT1, in addition to the adenosine A3 receptor and the neurokinin NK2 receptor<sup>18</sup>.

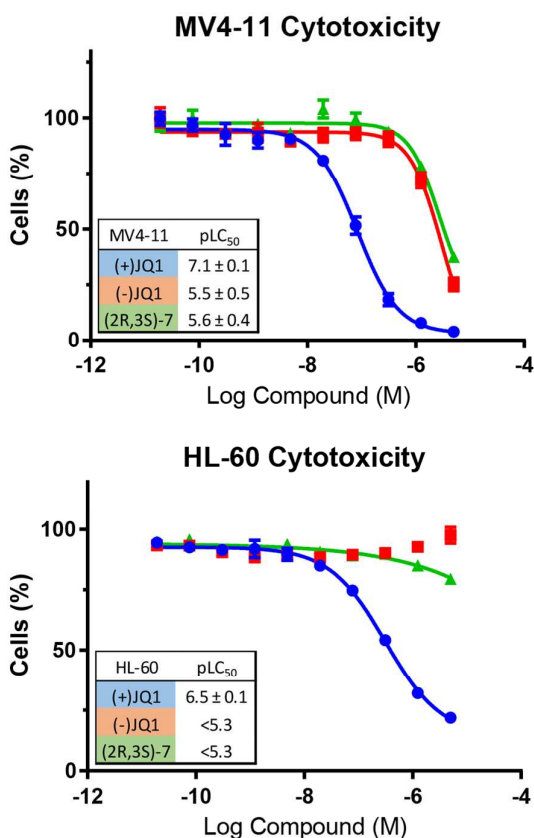


**Figure 7.** (2R,3S)-7 does not Perturb WT BET-Dependent Cells. Effects of compounds on viability of BET-dependent cell-lines MV4-11 & HL-60

### Application to a Biological Question

Some aspects of basic BET protein function are still unclear, such as the roles and relative importance of the first and second bromodomains within each protein. The BD1 of BRD4 has long been thought<sup>12</sup> to play a greater role in chromatin binding than its BD2. Experiments with ChIP-seq and acetylated nucleosome libraries<sup>42</sup> show that BRD4 BD1 is alone sufficient for chromatin binding, although it is enhanced by the BD2, while we have previously shown the BD1 of BRD4 is required for chromatin binding<sup>10</sup>. Recently it was shown that only the BD1 of BRDT is capable of binding acetylated nucleosomes, and the role of the BD2 may instead be to recruit acetylated non-histone proteins<sup>43</sup>. Currently little is known about the mechanisms of BRD2/BRD3 chromatin binding and the relative importance of their BD1s and BD2s.

Our development of the highly selective (2R,3S)-7 probe and improved L/V mutation motivated the application of the bump-&-hole system to answer these biological questions. By testing (2R,3S)-7 against GFP-BET constructs in our FRAP assay and comparing its effects on BD1 vs BD2 mutants we can observe their relative importance to chromatin binding. A dose of 200 nM was chosen as it showed no statistically significant blockade of WT BRD4 alongside almost complete displacement of L/V BRD4 (Figure 8A). As the L/V mutation has a minor impact on uninhibited recovery times (Fig. S5) the effects of inhibition on different constructs can be reliably compared.

Our data shows that, for all BET proteins, inhibition of BD1 has a greater effect than of BD2 (Figure 8B-E). Interestingly, the degree to which BD1 is dominant varies between the BET proteins. BD2 inhibition had no impact on BRDT (Figure 8E), and (2R,3S)-7 had the same effect on both the LV/WT and LV/LV constructs. These data are consistent with a model in which BRDT BD2 is not involved in chromatin binding, a conclusion recently drawn by Miller and colleagues<sup>43</sup>. BRD4 (Figure 8B) did see a small change in  $t_{1/2}$  in response to BD2 inhibition, suggesting (alongside previous experiments from us<sup>10</sup> and others<sup>42</sup>) that it has a minor role in chromatin binding. Finally BRD3 (Figure 8C) shows the greatest impact of BD2 inhibition, and mutation of both bromodomains is necessary for full displacement from chromatin, suggesting a much more balanced mechanism of bromodomain:histone. We cannot be certain of the role of BRD2 BD2 (Figure 8D) as the WT/LV construct shows no change in  $t_{1/2}$  but BD1 inhibition does not match that of the double mutant. Inhibition of the double mutant could not be quantified, as the GFP-BRD2 construct aggregated in the nucleus. This phenomenon was shown to be connected to strong inhibition and to occur with the WT construct and hence not be due to any destabilizing effect of the L/V mutation (Fig. S13). Inhibition-triggered aggregation of bromodomain constructs has previously been observed<sup>44</sup>.

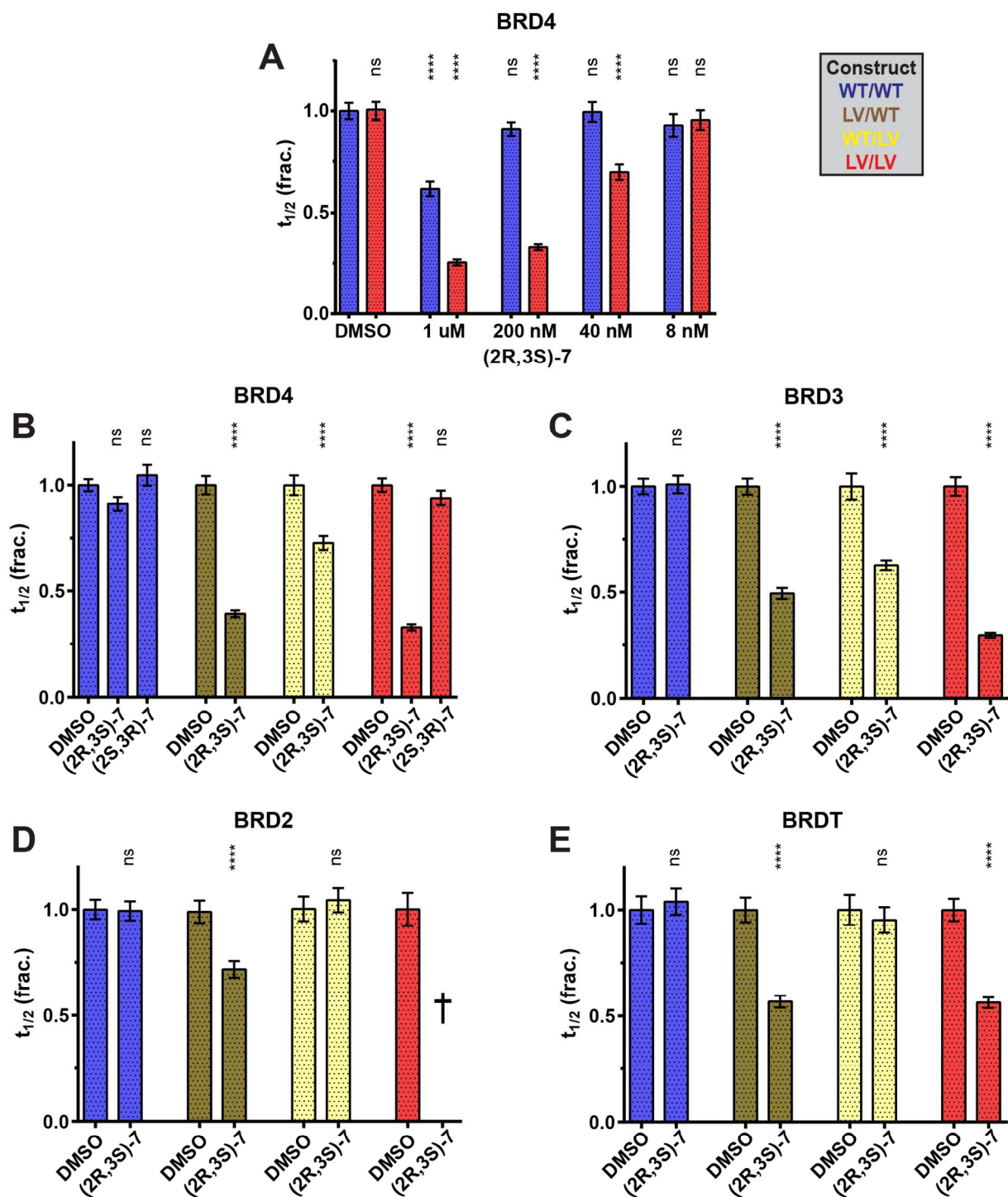


**Figure 8.** Application of the Bump-&-Hole System to a Biological Question. A-E) Effects of **7** enantiomers on the fluorescence recovery of GFP-labelled full-length BET constructs in U2OS cells, following 0.5s laser bleach event, at 2  $\mu$ M SAHA and 0.03% DMSO. Compound concentration is 200 nM unless stated otherwise. Unpaired t tests compare the effects of each compound to said construct's DMSO control. Results are mean and SEM of  $\sim$ 50 cells tested over 2 separate experiments. † - ‡ could not be determined due to inhibition-induced aggregation.

To provide additional functional insights into the individual roles of BD1 vs BD2 beyond chromatin binding, a luciferase assay was developed to monitor the expression of NF- $\kappa$ B target genes, inspired by work of Zou et al.<sup>45</sup>. Expression of our NF- $\kappa$ B-controlled luciferase was significantly increased by overexpression of GFP-BRD4 (on top of endogenous BET protein). This luciferase induction was maintained with L/V mutations (but not L/A), consistent again with more WT-like functionality of L/V compared to L/A.

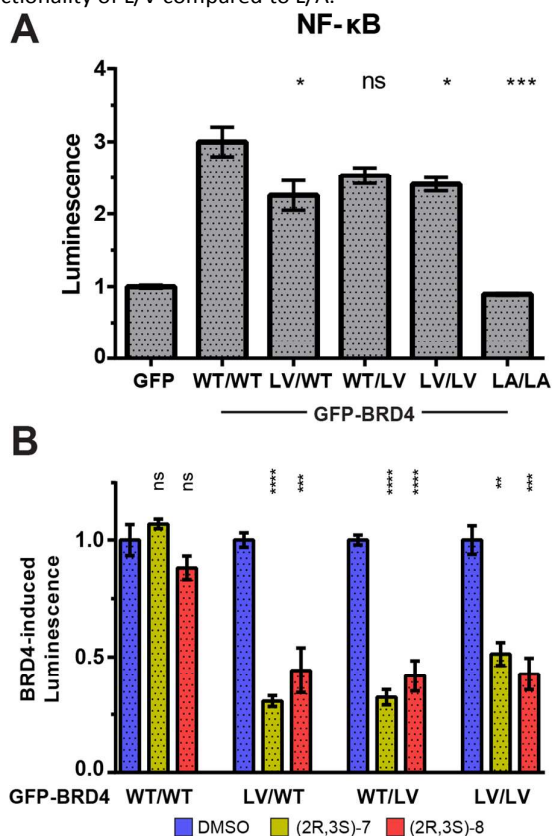


**Figure 9.** BRD4 and NF- $\kappa$ B-Target Gene Expression. Luminescence of HEK cells transfected with GFP-labelled BRD4 constructs and [a NF- $\kappa$ B luciferase reporter plasmid]. A) Luminescence normalised to GFP control. Statistical significance indicators relate to WT BRD4. B) Basal luciferase expression (with GFP plasmid) subtracted as background. Signal normalised to each construct's DMSO control. Results are mean and standard error of six technical replicates spread over two independent experiments.

Treatment of **(2R,3S)-7** and **(2R,3S)-8** against each GFP-BRD4 L/V construct showed that inhibiting either individual BD of BRD4 strongly impacted on NF- $\kappa$ B signalling, matching that of inhibiting both BDs. Together, the FRAP and luciferase data are consistent with the BD2 having little role in chromatin binding, but still being vital for initiating transcription and regulating gene expression, at least in the case of BRD4 and NF- $\kappa$ B.

## Discussion

Through a variety of techniques we have optimized both the biological and chemical aspects of our BET-bromodomain targeting bump-&-hole system. From our library of bumped

compounds we have highlighted **(2R,3S)-7** which shows high potency and strong selectivity for our L/V mutation, which we have shown to be more structurally and functionally conservative than the previous L/A mutation.

We applied our optimized system to address a biological question – the relative importance of the BD1s and BD2s of BET proteins to chromatin binding<sup>10, 42, 43</sup>. By dosing a variety of GFP-BET constructs in our FRAP assay we showed that, for all BET proteins, chromatin binding is primarily influenced by BD1s. Furthermore we could show that the degree to which the BD1 is dominant varies between BET proteins and that BRD3 is sensitive to BD2 inhibition. Interestingly our GFP-BRDT construct generates significantly slower recovery times ( $t_{1/2} \sim 1.5$ s) when uninhibited. This could indicate BRDT being a weaker binder of acetylated chromatin, or a result of U2OS not presenting BRDT's preferred epigenetic marks. These observations show that when using this bump-&-hole system it may be necessary to mutate both bromodomains to fully displace a given BET protein. If the BD2s of certain BET proteins do not primarily function through the binding of chromatin then an alternate function could be the recognition and recruitment of acetylated, non-histone proteins. Several such interactions have been reported recently<sup>46-49</sup>, such as an interaction between BRD4 BD2 and di-acetylated Twist<sup>50</sup>. The unusual BD1/BD2 balance displayed by BRD3 suggests its chromatin and non-chromatin mediated biological functions may also be atypical.

By combining our bump-&-hole system and a NF- $\kappa$ B luciferase assay we were able to assess the importance of the BD1 and BD2 of BRD4 to initiating transcription and regulating gene expression (for NF- $\kappa$ B target genes). Our data revealed that BRD4 BD2 is still vital for transcription initiation, despite having little role in chromatin binding. This suggests that recruitment of non-histone proteins is also essential. This is consistent with the model put forth by Shi et al<sup>50</sup> wherein BRD4 BD2 binds Twist, a transcriptional activator, giving the BRD4 – P-TEFb – RNA Pol II complex specificity for WNT5A. One can imagine that there are other non-histone proteins (NF- $\kappa$ B in our example<sup>45</sup>) recognised by BRD4 BD2, and other BET BDs not involved in chromatin binding, that can direct BET proteins to up-regulate other specific sets of genes. In the future, a more widespread and systematic investigation into such non-histone BET binding partners could reveal much about how they function on a molecular level, and present new opportunities for drug or chemical probe development.

Recently the results of BET-inhibitor clinical trials have highlighted the risks of on-target toxicity, especially thrombocytopenia<sup>23, 51-55</sup>. The BD2-selective RVX-208<sup>28</sup> is the only BET-inhibitor to progress to phase 3, hinting at reduced toxicity<sup>56</sup>. This low toxicity could be a result of the reduced role of BD2s in chromatin binding through three potential routes. As the BD2s are less important to chromatin binding RVX-208 may generate only partial BET inhibition and a greater therapeutic window. As the role of the BD2 differs between



BET proteins this could generate some inter-protein selectivity for BRD3 over BRD4, reducing any BRD4-mediated toxicity. Finally, RVX-208 may not function through chromatin displacement but by blocking interactions between BD2s and non-histone proteins (such as Twist) and hence act through a more precise, less toxic, mechanism.

Through a combination of selectivity screens we show **(2R,3S)-7** to have almost no off-target inhibition. The only significant off-target is the melatonin receptor MT1. MT1 has been shown to have a variety of functions<sup>57</sup>, primarily taking place in the CNS and regarding the circadian rhythm, which should not complicate the use of **(2R,3S)-7**. Based on the results of said selectivity screens, the observation of cytotoxicity in BET-dependent AML cell-lines above 1  $\mu$ M and our FRAP dose-response experiments we believe that, for cellular experiments, a dosage of 100-500 nM is optimal, and should allow for total or near-total inhibition of L/V BET proteins with no WT significant.

Although we show how the current system can be used to address biological questions, the investigation of more complex physiological and disease-relevant functions, for example comparing the genes regulated by each protein, will require the development of isogenic cell-lines and model organisms carrying the L/V mutation. Recent advances in the use of the CRISPR/cas9 system<sup>58</sup> as a gene-editing technology presents an ideal opportunity to introduce single-point mutations into a variety of cell-lines and model organisms, without introducing exogenous BET genes that may not be regulated or post-translationally processed correctly.

Our optimized bumped compounds could also provide useful chemical tools for sophisticated or unconventional chemical genetics experiments. Ethyl-amide containing compounds (**16**, **17** & **21**) could be converted into L/V-selective alternatives to Bio-JQ1<sup>40</sup> and a series of JQ1-based cross-linking compounds used for protein pulldown and fluorescence microscopy<sup>59</sup>. The 1,4-benzodiazepine scaffold used in BET inhibitors has also been derivatized to create PROTAC degraders<sup>32-35, 37</sup> and bivalent inhibitors<sup>60</sup>, and such modifications could be implemented in our bumped compounds.

Through optimizing our specific bump-&-hole system we believe we have revealed some observations relevant to the bump-&-hole technique in general. It is clear that any mutation introduced to target proteins must be very subtle, as even the relatively conservative L/A mutation had noticeable effects on BET bromodomain binding and function. Fortunately, major mutations and large 'holes' are not required for selectivity, as our L/V mutation allowed for over 100-fold selectivity despite the removal of only one methyl group. By association, the design of mutant-selective compounds should focus on minor modifications, and longer alkyl bumps can easily cause large drops in potency. Large bumps will also increase the molecular weight and LogP of the inhibitor, leading to poorer DMPK properties. Care should be taken with regard to bump placement, as our compounds featured the bump on a flexible side-group which allowed for some residual WT binding. This could be prevented by locking the bump in place, as we do with the amide side-groups, or by

placing the bump on a rigid part of the scaffold. Interestingly, we show the potential of introducing chemical modifications that are not located near the bump or mutation, as our best compounds contained a methoxy shift modification quite distant to our alkyl bump and L/V hole.

## Conclusions

In summary, we describe an iterative, step-wise and rational optimization of the bump-&-hole approach for allele-selective BET bromodomain inhibition, in both its biological and chemical aspects, which has led to the development of a more reliable and powerful system.

Through a three-stage process, several bumped analogues were identified with high potency, selectivity for the L/V mutant over WT bromodomains and desirable DMPK properties. This culminated in our selection of enantiomerically-pure **(2R,3S)-7** as a chemical probe targeting L/V BET bromodomains with  $\sim$ 200 nM potency, >100-fold selectivity across the BET subfamily and displaying an excellent DMPK profile.

This orthogonal **(2R,3S)-7**:L/V inhibitor:mutant pair was validated through a number of in vitro and cellular experiments, and then utilized to answer a biological question, revealing that the BD1 of all BET proteins is more important to chromatin binding than the BD2, albeit to varying degrees. Interestingly, the BD2 of BRD4 was shown to still be essential for transcription (with NF- $\kappa$ B target genes) highlighting the importance of BD:non-histone protein interactions. We present this optimized bump-&-hole system as a powerful and reliable tool for investigating the biological role of the BET proteins and for more advanced target validation.

## Conflicts of interest

There are no conflicts of interest to declare.

## Acknowledgements

This work was supported by awards to A.C. from the UK Biotechnology and Biological Sciences Research Council (BBSRC, grant BB/J001201/2 and David Phillips Fellowship BB/G023123/2) and the European Research Council (ERC starting grant, ERC-2012-StG-311460 DrugE3CRLs). A.C.R. was supported by a BBSRC EASTBIO Doctoral Training Partnership award (BB/J01446X/1). K.-H.C. was supported by a European Commission Marie Skłodowska-Curie Actions Individual Fellowship (H2020-MSCA-IF-2014-655516). L.V.B. was funded by a BBSRC Research Experience Placement award (BB/J01446X/1). Biophysics and drug discovery activities are supported by Wellcome Trust strategic awards to Dundee (100476/Z/12/Z and 094090/Z/10/Z, respectively). We would like to acknowledge P. Fyfe of the in-house X-ray Crystallography Facility at the University of Dundee, which is supported by The Wellcome Trust (award no. 094090); the staff at the Diamond Light Source for beamtime (BAG proposal

MX10071) and beamline support at beamline I04-1; and Dr. Sam Swift at the Dundee Imaging Facility, Dundee, which is supported by the 'Wellcome Trust Technology Platform' award [097945/B/11/Z] and the 'MRC Next Generation Optical Microscopy' award [MR/K015869/1].

## Notes

Crystal structure PDB codes:

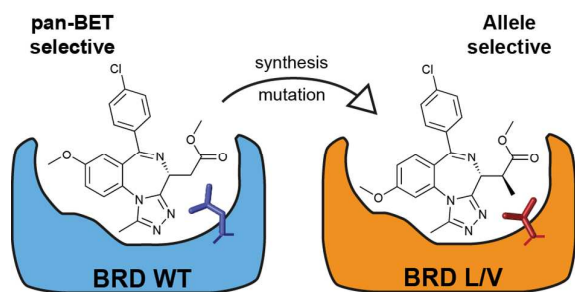
BRD2 BD2 L383V apo (5O38), in complex with compounds 3 (5O39), 4 (5O3A), 5 (5O3B), 7 (5O3C), 8 (5O3D), 16 (5O3E), 17(5O3F), 18 (5O3G) 21 (5O3H) and 24 (5O3I).

## References

1. A. C. Runcie, K. H. Chan, M. Zengerle and A. Ciulli, *Curr Opin Chem Biol*, 2016, 33, 186-194.
2. C. H. Arrowsmith, J. E. Audia, C. Austin, J. Baell, J. Bennett, J. Blagg, C. Bountra, P. E. Brennan, P. J. Brown, M. E. Bunnage, C. Buser-Doepner, R. M. Campbell, A. J. Carter, P. Cohen, R. A. Copeland, B. Cravatt, J. L. Dahlin, D. Dhanak, A. M. Edwards, M. Frederiksen, S. V. Frye, N. Gray, C. E. Grimshaw, D. Hepworth, T. Howe, K. V. Huber, J. Jin, S. Knapp, J. D. Kotz, R. G. Kruger, D. Lowe, M. M. Mader, B. Marsden, A. Mueller-Fahrnow, S. Muller, R. C. O'Hagan, J. P. Overington, D. R. Owen, S. H. Rosenberg, B. Roth, R. Ross, M. Schapira, S. L. Schreiber, B. Shoichet, M. Sundstrom, G. Superti-Furga, J. Taunton, L. Toledo-Sherman, C. Walpole, M. A. Walters, T. M. Willson, P. Workman, R. N. Young and W. J. Zuercher, *Nat Chem Biol*, 2015, 11, 536-541.
3. M. E. Bunnage, E. L. Chekler and L. H. Jones, *Nat Chem Biol*, 2013, 9, 195-199.
4. K. Islam, *ACS Chem Biol*, 2015, 10, 343-363.
5. A. C. Bishop, J. A. Ubersax, D. T. Petsch, D. P. Matheos, N. S. Gray, J. Blethrow, E. Shimizu, J. Z. Tsien, P. G. Schultz, M. D. Rose, J. L. Wood, D. O. Morgan and K. M. Shokat, *Nature*, 2000, 407, 395-401.
6. T. Clackson, W. Yang, L. W. Rozamus, M. Hatada, J. F. Amara, C. T. Rollins, L. F. Stevenson, S. R. Magari, S. A. Wood, N. L. Courage, X. Lu, F. Cerasoli, Jr., M. Gilman and D. A. Holt, *Proceedings of the National Academy of Sciences of the United States of America*, 1998, 95, 10437-10442.
7. W. Yang, L. W. Rozamus, S. Narula, C. T. Rollins, R. Yuan, L. J. Andrade, M. K. Ram, T. B. Phillips, M. R. van Schravendijk, D. Dalgarno, T. Clackson and D. A. Holt, *J Med Chem*, 2000, 43, 1135-1142.
8. R. Wang, K. Islam, Y. Liu, W. Zheng, H. Tang, N. Lailier, G. Blum, H. Deng and M. Luo, *J Am Chem Soc*, 2013, 135, 1048-1056.
9. Q. Lin, F. Jiang, P. G. Schultz and N. S. Gray, *J Am Chem Soc*, 2001, 123, 11608-11613.
10. M. G. Baud, E. Lin-Shiao, T. Cardote, C. Tallant, A. Pschibul, K. H. Chan, M. Zengerle, J. R. Garcia, T. T. Kwan, F. M. Ferguson and A. Ciulli, *Science*, 2014, 346, 638-641.
11. M. G. Baud, E. Lin-Shiao, M. Zengerle, C. Tallant and A. Ciulli, *J Med Chem*, 2016, 59, 1492-1500.
12. P. Filippakopoulos, S. Picaud, M. Mangos, T. Keates, J. P. Lambert, D. Barsyte-Lovejoy, I. Felletar, R. Volkmer, S. Muller, T. Pawson, A. C. Gingras, C. H. Arrowsmith and S. Knapp, *Cell*, 2012, 149, 214-231.
13. J. T. Deeney, A. C. Belkina, O. S. Shirihai, B. E. Corkey and G. V. Denis, *PLoS One*, 2016, 11, e0151329.
14. J. Zuber, J. Shi, E. Wang, A. R. Rappaport, H. Herrmann, E. A. Sison, D. Magoon, J. Qi, K. Blatt, M. Wunderlich, M. J. Taylor, C. Johns, A. Chicas, J. C. Mulloy, S. C. Kogan, P. Brown, P. Valent, J. E. Bradner, S. W. Lowe and C. R. Vakoc, *Nature*, 2011, 478, 524-528.
15. M. A. Dawson, R. K. Prinjha, A. Dittmann, G. Giotopoulos, M. Bantscheff, W. I. Chan, S. C. Robson, C. W. Chung, C. Hopf, M. M. Savitski, C. Huthmacher, E. Gudgin, D. Lugo, S. Beinke, T. D. Chapman, E. J. Roberts, P. E. Soden, K. R. Auger, O. Mirguet, K. Doehner, R. Delwel, A. K. Burnett, P. Jeffrey, G. Drewes, K. Lee, B. J. Huntly and T. Kouzarides, *Nature*, 2011, 478, 529-533.
16. J. E. Delmore, G. C. Issa, M. E. Lemieux, P. B. Rahl, J. Shi, H. M. Jacobs, E. Kastiris, T. Gilpatrick, R. M. Paranal, J. Qi, M. Chesi, A. C. Schinzel, M. R. McKeown, T. P. Heffernan, C. R. Vakoc, P. L. Bergsagel, I. M. Ghobrial, P. G. Richardson, R. A. Young, W. C. Hahn, K. C. Anderson, A. L. Kung, J. E. Bradner and C. S. Mitsiades, *Cell*, 2011, 146, 904-917.
17. J. Shi and C. R. Vakoc, *Mol Cell*, 2014, 54, 728-736.
18. P. Filippakopoulos, J. Qi, S. Picaud, Y. Shen, W. B. Smith, O. Fedorov, E. M. Morse, T. Keates, T. T. Hickman, I. Felletar, M. Philpott, S. Munro, M. R. McKeown, Y. Wang, A. L. Christie, N. West, M. J. Cameron, B. Schwartz, T. D. Heightman, N. La Thangue, C. A. French, O. Wiest, A. L. Kung, S. Knapp and J. E. Bradner, *Nature*, 2010, 468, 1067-1073.
19. E. Nicodeme, K. L. Jeffrey, U. Schaefer, S. Beinke, S. Dewell, C. W. Chung, R. Chandwani, I. Marazzi, P. Wilson, H. Coste, J. White, J. Kirilovsky, C. M. Rice, J. M. Lora, R. K. Prinjha, K. Lee and A. Tarakhovsky, *Nature*, 2010, 468, 1119-1123.
20. N. H. Theodoulou, N. C. Tomkinson, R. K. Prinjha and P. G. Humphreys, *Curr Opin Chem Biol*, 2016, 33, 58-66.
21. S. G. Smith and M. M. Zhou, *ACS Chem Biol*, 2016, 11, 598-608.
22. C. Galdeano and A. Ciulli, *Future Med Chem*, 2016, 8, 1655-1680.
23. G. Andrieu, A. C. Belkina and G. V. Denis, *Drug Discov Today Technol*, 2016, 19, 45-50.
24. P. Bamborough, C. W. Chung, R. C. Furze, P. Grandi, A. M. Michon, R. J. Sheppard, H. Barnett, H. Diallo, D. P. Dixon, C. Douault, E. J. Jones, B. Karamshi, D. J. Mitchell, R. K. Prinjha, C. Rau, R. J. Watson, T. Werner and E. H. Demont, *J Med Chem*, 2015, 58, 6151-6178.
25. P. Bamborough, H. A. Barnett, I. Becher, M. J. Bird, C. W. Chung, P. D. Craggs, E. H. Demont, H. Diallo, D. J. Fallon, L. J. Gordon, P. Grandi, C. I. Hobbs, E. Hooper-Greenhill, E. J. Jones, R. P. Law, A. Le Gall, D. Lugo, A. M. Michon, D. J. Mitchell, R. K. Prinjha, R. J. Sheppard, A. J. Watson and R. J. Watson, *ACS Med Chem Lett*, 2016, 7, 552-557.
26. N. H. Theodoulou, P. Bamborough, A. J. Bannister, I. Becher, R. A. Bit, K. H. Che, C. W. Chung, A. Dittmann, G. Drewes, D. H. Drewry, L. Gordon, P. Grandi, M. Leveridge, M. Lindon, A. M. Michon, J. Molnar, S. C. Robson, N. C. Tomkinson, T. Kouzarides, R. K. Prinjha and P. G. Humphreys, *J Med Chem*, 2016, 59, 1425-1439.
27. S. Muller and S. Knapp, *Medchemcomm*, 2014, 5, 288-296.

28. S. Picaud, C. Wells, I. Felletar, D. Brotherton, S. Martin, P. Savitsky, B. Diez-Dacal, M. Philpott, C. Bountra, H. Lingard, O. Fedorov, S. Muller, P. E. Brennan, S. Knapp and P. Filippakopoulos, *Proceedings of the National Academy of Sciences of the United States of America*, 2013, 110, 19754-19759.
29. K. Cheung, G. Lu, R. Sharma, A. Vincek, R. Zhang, A. N. Plotnikov, F. Zhang, Q. Zhang, Y. Ju, Y. Hu, L. Zhao, X. Han, J. Meslamani, F. Xu, A. Jaganathan, T. Shen, H. Zhu, E. Rusinova, L. Zeng, J. Zhou, J. Yang, L. Peng, M. Ohlmeyer, M. J. Walsh, D. Y. Zhang, H. Xiong and M. M. Zhou, *Proceedings of the National Academy of Sciences of the United States of America*, 2017, 114, 2952-2957.
30. M. Gacias, G. Gerona-Navarro, A. N. Plotnikov, G. Zhang, L. Zeng, J. Kaur, G. Moy, E. Rusinova, Y. Rodriguez, B. Matikainen, A. Vincek, J. Joshua, P. Casaccia and M. M. Zhou, *Chem Biol*, 2014, 21, 841-854.
31. B. Raux, Y. Voitovich, C. Derviaux, A. Lugari, E. Rebuffet, S. Milhas, S. Priet, T. Roux, E. Trinquet, J. C. Guillemot, S. Knapp, J. M. Brunel, A. Y. Fedorov, Y. Collette, P. Roche, S. Betzi, S. Combes and X. Morelli, *J Med Chem*, 2016, 59, 1634-1641.
32. G. E. Winter, D. L. Buckley, J. Paulk, J. M. Roberts, A. Souza, S. Dhe-Paganon and J. E. Bradner, *Science*, 2015, 348, 1376-1381.
33. M. Zengerle, K. H. Chan and A. Ciulli, *ACS Chem Biol*, 2015, 10, 1770-1777.
34. J. Lu, Y. Qian, M. Altieri, H. Dong, J. Wang, K. Raina, J. Hines, J. D. Winkler, A. P. Crew, K. Coleman and C. M. Crews, *Chem Biol*, 2015, 22, 755-763.
35. K. Raina, J. Lu, Y. Qian, M. Altieri, D. Gordon, A. M. Rossi, J. Wang, X. Chen, H. Dong, K. Siu, J. D. Winkler, A. P. Crew, C. M. Crews and K. G. Coleman, *Proceedings of the National Academy of Sciences of the United States of America*, 2016, 113, 7124-7129.
36. B. Zhou, J. Hu, F. Xu, Z. Chen, L. Bai, E. Fernandez-Salas, M. Lin, L. Liu, C. Y. Yang, Y. Zhao, D. McEachern, S. Przybranowski, B. Wen, D. Sun and S. Wang, *J Med Chem*, 2017, DOI: 10.1021/acs.jmedchem.6b01816.
37. M. S. Gadd, A. Testa, X. Lucas, K. H. Chan, W. Chen, D. J. Lamont, M. Zengerle and A. Ciulli, *Nat Chem Biol*, 2017, 13, 514-521.
38. M. Philpott, C. M. Rogers, C. Yapp, C. Wells, J. P. Lambert, C. Strain-Damerell, N. A. Burgess-Brown, A. C. Gingras, S. Knapp and S. Muller, *Epigenetics Chromatin*, 2014, 7, 14.
39. O. Mirguet, R. Gosmini, J. Toum, C. A. Clement, M. Barnathan, J. M. Brusq, J. E. Mordaunt, R. M. Grimes, M. Crowe, O. Pineau, M. Ajakane, A. Daugan, P. Jeffrey, L. Cutler, A. C. Haynes, N. N. Smithers, C. W. Chung, P. Bamborough, I. J. Uings, A. Lewis, J. Witherington, N. Parr, R. K. Prinjha and E. Nicodeme, *J Med Chem*, 2013, 56, 7501-7515.
40. L. Anders, M. G. Guenther, J. Qi, Z. P. Fan, J. J. Marineau, P. B. Rahl, J. Loven, A. A. Sigova, W. B. Smith, T. I. Lee, J. E. Bradner and R. A. Young, *Nat Biotechnol*, 2014, 32, 92-96.
41. A. E. Nassar, A. M. Kamel and C. Clarimont, *Drug Discov Today*, 2004, 9, 1020-1028.
42. U. T. Nguyen, L. Bittova, M. M. Muller, B. Fierz, Y. David, B. Houck-Loomis, V. Feng, G. P. Dann and T. W. Muir, *Nat Methods*, 2014, 11, 834-840.
43. T. C. Miller, B. Simon, V. Rybin, H. Grotsch, S. Curtet, S. Khochbin, T. Carlomagno and C. W. Muller, *Nat Commun*, 2016, 7, 13855.
44. A. R. Conery, R. C. Centore, A. Neiss, P. J. Keller, S. Joshi, K. L. Spillane, P. Sandy, C. Hatton, E. Pardo, L. Zawadzke, A. Bommi-Reddy, K. E. Gascoigne, B. M. Bryant, J. A. Mertz and R. J. Sims, *Elife*, 2016, 5.
45. Z. Zou, B. Huang, X. Wu, H. Zhang, J. Qi, J. Bradner, S. Nair and L. F. Chen, *Oncogene*, 2014, 33, 2395-2404.
46. B. Huang, X. D. Yang, M. M. Zhou, K. Ozato and L. F. Chen, *Mol Cell Biol*, 2009, 29, 1375-1387.
47. R. Gamsjaeger, S. R. Webb, J. M. Lamonica, A. Billin, G. A. Blobel and J. P. Mackay, *Mol Cell Biol*, 2011, 31, 2632-2640.
48. J. M. Lamonica, W. Deng, S. Kadauke, A. E. Campbell, R. Gamsjaeger, H. Wang, Y. Cheng, A. N. Billin, R. C. Hardison, J. P. Mackay and G. A. Blobel, *Proceedings of the National Academy of Sciences of the United States of America*, 2011, 108, E159-168.
49. S. Schroder, S. Cho, L. Zeng, Q. Zhang, K. Kaehlecke, L. Mak, J. Lau, D. Bisgrove, M. Schnolzer, E. Verdin, M. M. Zhou and M. Ott, *J Biol Chem*, 2012, 287, 1090-1099.
50. J. Shi, Y. Wang, L. Zeng, Y. Wu, J. Deng, Q. Zhang, Y. Lin, J. Li, T. Kang, M. Tao, E. Rusinova, G. Zhang, C. Wang, H. Zhu, J. Yao, Y. X. Zeng, B. M. Evers, M. M. Zhou and B. P. Zhou, *Cancer Cell*, 2014, 25, 210-225.
51. A. Stathis, E. Zucca, M. Bekradda, C. Gomez-Roca, J. P. Delord, T. de La Motte Rouge, E. Uro-Coste, F. de Braud, G. Pelosi and C. A. French, *Cancer Discov*, 2016, 6, 492-500.
52. S. Amorim, A. Stathis, M. Gleeson, S. Iyengar, V. Magarotto, X. Leleu, F. Morschhauser, L. Karlin, F. Broussais, K. Rezai, P. Herait, C. Kahatt, F. Lokiec, G. Salles, T. Facon, A. Palumbo, D. Cunningham, E. Zucca and C. Thieblemont, *Lancet Haematol*, 2016, 3, e196-204.
53. J. E. Bolden, N. Tasdemir, L. E. Dow, J. H. van Es, J. E. Wilkinson, Z. Zhao, H. Clevers and S. W. Lowe, *Cell Rep*, 2014, 8, 1919-1929.
54. B. K. Albrecht, V. S. Gehling, M. C. Hewitt, R. G. Vaswani, A. Cote, Y. Leblanc, C. G. Nasveschuk, S. Bellon, L. Bergeron, R. Campbell, N. Cantone, M. R. Cooper, R. T. Cummings, H. Jayaram, S. Joshi, J. A. Mertz, A. Neiss, E. Normant, M. O'Meara, E. Pardo, F. Poy, P. Sandy, J. Supko, R. J. Sims, 3rd, J. C. Harmange, A. M. Taylor and J. E. Audia, *J Med Chem*, 2016, 59, 1330-1339.
55. A. J. Stonestrom, S. C. Hsu, M. T. Werner and G. A. Blobel, *Drug Discov Today Technol*, 2016, 19, 23-28.
56. S. J. Nicholls, A. Gordon, J. Johansson, K. Wolski, C. M. Ballantyne, J. J. Kastelein, A. Taylor, M. Borgman and S. E. Nissen, *J Am Coll Cardiol*, 2011, 57, 1111-1119.
57. M. L. Dubocovich and M. Markowska, *Endocrine*, 2005, 27, 101-110.
58. J. D. Sander and J. K. Joung, *Nat Biotechnol*, 2014, 32, 347-355.
59. Z. Li, D. Wang, L. Li, S. Pan, Z. Na, C. Y. Tan and S. Q. Yao, *J Am Chem Soc*, 2014, 136, 9990-9998.
60. M. Tanaka, J. M. Roberts, H. S. Seo, A. Souza, J. Paulk, T. G. Scott, S. L. DeAngelo, S. Dhe-Paganon and J. E. Bradner, *Nat Chem Biol*, 2016, 12, 1089-1096.

## Graphical Abstract



## Optimization of a “Bump-and-Hole” Approach to Allele-Selective BET Bromodomain Inhibition

A. C. Runcie<sup>a†</sup>, M. Zengerle<sup>a†</sup>, K.-H. Chan<sup>a†</sup>, A. Testa<sup>a</sup>, L. van Beurden<sup>a</sup>, M. G. J. Baud<sup>a</sup>, O. Epemolu<sup>a</sup>, L. C.J. Ellis<sup>a</sup>, K. D. Read<sup>a</sup>, V. Coulthard<sup>b</sup>, A. Brien<sup>b</sup>, A. Ciulli<sup>a\*</sup>

<sup>a</sup> Division of Biological Chemistry and Drug Discovery, School of Life Sciences, University of Dundee, Dundee, Scotland, UK.

<sup>b</sup> Reach Separations Ltd, BioCity Nottingham, Nottingham, UK.

### Supplementary Information

Supplementary Figures & Tables	S2
X-Ray Crystallography: Data Collection & Refinement Statistics	S20
Materials & Methods	S22
Compound Synthesis & Characterization	S26
Supplemental References	S37

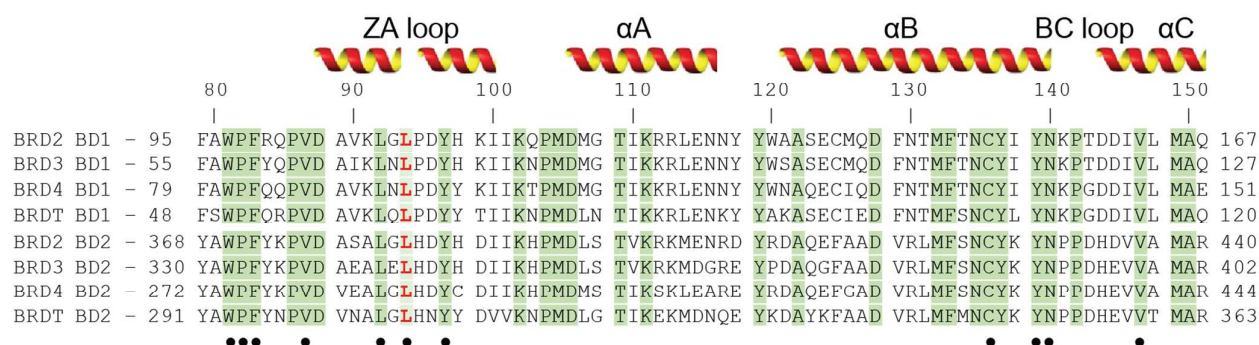


**Figure S1 – BET Bromodomain Sequence alignment**

Sequence alignment of the eight human BET bromodomains, with positions of  $\alpha$ -helices and associated loops. Conserved residues highlighted in green, with mutated leucine in red. Conserved residues making direct contact with I-BET shown with black dot. Ruler numbering based on BRD4 BD1 sequence.

Bromodomain	T <sub>m</sub> (°C) $\pm$ SE			$\Delta$ T <sub>m</sub> (°C) $\pm$ SE	
	WT	L/V	L/A	L/V	L/A
BRD2 BD1	45 $\pm$ 0.0	43 $\pm$ 0.6	45 $\pm$ 0.5	-2 $\pm$ 0.6	-1 $\pm$ 0.6
BRD2 BD2	49 $\pm$ 0.1	48 $\pm$ 0.1	48 $\pm$ 0.3	-1 $\pm$ 0.1	-1 $\pm$ 0.3
BRD3 BD1	46 $\pm$ 0.1	43 $\pm$ 0.2	44 $\pm$ 0.1	-3 $\pm$ 0.2	-2 $\pm$ 0.1
BRD3 BD2	44 $\pm$ 0.1	45 $\pm$ 0.9	44 $\pm$ 0.0	1 $\pm$ 0.9	0 $\pm$ 0.1
BRD4 BD1	43 $\pm$ 0.2	41 $\pm$ 0.2	44 $\pm$ 0.2	-2 $\pm$ 0.3	0 $\pm$ 0.3
BRD4 BD2	46 $\pm$ 0.1	45 $\pm$ 0.3	43 $\pm$ 0.1	-1 $\pm$ 0.3	-4 $\pm$ 0.1
BRDT BD1	45 $\pm$ 0.2	45 $\pm$ 0.1	43 $\pm$ 0.2	1 $\pm$ 0.2	-1 $\pm$ 0.3
BRDT BD2	44 $\pm$ 0.1	42 $\pm$ 1.6	47 $\pm$ 0.1	-2 $\pm$ 1.6	3 $\pm$ 0.2

**Table S1 – Thermal Stability of BET Bromodomain Constructs**

Differential Scanning Fluorimetry –derived melting points of WT, L/V and L/A BET bromodomains. Mean and standard error of three replications.

H4 K5,8ac	BRD2 BD1	BRD2 BD2	BRD3 BD1	BRD3 BD2	BRD4 BD1	BRD4 BD2	BRDT BD1
-----------	----------	----------	----------	----------	----------	----------	----------

	WT	L/V	WT	L/V	WT	L/V	WT	L/V	WT	L/V	WT	L/V	WT	L/V
Kd ( $\mu\text{M}$ )	31	42	91	138	18	22	105	154	8	10	83	198	23	40
SE	2	3	19	16	1	1	12	16	1	1	2	22	4	8
$\Delta\text{H}$ (kcal/mol)	-8.8	-9.8	-1.7	-1.4	-9.4	-10.7	-6.7	-11.6	-10.5	-10.9	-4.1	-5.6	-14.4	-16.9
SE	0.2	0.5	0.2	0.2	0.1	0.2	1.1	5.7	0.1	0.1	0.1	0.9	1.4	3.0
N	2.1	1.8	2.3	2.0	2.0	1.7	1.2	0.5	1.7	1.7	1.4	1.6	1.3	1.1
SE	0.04	0.06	1.14	0.17	0.02	0.02	0.18	0.22	0.02	0.01	0.02	0.21	0.10	0.16
H4 K5,8, 12,16ac	BRD2 BD1		BRD2 BD2		BRD3 BD1		BRD3 BD2		BRD4 BD1		BRD4 BD2		BRDT BD1	
	WT	L/V	WT	L/V	WT	L/V	WT	L/V	WT	L/V	WT	L/V	WT	L/V
Kd ( $\mu\text{M}$ )	16	34	133	169	20	36	63	128	9	13	83	138	15	33
SE	1	1	7	12	1	3	6	7	1	1	3	10	1	4
$\Delta\text{H}$ (kcal/mol)	-11.9	-15.7	-6.3	-3.8	-9.1	-10.5	-9.3	-7.0	-9.7	-9.8	-8.3	-7.3	-14.8	-14.9
SE	0.1	0.2	0.4	0.3	0.1	0.3	0.9	1.0	1.8	0.1	0.2	0.4	0.4	1.0
N	1.1	1.2	1.1	1.5	2.3	2.0	0.9	1.0	1.8	1.6	0.9	1.1	1.3	1.1
SE	0.01	0.01	0.05	0.08	0.01	0.03	0.08	(FIX)	0.02	0.02	0.02	0.04	0.02	0.06

**Table S2 – Effect of L/V Mutation on BRD:Peptide Affinity**

Results of ITC titrations of di- and tetra-acetylated H4 peptides titrated into WT and L/V BET bromodomains.

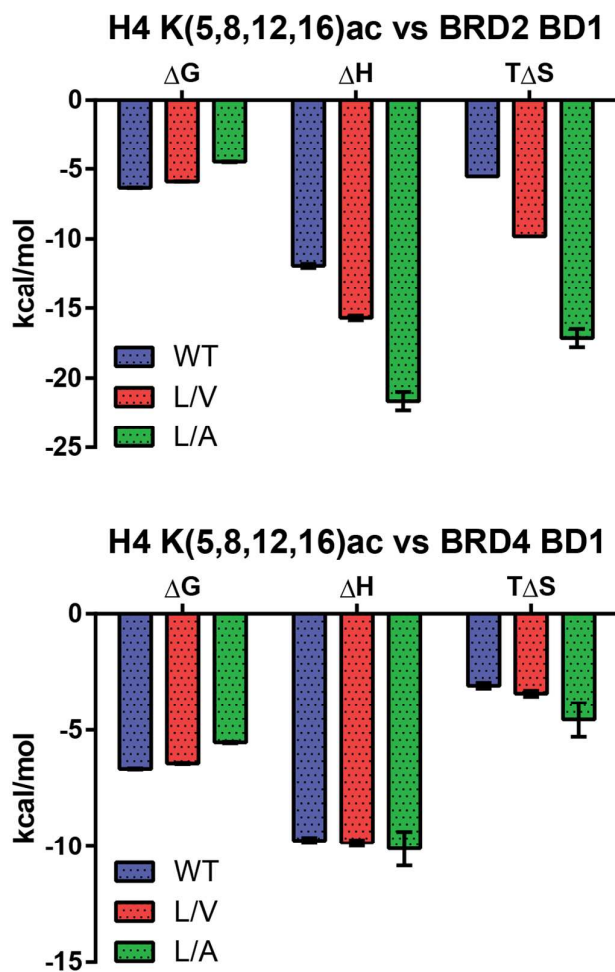


**Figure S2 – Effect of L/V Mutation on Binding Energies of BRD:Peptide Interactions**

Thermodynamic measurements of tetra-acetylated H4 peptide titrated into WT and mutant BET bromodomains.



Peptide	BRD2 BD1		BRD2 BD2		BRD3 BD1		BRD3 BD2		BRD4 BD1		BRD4 BD2		BRDT BD1		BRDT BD2	
	WT	L/V	WT	L/V	WT	L/V	WT	L/V	WT	L/V	WT	L/V	WT	L/V	WT	L/V
H4 1-21	0.62	0.21	0.07	-0.03	0.14	-0.01	0.08	0.04	0.05	0.03	0.00	0.19	-0.23	0.00	0.06	-0.04
H4 1-21 K5ac	0.53	0.21	0.18	0.06	0.23	0.10	0.23	0.21	0.14	0.18	0.16	0.29	-0.11	0.07	0.19	-0.03
H4 1-21 K8ac	0.44	0.17	0.15	0.03	0.17	0.08	0.21	0.12	0.10	0.19	0.11	0.22	-0.17	0.03	0.09	-0.04
H4 1-21 K12ac	0.56	0.23	0.23	0.06	0.26	0.14	0.26	0.20	0.21	0.37	0.20	0.27	-0.01	0.12	0.13	-0.02
H4 1-21 K16ac	0.26	0.08	0.02	-0.02	0.09	0.02	0.09	0.06	0.04	0.10	0.03	0.15	-0.17	0.01	0.02	-0.04
H4 1-21 K5acK8ac	2.70	1.40	0.54	0.16	3.77	2.18	0.54	0.31	2.74	2.12	0.38	0.53	1.00	0.59	0.26	0.11
H4 1-21 K5K9ac	0.46	0.25	0.37	0.04	0.40	0.23	0.51	0.32	0.33	0.55	0.37	0.32	0.09	0.15	0.07	0.02
H4 1-21 K5K16ac	0.16	0.11	0.16	0.06	0.16	0.12	0.24	0.18	0.12	0.32	0.17	0.18	-0.05	0.07	0.07	-0.01
H4 1-21 K8K12ac	0.49	0.28	0.37	0.07	0.49	0.34	0.33	0.24	0.42	0.68	0.33	0.28	0.13	0.18	0.10	-0.03
H4 1-21 K8K16ac	0.15	0.12	0.16	0.07	0.17	0.15	0.23	0.16	0.13	0.37	0.17	0.17	-0.05	0.07	0.11	0.00
H4 1-21 K12K16ac	0.52	0.29	0.29	0.09	0.66	0.43	0.32	0.20	0.59	0.82	0.26	0.24	0.17	0.17	0.08	0.03
H4 1-21 K5K8K12ac	3.38	2.01	1.10	0.33	3.93	2.60	0.89	0.42	3.12	2.72	0.65	0.64	1.43	0.86	0.31	0.17
H4 1-21 K8K12K16ac	1.06	0.75	0.62	0.18	1.26	0.90	0.53	0.29	1.22	1.33	0.38	0.37	0.51	0.43	0.18	0.08
H4 1-21 K5K12K16ac	0.79	0.51	0.56	0.18	0.99	0.66	0.57	0.38	0.81	1.20	0.43	0.35	0.38	0.30	0.15	0.05
H4 1-21 K5K8K16ac	2.51	1.54	0.69	0.21	3.65	2.28	0.62	0.31	2.88	2.37	0.35	0.49	1.10	0.62	0.20	0.14
H4 1-21 K5K8K12K16ac	3.31	2.12	1.12	0.29	4.34	2.86	0.80	0.36	3.11	3.05	0.55	0.56	1.61	0.95	0.26	0.23
H4 9-29	0.04	0.04	0.01	-0.02	0.07	0.04	0.01	0.06	0.03	0.05	0.02	0.04	-0.09	0.01	0.03	0.00
H4 9-29 K20ac	0.11	0.18	0.26	0.17	0.10	0.14	0.34	0.46	0.13	0.38	0.22	0.25	0.11	0.33	0.06	0.11
H4 9-29 K16ac	0.05	0.06	0.02	0.01	0.04	0.05	0.05	0.06	0.03	0.09	0.03	0.03	0.01	0.04	0.01	0.02
H4 9-29 K12K16ac	0.36	0.47	0.27	0.12	0.40	0.41	0.23	0.18	0.23	0.63	0.18	0.13	0.23	0.32	0.06	0.10
H4 9-29 K12K16K20ac	0.50	0.90	0.48	0.23	0.53	0.66	0.35	0.32	0.33	1.07	0.22	0.23	0.33	0.68	0.06	0.17
H2a 1-21	0.45	0.09	0.04	-0.02	0.09	0.03	0.01	0.08	0.03	0.07	0.02	0.21	-0.14	0.01	0.04	-0.03
H2a 1-21 K5ac	0.54	0.23	0.17	0.04	0.22	0.04	0.18	0.17	0.14	0.17	0.16	0.32	-0.12	0.06	0.11	-0.02
H2a 1-21 K9ac	0.50	0.20	0.20	0.03	0.22	0.03	0.16	0.12	0.11	0.13	0.13	0.25	-0.16	0.04	0.10	-0.03
H2a 1-21 K13ac	0.36	0.13	0.07	0.01	0.16	0.05	0.03	0.08	0.07	0.08	0.04	0.20	-0.12	0.04	0.09	-0.02
H2a 1-21 K15ac	0.33	0.10	0.07	0.00	0.15	0.04	0.04	0.07	0.06	0.07	0.04	0.17	-0.15	0.03	0.08	-0.03
H2a 1-21 K5K9ac	0.24	0.12	0.30	0.10	0.22	0.13	0.34	0.24	0.16	0.28	0.28	0.31	-0.07	0.08	0.12	0.01
H2a 1-21 K5K13ac	0.10	0.07	0.14	0.03	0.17	0.09	0.20	0.17	0.11	0.18	0.15	0.19	-0.11	0.05	0.08	0.00
H2a 1-21 K5K15ac	0.12	0.07	0.07	0.09	0.14	0.07	0.20	0.17	0.09	0.19	0.07	0.21	-0.10	0.05	0.07	-0.01
H2a 1-21 K9K13ac	0.18	0.09	0.17	0.04	0.22	0.11	0.21	0.07	0.13	0.24	0.18	0.17	-0.09	0.06	0.09	0.00
H2a 1-21 K9K15ac	0.16	0.12	0.29	0.09	0.22	0.14	0.29	0.18	0.16	0.29	0.27	0.21	-0.03	0.06	0.11	0.02
H2a 1-21 K13K15ac	0.10	0.04	0.04	-0.01	0.13	0.06	0.05	0.07	0.05	0.10	0.06	0.09	-0.12	0.03	0.04	-0.02
H2a 1-21 K5K9K13ac	0.02	0.05	0.00	0.03	0.01	0.06	0.10	0.04	0.01	0.05	0.05	0.03	0.07	0.05	0.03	0.07
H2a 1-21 K5K13K15ac	0.12	0.08	0.17	0.06	0.15	0.11	0.20	0.17	0.13	0.23	0.17	0.15	0.02	0.05	0.03	0.00
H2a 1-21 K9K13K15ac	0.20	0.13	0.30	0.08	0.30	0.11	0.19	0.12	0.18	0.31	0.21	0.13	-0.03	0.06	0.12	-0.01
H2a 1-21 K5K9K15ac	0.19	0.13	0.18	0.15	0.32	0.13	0.40	0.20	0.22	0.35	0.35	0.26	-0.02	0.08	0.11	-0.02
H2a 1-21 K5K9K13K15ac	0.30	0.23	0.51	0.15	0.35	0.28	0.40	0.23	0.29	0.49	0.35	0.23	0.14	0.12	0.12	0.05
H2b 1-21	0.02	0.00	0.00	0.00	0.08	0.02	-0.02	0.04	0.01	0.01	0.02	0.04	-0.14	0.02	0.04	-0.02
H2b 1-21 K5ac	0.01	0.02	0.06	0.07	0.06	0.05	-0.02	0.06	0.02	0.06	0.02	0.02	-0.03	0.03	0.06	0.01
H2b 1-21 K11ac	0.00	0.00	0.00	0.01	0.00	0.02	0.00	0.04	0.01	0.01	0.01	0.02	-0.04	0.02	0.02	-0.01
H2b 1-21 K12ac	0.01	0.02	0.00	0.00	0.02	0.04	0.03	0.06	0.02	0.05	0.03	0.02	-0.01	0.02	0.04	0.01
H2b 1-21 K15ac	0.01	0.04	0.00	0.01	0.03	0.06	0.05	0.06	0.02	0.08	0.02	0.03	0.00	0.04	0.04	0.01
H2b 1-21 K5K11K16ac	0.04	0.04	0.02	0.03	0.04	0.08	0.04	0.04	0.03	0.10	0.03	0.03	0.04	0.04	0.04	0.02
H2b 1-21 K5K12ac	0.02	0.01	0.00	0.02	0.00	0.03	0.02	0.03	0.01	0.02	0.02	0.02	0.00	0.03	0.01	0.00
H2b 1-21 K5K15ac	0.01	0.03	0.01	0.01	0.02	0.06	0.06	0.04	0.02	0.08	0.02	0.03	0.01	0.04	0.02	0.01
H2b 1-21 K5K16ac	0.02	0.03	0.01	0.02	0.04	0.05	0.03	0.03	0.02	0.09	0.02	0.02	0.03	0.03	0.06	0.01
H2b 1-21 K11K12ac	0.03	-0.02	0.06	0.01	0.03	-0.02	0.01	0.00	0.02	0.00	0.01	0.00	-0.02	0.00	0.00	-0.01
H2b 1-21 K11K15ac	0.04	0.03	0.11	0.05	0.07	0.02	0.04	0.01	0.03	0.07	0.02	0.01	0.00	0.02	0.01	0.00
H2b 1-21 K11K16ac	0.04	0.05	0.03	0.04	0.00	0.05	0.04	0.03	0.03	0.08	0.02	0.02	0.02	0.03	0.03	0.01
H2b 1-21 K5K11K12ac	0.03	0.01	0.05	0.03	0.03	0.04	0.04	0.03	0.02	0.05	0.02	0.02	0.01	0.01	0.03	0.01
H2b 1-21 K5K15K16ac	0.03	0.06	0.06	0.03	0.04	0.06	0.03	0.03	0.04	0.09	0.03	0.03	0.04	0.04	0.02	0.02
H2b 1-21 K5K15K16ac	0.26	0.12	0.17	0.03	0.50	0.20	0.06	0.03	0.17	0.17	0.03	0.03	0.13	0.06	0.04	0.03
H2b 1-21 K11K15K16ac	0.02	0.04	0.02	0.00	0.05	0.08	0.04	0.03	0.03	0.08	0.02	0.02	0.04	0.05	0.02	0.02
H2b 1-21 K12K15K16ac	0.47	0.17	0.20	0.04	1.02	0.30	0.07	0.02	0.45	0.34	0.05	0.03	0.30	0.10	0.03	0.02
H2b 1-21 K11K12K15ac	0.17	0.10	0.13	0.04	0.30	0.16	0.06	0.03	0.11	0.15	0.03	0.03	0.11	0.06	0.04	0.03
H2b 1-21 K11K12K16ac	0.04	0.04	0.01	0.02	0.06	0.07	0.05	0.04	0.04	0.07	0.02	0.03	0.05	0.04	0.02	0.02
H2b 1-21 K5K11K12K15K16ac	0.07	0.12	0.01	0.06	0.01	0.05	0.09	0.04	0.03	0.03	0.03	0.01	0.07	0.09	0.01	0.05
H2b 13-33	0.73	0.14	0.09	-0.02	0.18	0.06	0.02	0.11	0.05	0.08	0.02	0.25	-0.25	0.02	0.08	-0.04
H2b 13-33 K20ac	1.09	0.39	0.18	0.01	0.19	0.04	0.04	0.10	0.09	0.09	0.03	0.29	-0.28	0.03	0.12	-0.02
H2b 13-33 K23ac	0.88	0.35	0.14	-0.01	0.20	0.02	0.07	0.09	0.06	0.05	0.02	0.26	-0.27	0.02	0.10	-0.05
H2b 13-33 K24ac	0.83	0.26	0.11	0.00	0.14	0.06	0.02	0.10	0.07	0.10	0.02	0.26	-0.24	0.03	0.11	-0.03
H2b 13-33 K20K23K24ac	0.43	0.18	0.23	0.02	0.23	0.09	0.08	0.10	0.09	0.12	0.07	0.19	-0.21	0.05	0.10	-0.05
H3 1-21	0.09	0.02	0.01	0.01	0.08	0.03	-0.01	0.06	0.03	0.02	0.01	0.10	-0.10	0.02	0.04	-0.02
H3 1-21 K4ac	0.02	0.02	0.01	0.00	0.10	0.05	0.03	0.07	0.03	0.07	0.04	0.06	-0.13	0.03	0.04	-0.01
H3 1-21 K9ac	0.02	0.01	-0.01	0.00	0.07	0.05	0.03	0.06	0.02	0.04	0.02	0.05	-0.11	0.02	0.04	0.00
H3 1-21 K14ac	0.07	0.03	0.06	0.03	0.12	0.06	0.10	0.10	0.04	0.09	0.10	0.10	-0.09	0.03	0.05	0.00
H3 1-21 K4K9ac	0.04	0.05	0.05	0.02	0.07	0.09	0.06	0.09	0.06	0.13	0.06	0.06	0.00	0.05	0.06	0.02
H3 1-21 K4K14ac	0.07	0.04	0.08	0.03	0.10	0.07	0.10	0.12	0.05	0.12	0.11	0.08	-0.02	0.04	0.03	0.00
H3 1-21 K9K14ac	0.05	0.04	0.04	0.02	0.04	0.08	0.05	0.05	0.03	0.10	0.03	0.03	0.05	0.03	0.03	0.02
H3 1-21 K4K9K14ac	0.11	0.07	0.10	0.04	0.09	0.09	0.15	0.10	0.07	0.17	0.10	0.07	0.06	0.05	0.05	0.02
H3 11-31	0.01	-0.03	0.05	0.01	0.11	-0.01	-0.03	0.05	0.02	0.02	0.00	0.04	-0.17	-0.01	0.04	-0.03
H3 11-31 K14ac	0.03	-0.02	0.04	0.00	0.09	0.01	0.00	0.05	0.01	0.03	0.04	0.03	-0.07	-0.01	0.02	-0.03

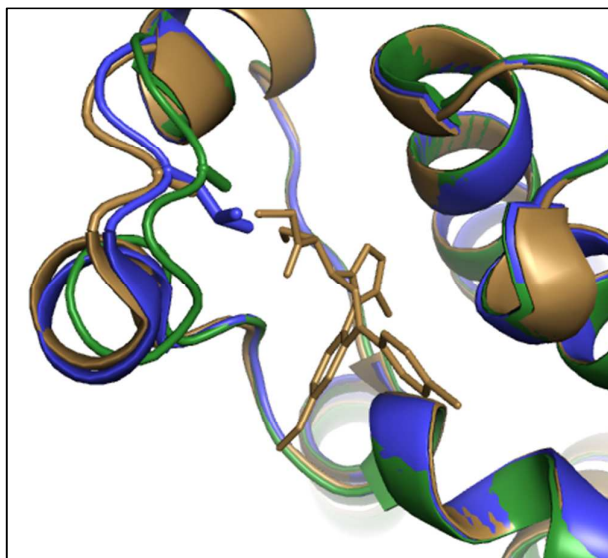


**Figure S4 – Crystallographic Analysis of ZA Loop during Binding**

Aligned X-ray crystal structures of BRD2 BD2 L/A apo (green) (4QEU) and bound to ET (brown) (4QEW), as well as BRD2 BD2 WT bound to an acetylated H4 peptide (blue) (2E3K). Bound peptide not shown. Mutated leucine/alanine side-chain highlighted.

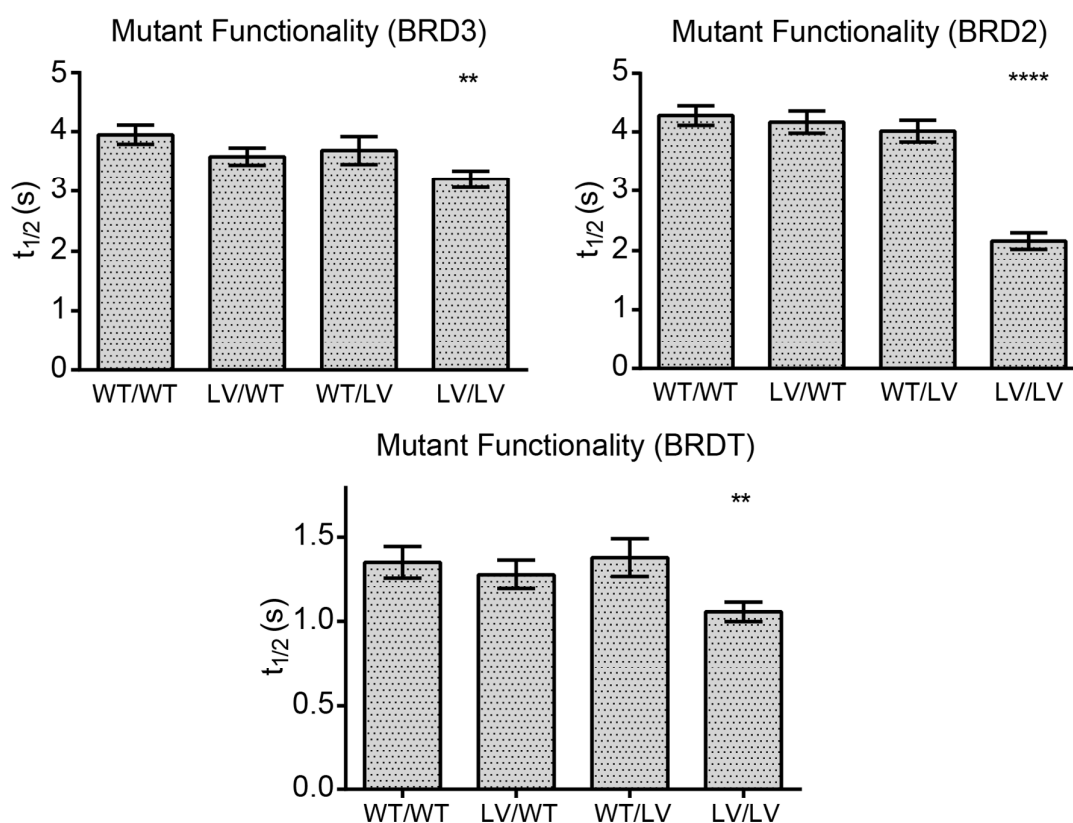


**Figure S5 – Effect of L/V Mutation on BET Protein Construct's FRAP Recovery Times**

Recovery times of GFP-labelled BET bromodomain constructs in FRAP assay, following 0.5s laser bleach event, at 2  $\mu$ M SAHA. Each bar is mean and SE of ~50 U2OS cells tested over two separate experiments.

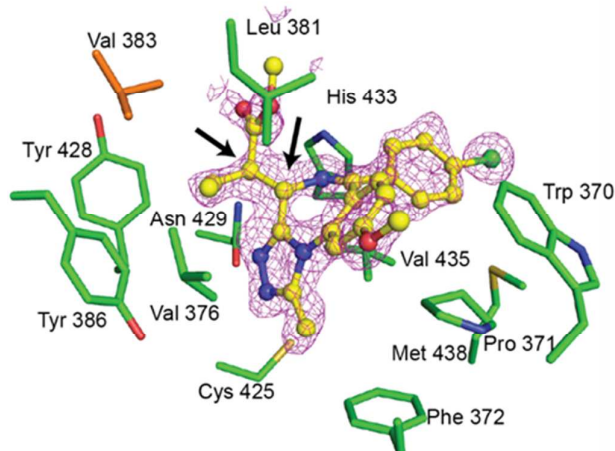
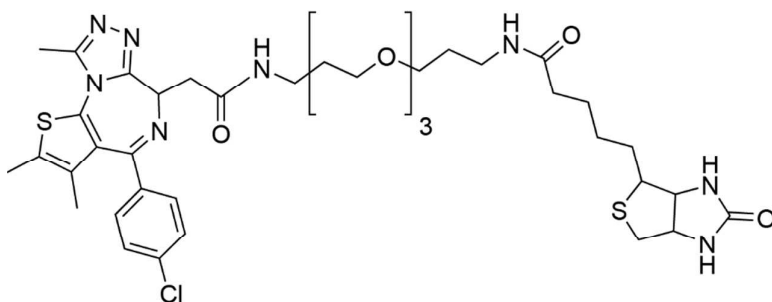


**Figure S6 – 2R,3S is the Potent Enantiomer that Binds to BET Bromodomains**

X-ray structure of BRD2 BD2 (L/V) (green, with mutant valine in orange) co-crystallised with (2R,3S)-8 (yellow). Fo-Fc ligand omit map (magenta mesh surface, contour: 2 sigma) shows clearly defined electron density around chiral centres of (2R,3S)-8 (marked with arrows).



	Positive	Negative
Mean	$1.7 \times 10^6$	$1.7 \times 10^4$
SD	$1.3 \times 10^5$	$2.1 \times 10^3$
S/N	102	
Z'	0.77	

**Figure S7 – Structure of Biotinylated-JQ1 and Associated Assay Robustness**

Structure of biotinylated JQ1. Z' calculated using BRD2 BD2 WT with 0 and 300  $\mu$ M JQ1 (positive and negative controls) (12 replicates).

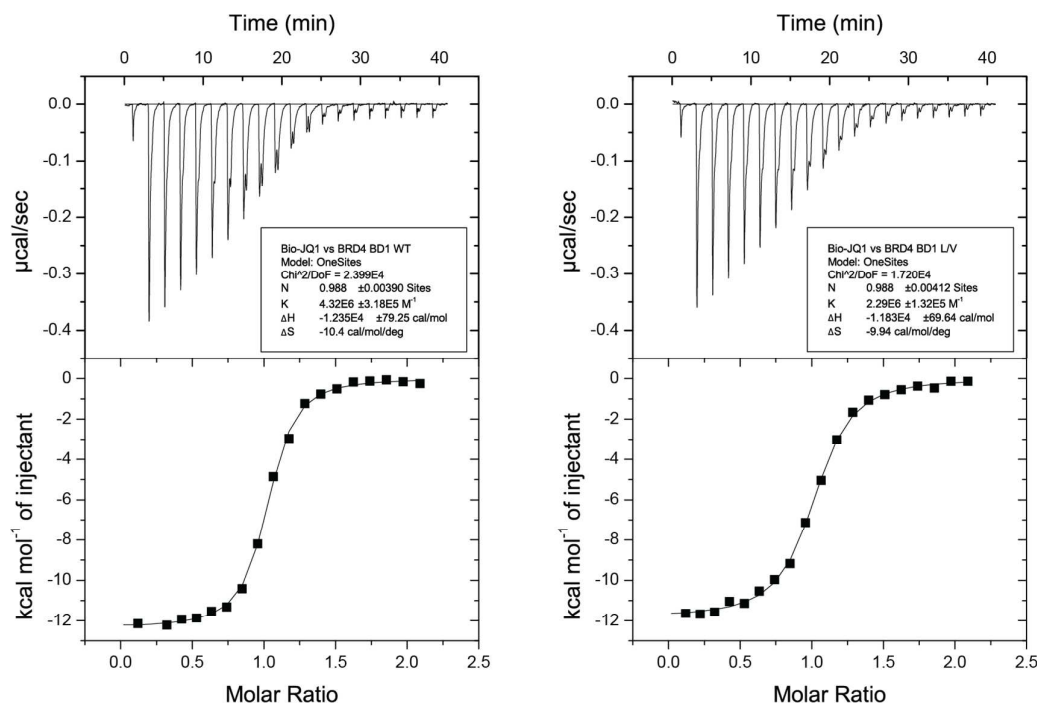


**Figure S8 – ITC Titrations of Biotinylated-JQ1**

ITC Titrations of biotinylated JQ1 into WT and LV BRD4 BD1.

Bio-JQ1	BRD2 BD1		BRD2 BD2		BRD3 BD1		BRD3 BD2		BRD4 BD1		BRD4 BD2		BRDT BD1		BRDT BD2	
	WT	L/V	WT	L/V	WT	L/V	WT	L/V	WT	L/V	WT	L/V	WT	L/V	WT	L/V
EC <sub>50</sub> (nM)	1.4	3.2	2.3	1.8	0.9	1.2	1.9	4.0	1.0	2.0	1.3	2.9	3.2	4.0	3.1	4.9
95% C.I.	1.0- 2.6	1.2- 2.1	1.6- 3.2	1.6- 2.2	0.6- 1.3	1.1- 1.4	1.7- 2.3	3.7- 4.4	0.7- 1.5	1.6- 2.6	0.8- 2.2	2.7- 3.8	2.7- 3.7	3.7- 4.4	2.4- 3.9	3.9- 6.1
LV/WT	2.3		0.8		1.3		2.1		2.0		2.2		1.3		1.6	

**Table S3 – AlphaLISA Titrations of Biotinylated-JQ1**

Results of dose-response curves of JPB titrated against 100 nM WT and L/V BET bromodomains. Data points after the 'hook' point excluded from analysis

Compound	AlphaLISA pIC <sub>50</sub> Value															
	BRD2 BD1		BRD2 BD2		BRD3 BD1		BRD3 BD2		BRD4 BD1		BRD4 BD2		BRDT BD1		BRDT BD2	
	WT	L/V	WT	L/V	WT	L/V	WT	L/V	WT	L/V	WT	L/V	WT	L/V	WT	L/V
(+)JQ1	6.4	6.5	6.5	6.5	6.8	6.6	6.5	6.4	6.6	6.5	6.5	6.4	6.6	6.0	6.3	6.1
(-)JQ1	4.8	4.8	4.8	4.4	5.0	5.0	4.6	4.4	4.9	4.6	4.7	4.5	4.7	4.6	4.6	4.6
I-BET	6.2	6.1	6.3	6.7	6.7	6.9	6.6	6.3	6.6	6.3	6.5	6.5	6.3	6.0	6.3	6.3
1	6.5	6.6	6.5	6.5	6.9	7.2	6.6	6.3	6.9	6.6	6.4	6.6	6.3	6.2	6.6	6.0
2	5.7	5.8	5.6	5.7	6.2	6.3	5.6	6.0	6.0	6.0	5.6	5.6	5.7	5.8	5.4	5.5
3	5.7	7.2	6.0	7.3	6.6	7.5	6.3	7.5	6.2	7.4	6.1	7.3	5.7	7.3	5.9	7.1
4	4.9	6.5	5.0	6.8	5.2	7.0	5.0	7.0	5.1	6.6	4.9	6.6	4.8	6.3	4.8	6.2
5	5.0	6.0	5.0	6.8	5.4	6.9	5.0	6.9	5.1	6.5	5.0	6.6	4.7	5.7	4.9	6.2
6	4.5	5.0	<4	5.0	4.7	5.2	4.7	5.0	4.6	5.1	4.2	4.9	4.5	4.6	4.9	6.2
7	5.5	6.7	5.1	6.5	5.8	7.0	5.3	7.0	5.5	6.7	5.2	6.7	5.3	6.6	5.1	6.2
8	5.0	6.5	5.4	6.7	5.6	6.9	5.4	7.1	5.8	6.9	5.5	6.7	4.8	6.2	5.4	6.4
9	4.3	5.4	4.4	5.9	4.5	5.8	4.3	6.0	4.4	5.5	4.2	5.5	4.2	5.2	4.3	5.3
16	4.9	6.4	5.3	6.6	5.7	7.0	5.4	7.1	5.4	6.6	5.3	6.6	4.9	6.2	5.1	6.4
17	4.2	5.5	4.6	5.9	4.5	6.3	4.4	6.1	4.3	5.7	4.2	5.7	4.2	4.9	4.1	5.3
18	4.3	5.6	4.3	6.0	4.5	6.1	4.3	5.9	4.4	5.9	4.2	5.7	4.1	5.3	4.1	5.3
19	4.9	6.0	4.6	6.0	5.3	6.4	4.9	6.3	4.9	5.9	4.6	5.9	4.4	5.4	4.6	5.5
20	4.5	5.7	4.8	5.8	4.7	6.3	4.6	5.8	4.6	5.9	4.5	5.5	4.4	5.2	4.4	5.2
21	4.4	5.7	4.8	6.0	5.3	6.3	4.8	6.3	4.6	6.0	4.5	5.9	4.3	5.6	4.6	5.8
22	<4	5.2	<4	5.1	4.2	5.5	<4	5.4	4.2	5.1	<4	4.9	<4	4.7	<4	4.7
23	5.3	5.8	5.3	6.0	5.6	6.4	5.3	6.1	5.3	6.1	5.2	5.8	5.2	5.6	5.2	5.6
24	5.3	5.9	5.1	6.3	5.4	6.5	5.2	6.1	5.3	6.2	5.4	6.0	5.1	5.7	5.0	5.8
25	4.4	5.0	4.7	4.9	4.7	5.3	4.6	5.0	4.8	5.1	4.6	4.7	4.6	4.9	4.4	4.9
26	5.1	5.6	5.2	5.8	5.5	5.9	5.3	5.9	5.2	5.8	5.0	5.5	5.0	5.4	5.0	5.6

Table S4- Results of AlphaLISA Assay Screen

Compound	AlphaLISA pIC <sub>50</sub>			Plasma t <sub>1/2</sub> (mins)	CL <sub>int</sub> (ml/min/g)	P <sub>e</sub> (nm/s)	ClogP	ITC pKd		
	WT	L/V	Δ					WT	L/V	Δ
(+) JQ1	6.6	6.5	-0.1	>180	7.5		4.8			
(-) JQ1	4.8	4.6	-0.2				4.8			
I-BET762	6.5	6.5	0.0	>180	1.3	25	2.8			
1	6.6	6.6	0.0	54	<0.5	149	3.3			
2	5.8	5.9	0.1	67	1.7		3.3			
3	6.2	7.4	1.2	>180	0.7	185	3.5			
4	5.0	6.8	1.7	>180	1.5	153	3.9	5.1	6.9	1.8
5	5.1	6.6	1.5	>180	6.7	127	3.9	5.1	6.6	1.5
6	4.5	5.0	0.6	>180	5.2		4.3			
7	5.4	6.8	1.4	>180	<0.5	158	3.5	4.5	6.6	2.0
8	5.5	6.8	1.4	>180	4.1	155	3.9	<4.2	6.4	>2.2
9	4.4	5.7	1.3	>180	9.4	136	3.9			
16	5.3	6.7	1.4	>180	1.2	26	3.1	5.6	6.9	1.3
17	4.4	5.9	1.5	>180	1.4	45	3.5	<4.2	6.0	>1.8
18	4.3	5.9	1.5	>180	2.6	52	3.5			
19	4.9	6.1	1.2	>180	>50		3.8			
20	4.6	5.8	1.2	>180	>50		4.1			
21	4.7	6.0	1.3	>180	1.5	40	3.1	4.5	6.3	1.8
22	<4.0	5.2		>180	2.1	59	3.5			
23	5.3	6.0	0.7	>180	30.7		4.8			
24	5.3	6.2	0.9	>180	39.7		4.9			
25	4.6	5.0	0.4	>180	31.0		4.8			
26	5.2	5.8	0.5	>180	39.4		4.9			



**Figure S9. Color-Coded SAR**

Data from table 1, with potency/selectivity data color-coded.

Compound	BRD2 BD1		BRD2 BD2		BRD3 BD1		BRD3 BD2		BRD4 BD1		BRD4 BD2		
	WT	L/V	WT	L/V	WT	L/V	WT	L/V	WT	L/V	WT	L/V	
4	$K_d$ (nM)	22000 ±9000	240 ±50	3300 ±1400	50 ±10	3300 ±1000	80 ±10	16000 ±8000	100 ±30	2500 ±1000	160 ±10	35000 ±10000	330 ±50
	$\Delta H$ (kcal/mol)	-5.3 ±0.9	-12.6 ±0.2	-1.2 ±0.1	-8.5 ±0.1	-4.9 ±0.4	-14.1 ±0.1	-3.8 ±1.4	-9.5 ±0.2	-2.6 ±0.2	-10.3 ±0.1	-3.4 ±0.5	-7.9 ±0.1
	N	1 (FIX)	0.96 ±0.01	0.91 ±0.07	0.85 ±0.01	0.81 ±0.05	0.94 ±0.00	0.85 ±0.20	0.94 ±0.01	0.99 ±0.06	0.87 ±0.00	1 (FIX)	0.82 ±0.01
5	$K_d$ (nM)	8400 ±3400	470 ±100	5800 ±600	240 ±60	1500 ±600	270 ±30	23000 ±8000	310 ±60	9700 ±1800	180 ±10	16000 ±9000	170 ±20
	$\Delta H$ (kcal/mol)	-4.0 ±0.7	-10.3 ±0.2	-2.3 ±0.1	-5.9 ±0.1	-2.3 ±0.2	-11.3 ±0.1	-3.7 ±0.6	-8.5 ±0.2	-3.5 ±0.3	-7.4 ±0.0	-2.2 ±0.8	-6.4 ±0.5
	N	1.0 ±0.10	0.87 ±0.01	0.75 ±0.02	1.16 ±0.01	0.85 ±0.05	0.84 ±0.01	1 (FIX)	0.78 ±0.01	1.10 ±0.05	0.88 ±0.00	0.98 ±0.20	0.89 ±0.01
16	$K_d$ (nM)	2200 ±900	120 ±20	2400 ±500	190 ±20	1600 ±300	60 ±10	1500 ±300	130 ±20	9400 ±1100	160 ±20	1700 ±300	80 ±10
	$\Delta H$ (kcal/mol)	-4.5 ±0.4	-16.3 ±0.2	-3.9 ±0.2	-9.9 ±0.1	-8.8 ±0.3	-19.0 ±0.2	-6.0 ±0.2	-12.9 ±0.2	-10.2 ±0.5	-9.5 ±0.1	-3.6 ±0.1	-8.6 ±0.1
	N	0.94 ±0.05	0.75 ±0.01	0.65 ±0.03	0.62 ±0.00	0.81 ±0.02	0.64 ±0.00	0.88 ±0.03	0.74 ±0.01	0.96 ±0.03	0.92 ±0.01	0.81 ±0.02	0.83 ±0.00
17	$K_d$ (nM)	>60000	960 ±180	>60000	1300 ±200	>60000	740 ±130	>60000	610 ±90	>60000	1600 ±300	>60000	1000 ±200
	$\Delta H$ (kcal/mol)		-10.2 ±0.3		-5.3 ±0.1		-9.4 ±0.2		-4.7 ±0.1		-5.9 ±0.2		-3.7 ±0.1
	N		0.97 ±0.02		0.94 ±0.01		1.07 ±0.02		0.68 ±0.01		0.99 ±0.02		0.99 ±0.02
21	$K_d$ (nM)	>60000	990 ±50	7400 ±600	230 ±50	7400 ±600	410 ±20	11000 ±3000	800 ±50	39000 ±6000	370 ±50	>60000	320 ±20
	$\Delta H$ (kcal/mol)		-8.8 ±0.1	-5.1 ±0.2	-4.8 ±0.1	-5.1 ±0.2	-10.7 ±0.1	-4.5 ±1.3	-6.7 ±0.1	-3.3 ±0.3	-5.9 ±0.1		-4.4 ±0.0
	N		0.97 ±0.01	0.86 ±0.02	0.84 ±0.03	0.86 ±0.02	0.92 ±0.00	0.46 ±0.10	0.90 ±0.01	1 (FIX)	0.88 ±0.01		1.06 ±0.01

**Table S5 – Results of ITC Profiling**

Results of ITC titrations of compound titrated into BET bromodomains. For very weak interactions N value fixed to 1.0.

7								8							
L/V	2.1	2.2	3.1	3.2	4.1	4.2		L/V	2.1	2.2	3.1	3.2	4.1	4.2	
WT	Kd (nM)	310	330	140	230	140	980	WT	Kd (nM)	340	300	270	410	530	740
2.1	32000	100	100	230	140	230	30	2.1	>60000	>180	>200	>230	>150	>110	>80
2.2	>60000	>190	>180	>430	>260	>430	>60	2.2	>60000	>180	>200	>230	>150	>100	>80
3.1	12000	40	40	90	50	90	10	3.1	29000	90	100	110	70	60	40
3.2	34000	110	100	240	150	240	40	3.2	>60000	>180	>200	>230	>150	>110	>80
4.1	28000	90	90	200	120	200	30	4.1	>60000	>180	>200	>230	>150	>100	>80
4.2	33000	110	100	240	140	240	30	4.2	>60000	>180	>200	>230	>150	>100	>80

**Table S6. Selectivity Plots of 9-ME & 9-ET**

Results are means of three consistent ITC titrations of ligand into WT and L/V BET bromodomains. For some weak interactions N was fixed to 1

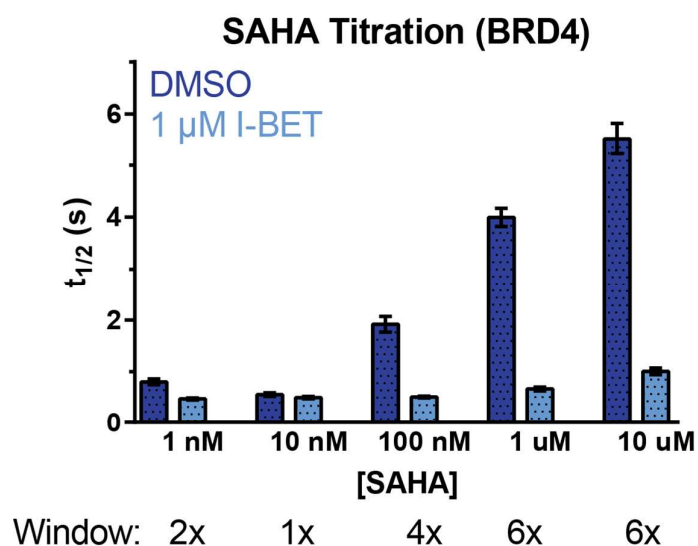


**Figure S10 – Effects of SAHA treatment on FRAP assay window.**

Recovery times of GFP-labelled BRD4 WT/WT in FRAP assay, following 0.5s laser bleach event, at a range of SAHA concentrations. Each bar is mean and SE of ~30 U2OS cells.



BRD4 BD1	7		(2R,3S)-7		(2S,3R)-7		8		(2R,3S)-8		(2S,3R)-8	
	WT	L/V	WT	L/V	WT	L/V	WT	L/V	WT	L/V	WT	L/V
pIC <sub>50</sub>	4.9	6.2	5.1	6.8	4.2	5.6	4.3	5.7	4.1	5.9	4.6	5.0
SE	0.07	0.04	0.03	0.07	0.07	0.05	0.08	0.06	0.11	0.06	0.18	0.12
ΔpIC <sub>50</sub>	1.4		1.7		1.4		1.4		1.8		0.4	

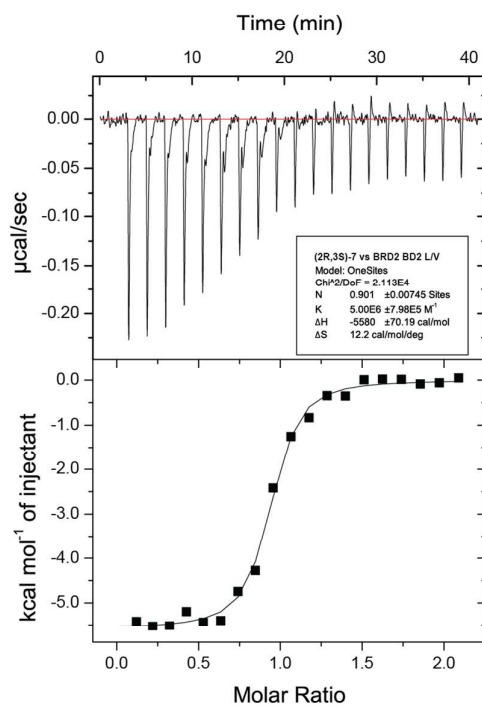
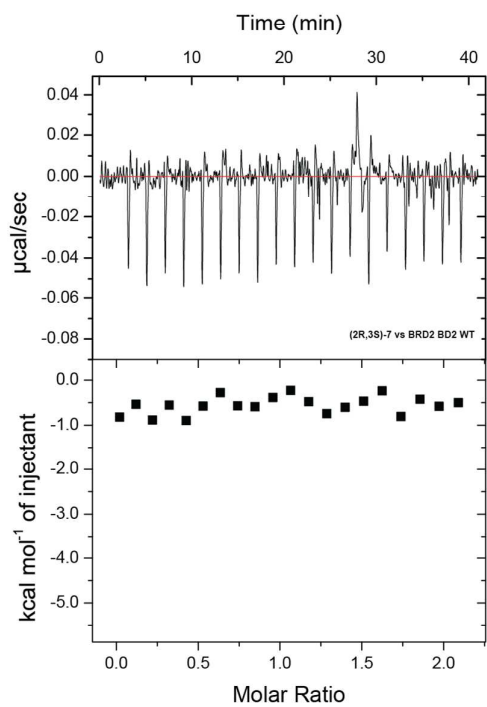
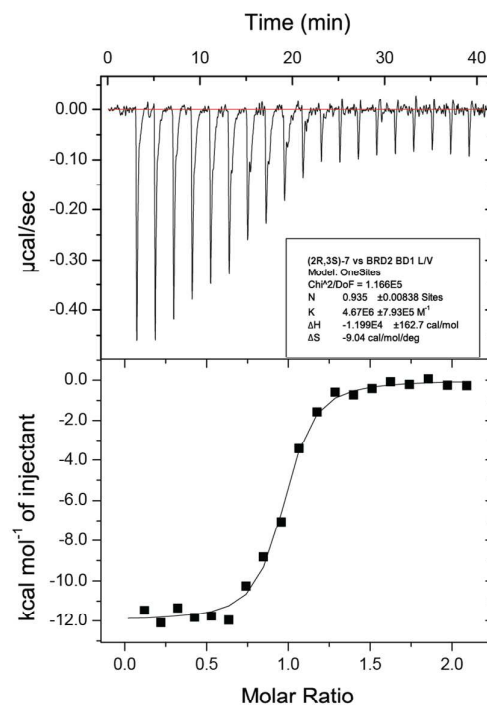
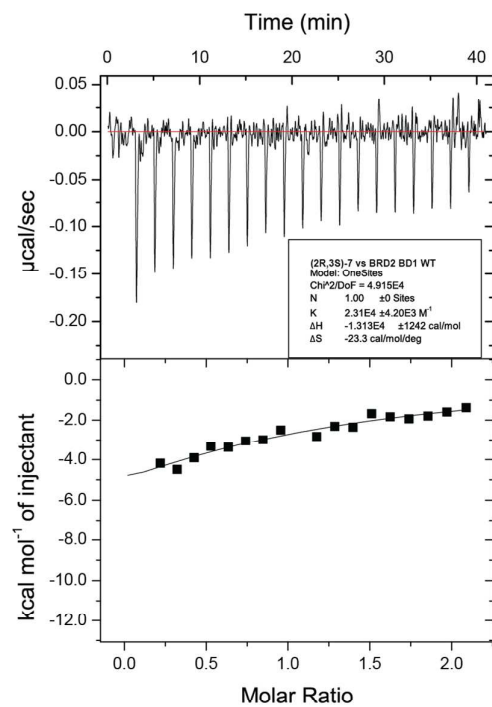
**Table S7 – AlphaLISA Testing of Separated Enantiomers**

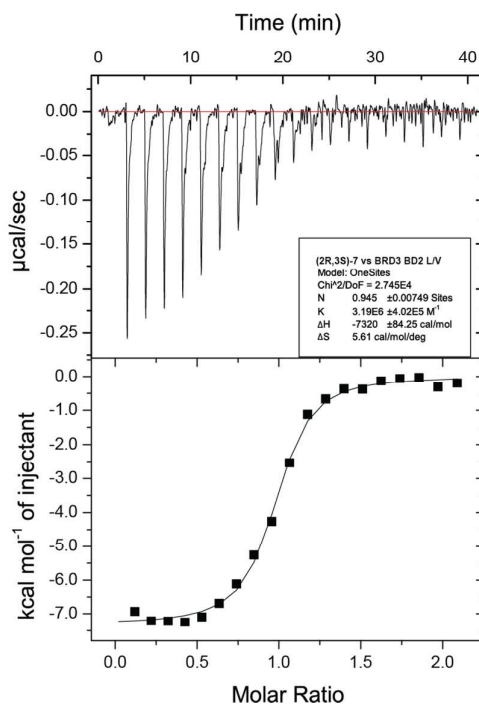
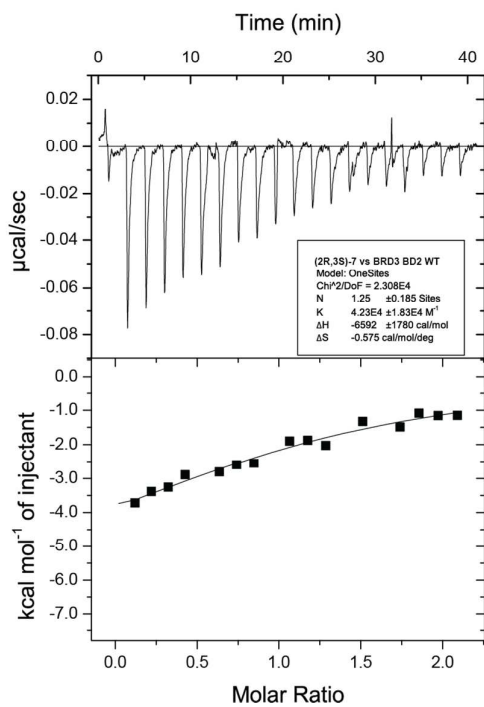
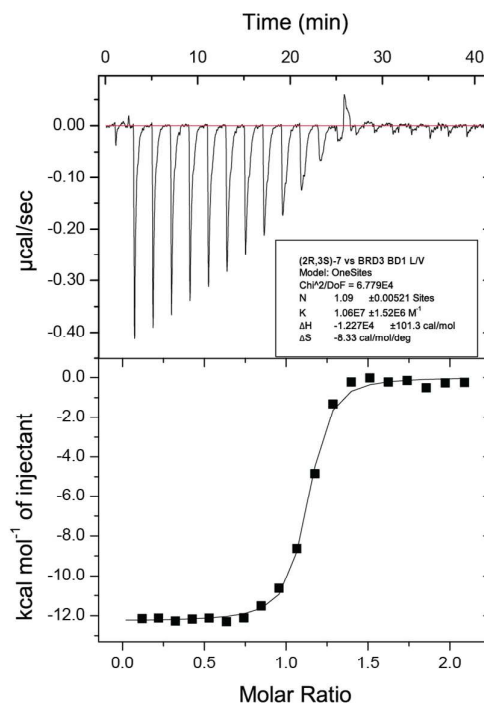
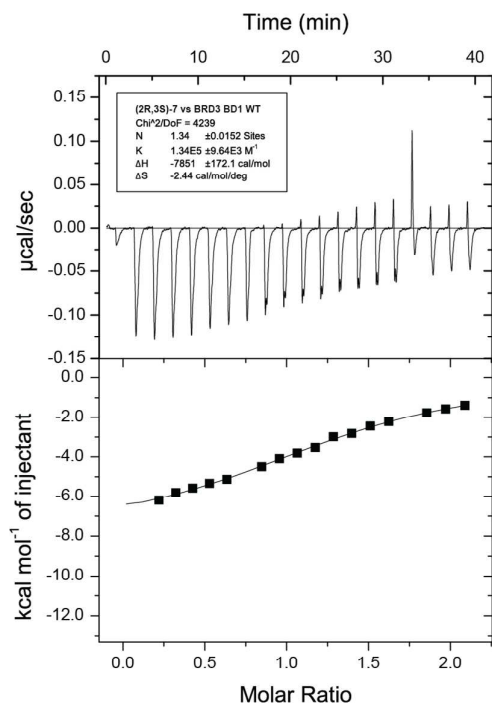
Results of titrations of 7 and 8 enantiomers and racemic mixtures against WT and L/V BRD4 BD1 in competitive AlphaLISA assay. Values refer to total compound concentration.

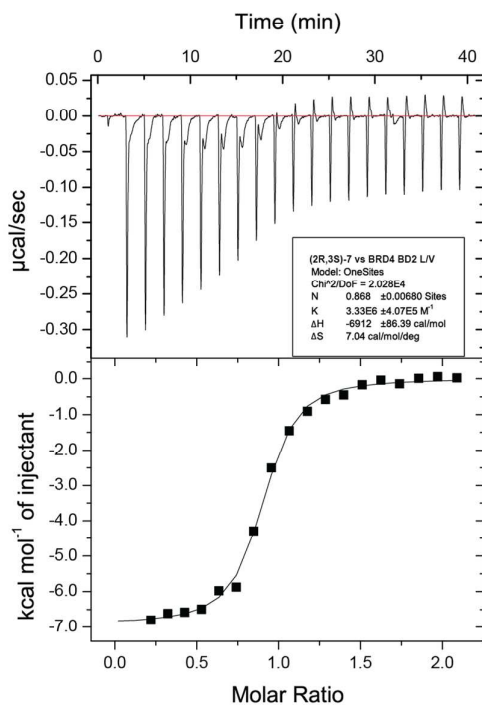
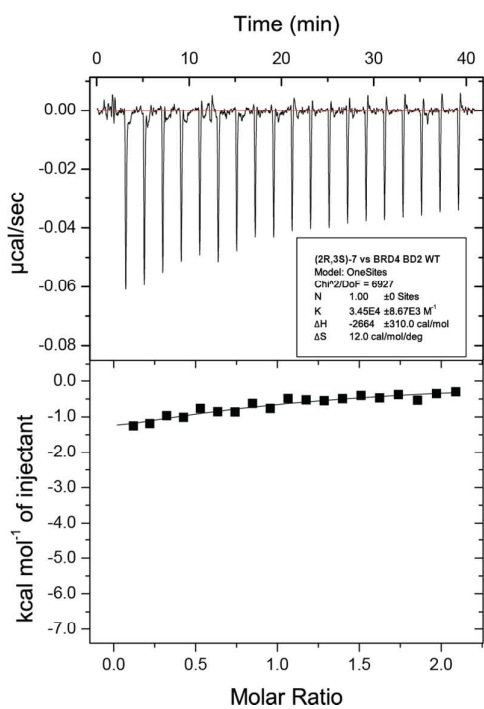
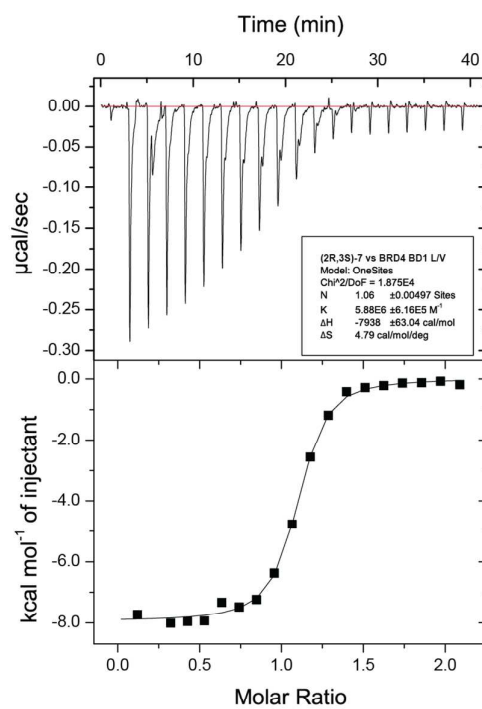
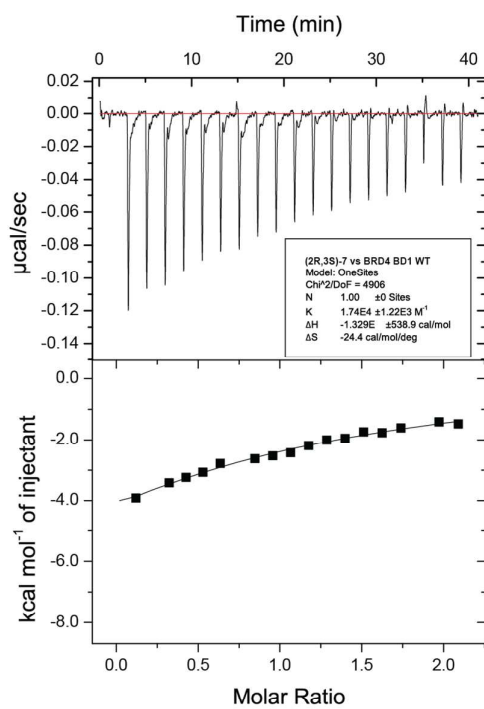
BRD4 BD1	(2R,3S)-7		(2S,3R)-7		7
	WT	L/V	WT	L/V	L/V
Kd (nM)	58000 ±4000	170 ±20	>60 000	>60 000	500 ±50
ΔH (kcal/mol)	-13.3 ±0.5	-7.9 ±0.1			-4.2 ±0.0
N	1 (FIX)	1.06 ±0.01			1.68 ±0.01
BRD4 BD1	(2R,3S)-8		(2S,3R)-8		8
	WT	L/V	WT	L/V	L/V
Kd (nM)	>60 000	440 ±50	>60 000	>60 000	840 ±170
ΔH (kcal/mol)		-6.5 ±0.1			-3.5 ±0.1
N		0.85 ±0.01			1.42 ±0.02

**Table S8 – ITC Testing of Separated Enantiomers**

7 and 8 enantiomers and racemic mixtures titrated against WT and L/V BRD4 BD1 in ITC. Values refer to total compound concentration. For some weak interactions N was fixed to 1.0.







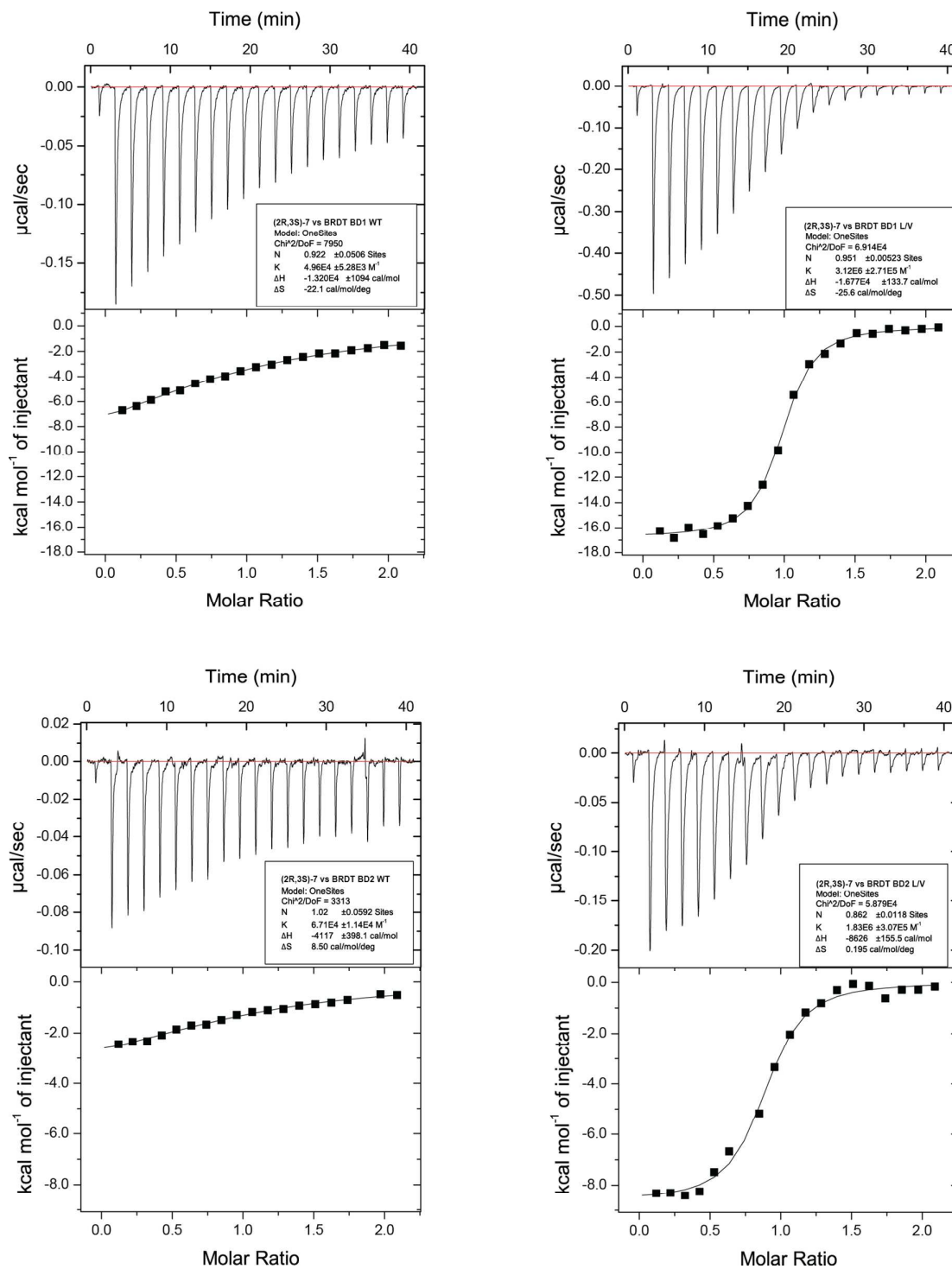


**Figure S11. 9-ME-1 ITC Profile**

Titration of 9-ME-1 (7a) into WT and L/V BET bromodomains. For some weak interactions N value fixed to 1.0.

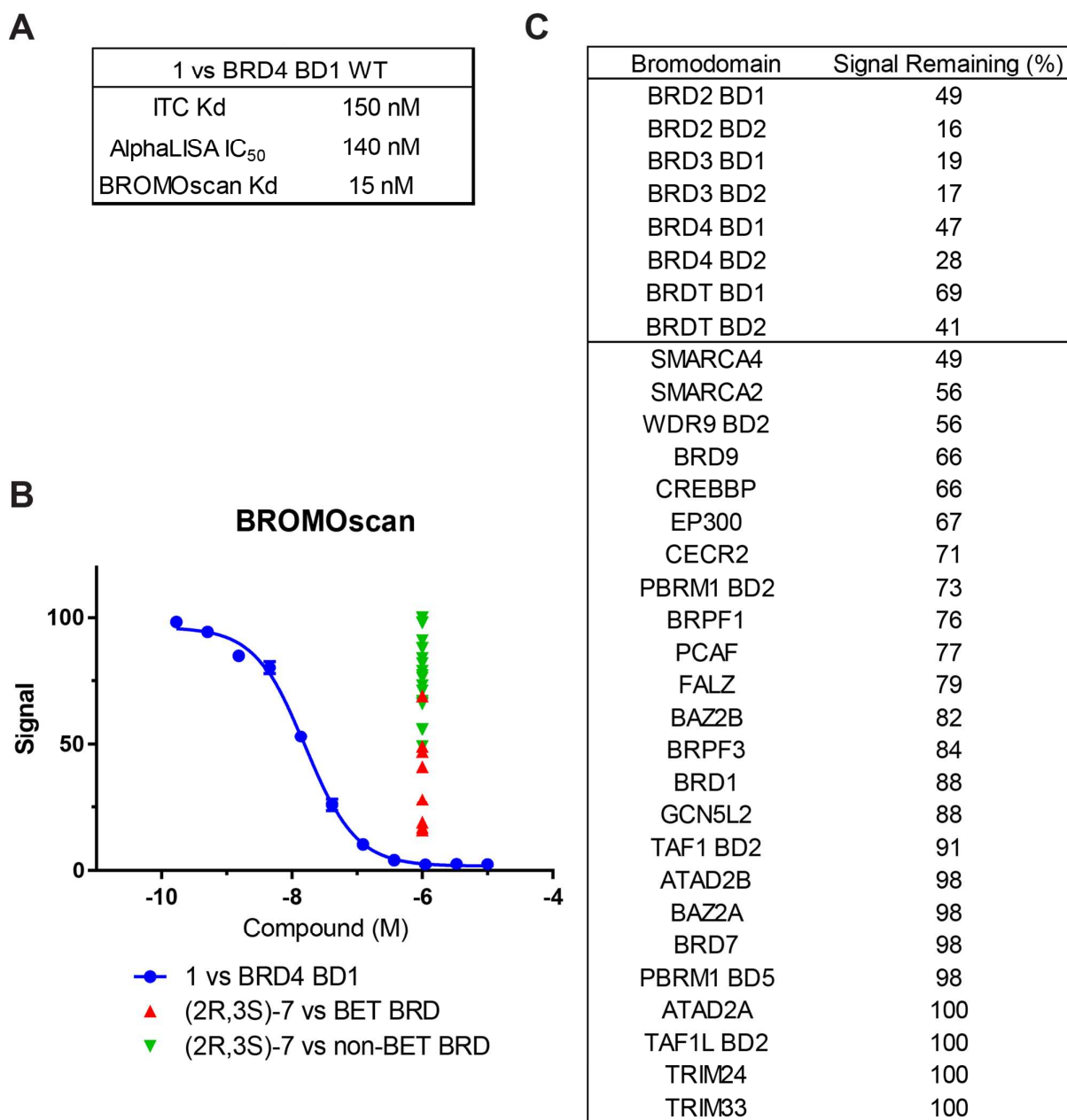


**Figure S12. BROMOscan Screen.**

A) Binding constants for **1** binding to BRD4 BD1 WT. B) BROMOscan titration of **1** against BRD4 BD1 WT, overlaid with results of C. C) BROMOscan signal generated by panel of human bromodomains following treatment with 1  $\mu$ M **(2R, 3S)-7**. **1** tested through bromoKdELECT (DiscoverRX) and **(2R, 3S)-7** tested in bromoMAX (DiscoverRX).

<https://www.discoverx.com/services/drug-discovery-development-services/epigenetic-profiling/bromoscan>

Kinase	Remaining activity	
	(%)	S.D.
MST2	118	14
IRAK4	114	10
HER4	114	9
SmMLCK	112	1
NEK6	109	12
TAK1	108	1
CHK2	107	8
PIM1	106	10
PAK4	104	11
AMPK (hum)	104	3
SGK1	103	5
RIPK2	103	20
TTK	102	6
p38a MAPK	101	6
CAMKKb	101	1
PRK2	100	1
MLK3	100	4
HIPK2	99	1
RSK1	99	2
TrkA	98	0
SYK	98	13
TBK1	98	2
EF2K	97	6
CK2	97	0
PDK1	97	5
PKCa	96	5
BTK	96	4
JAK3	95	7
GSK3b	95	10
PKBa	95	9
MSK1	94	1

CAMK1	94	5
MARK3	94	1
Aurora B	94	16
IGF-1R	93	2
CK1 $\delta$	93	11
S6K1	93	4
PKA	92	12
LKB1	91	9
JNK1	89	16
VEG-FR	89	13
MKK1	89	2
PLK1	89	3
ROCK 2	88	3
EPH-A2	86	15
Lck	86	4
Src	82	4
DYRK1A	80	8
SRPK1	79	6
PKD1	78	4

**Table S9. 9-ME-1 Kinase Screen**

Activity of panel of human kinases following treatment with 1  $\mu$ M (**2R**, **3S**)-7. Dundee MRC-PPU Express Screen (<http://www.kinase-screen.mrc.ac.uk/services/express-screen>)



Receptor	Reference Compound	Mean % of control specific binding ( $\pm$ SD)
Y1 (h)	NPY	122 (16)
mu (MOP) (h)	DAMGO	119 (3)
H2 (h)	cimetidine	117 (28)
D1 (h)	SCH 23390	116 (6)
5-HT6 (h)	serotonin	112 (4)
Y2 (h)	NPY	110 (13)
GABA (non-selective)	GABA	110 (1)
5-HT2B (h)	( $\pm$ )DOI	109 (0)
5-HT5a (h)	serotonin	109 (6)
sst (non-selective)	somatostatin-14	108 (6)
Ca <sup>2+</sup> channel (L, verapamil site)	D 600	108 (6)
H1 (h)	pyrilamine	108 (3)
NTS1 (NT1) (h)	neurotensin	106 (3)
5-HT7 (h)	serotonin	106 (6)
beta 2 (h)	ICI 118551	105 (4)
Na <sup>+</sup> channel (site 2)	veratridine	105 (6)
BZD (central)	diazepam	105 (10)
M2 (h)	methoctramine	105 (0)
M1 (h)	pirenzepine	104 (13)
5-HT1A (h)	8-OH-DPAT	104 (1)
SKCa channel	apamin	103 (10)
CCR1 (h)	MIP-1alpha	102 (4)
V1a (h)	[d(CH <sub>2</sub> ) <sup>5</sup> 1,Tyr(Me) <sup>2</sup> ]-AVP	102 (3)
NK2 (h)	[Nleu <sup>10</sup> ]-NKA (4-10)	101 (4)
M3 (h)	4-DAMP	101 (2)
A1 (h)	DPCPX	100 (0)
delta (DOP) (h)	DPDPE	100 (4)
5-HT2A (h)	ketanserin	100 (3)
KV channel	alpha -dendrotoxin	100 (0)
NK3 (h)	SB 222200	99 (7)
A2A (h)	NECA	99 (5)
AT1 (h)	saralasin	99 (0)

alpha 1 (non-selective)	prazosin	99 (12)
B2 (h)	NPC 567	98 (1)
5-HT1B	serotonin	98 (9)
Cl- channel (GABA-gated)	picROTOXININ	98 (4)
VPAC1 (VIP1) (h)	VIP	98 (13)
alpha 2 (non-selective)	yohimbine	98 (0)
CXCR2 (IL-8B) (h)	IL-8	96 (10)
5-HT3 (h)	MDL 72222	96 (1)
kappa (KOP)	U 50488	96 (9)
GAL2 (h)	galanin	96 (1)
5-HT transporter (h)	imipramine	96 (2)
D2S (h)	(+)butaclamol	95 (3)
beta 1 (h)	atenolol	95 (8)
NOP (ORL1) (h)	nociceptin	94 (4)
EP4 (h)	PGE2	93 (2)
A3 (h)	IB-MECA	91 (7)
CB1 (h)	CP 55940	90 (4)
CCK1 (CCKA) (h)	CCK-8s	90 (15)
MC4 (h)	NDP-alpha -MSH	89 (15)
norepinephrine transporter (h)	protriptyline	88 (4)
ETA (h)	endothelin-1	87 (3)
dopamine transporter (h)	BTCP	84 (1)
MT1 (ML1A) (h)	melatonin	23 (2)

**Table S10. Receptor & Ion-Channel Screening**

Activity of panel of receptors and ion channels following treatment with 1  $\mu$ M (**2R, 3S**)-7. CEREP ExpresSProfile panel [http://www.cerep.fr/cerep/utilisateurs/pages/downloads/Documents/Marketing/Pharmacology%20&%20ADME/Standard%20profiles/ExpresSProfile\\_2014v2LD.pdf](http://www.cerep.fr/cerep/utilisateurs/pages/downloads/Documents/Marketing/Pharmacology%20&%20ADME/Standard%20profiles/ExpresSProfile_2014v2LD.pdf)

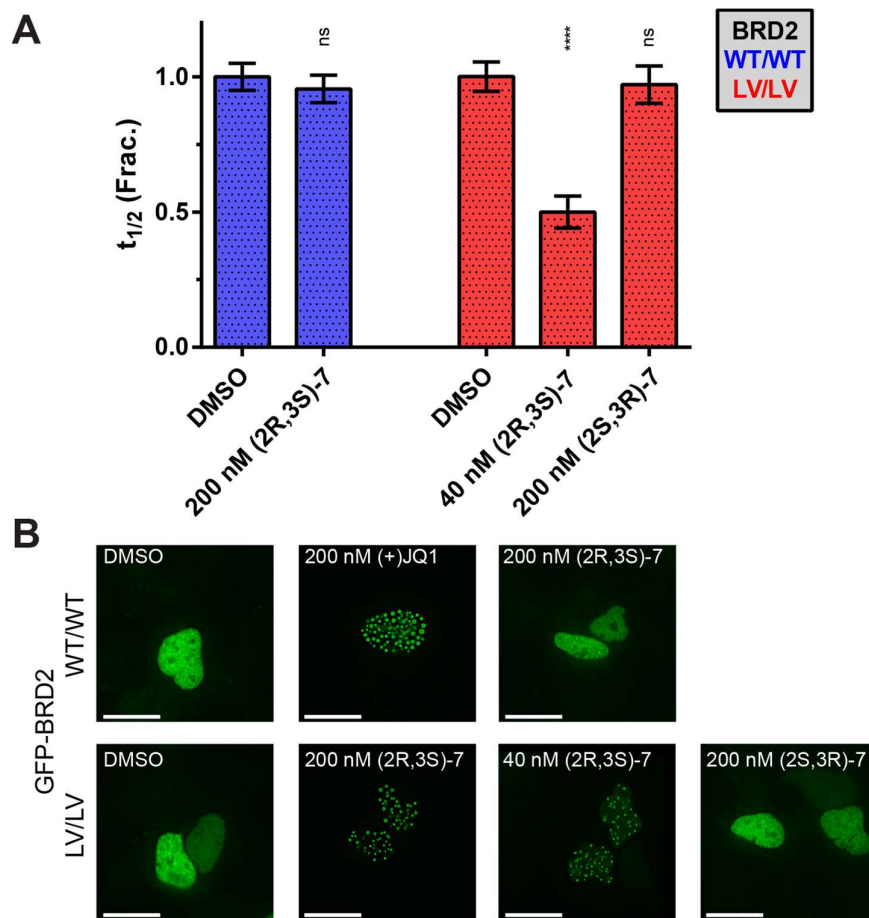


**Figure S13 – GFP-BRD2 Aggregates upon Inhibition**

A) Recovery times of GFP-labelled BRD2 constructs in FRAP assay, following 0.5s laser bleach event, at 2 μM SAHA and 0.03% DMSO. Each bar is mean and SE of ~30 U2OS cells. BRD2 LV/LV + 40 nM (2R, 3S)-7 showed some aggregation but recovery time could still be determined.

B) Nuclei of transfected U2OS cells, treated with 2 μM SAHA, 0.03% DMSO and test compound. Scale bar = 20 μm.

**X-Ray Crystallography: Data Collection & Refinement Statistics**

Structure	Apo	3	4	5	7	8
PDB code	5O38	5O39	5O3A	5O3B	5O3C	5O3D
Data Collection						
Space group	P 21 21 2	P 21 21 2	I 41 2 2	I 222	P 2 21 21	P 21 21 2
Cell dimensions						
a, b, c (Å)	52.420, 71.409, 31.969	52.406 72.129 31.990	126.799, 126.799, 43.194	88.075 101.893 123.534	31.852 52.082 71.789	52.407 71.83 32.003
$\alpha, \beta, \gamma$ (°)	90, 90, 90	90, 90, 90	90, 90, 90	90, 90, 90	90, 90, 90	90, 90, 90
Resolution (Å)	19.50 - 1.20 (1.243 - 1.20)	21.77-1.74 (1.802-1.74)	40.10 - 2.40 (2.486 - 2.40)	44.04 - 1.95 (2.02 - 1.95)	31.85 - 1.60 (1.657 - 1.60)	32.00 - 1.60 (1.657 - 1.60)
<i>R</i> merge	0.05918 (0.06509)	0.04883 (0.05565)	0.09961 (0.3312)	0.2827 (0.9697)	0.1111 (0.5627)	0.05236 (0.07519)
<i>I</i> /sigma( <i>I</i> )	17.14 (14.31)	43.16 (37.50)	17.11 (5.14)	10.53 (2.26)	7.67 (2.04)	32.70 (18.62)
<i>CC</i> <sub>1/2</sub>	0.997 (0.998)	1 (0.999)	0.999 (0.984)	0.984 (0.535)	0.992 (0.755)	0.999 (0.994)
Completeness (%)	98.26 (93.37)	97.12 (79.28)	99.18 (100.00)	99.92 (99.98)	99.51 (99.56)	98.83 (94.76)
Redundancy	5.7 (5.7)	17.1 (15.3)	15.3 (14.6)	8.6 (7.8)	4.3 (4.2)	10.3 (7.2)
<b>Refinement</b>						
Resolution (Å)	19.50 - 1.20 (1.243 - 1.20)	21.77-1.74 (1.802-1.74)	40.10 - 2.40 (2.486 - 2.40)	44.04 - 1.95 (2.02 - 1.95)	31.85 - 1.60 (1.657 - 1.60)	32.00 - 1.60 (1.657 - 1.60)
No. reflections	122513 (5072)	123746 (4452)	109065 (10146)	349867 (31395)	69717 (6561)	168336 (11018)
Unique no. of reflections	37657 (894)	12633 (291)	7114 (696)	40791 (4007)	16285 (1575)	16364 (1536)
<i>R</i> work	0.1178 (0.1068)	0.1443 (0.1466)	0.2055 (0.3278)	0.1972 (0.2710)	0.1615 (0.2197)	0.1483 (0.1324)
<i>R</i> free	0.1413 (0.1365)	0.1897 (0.2237)	0.2547 (0.3512)	0.2442 (0.3180)	0.1945 (0.2670)	0.1711 (0.1608)
No. atoms						
Protein	991	922	893	3613	918	948
Ligand/ion	31	40	31	128	40	41
Water	237	203	57	559	212	219
<i>B</i> factors						
Average	13.3	12.9	43.2	19.3	16.7	11.8

Protein	10.1	10.4	43.3	18.4	14.3	8.9
Ligand/ion	16.9	11.0	37.9	15.4	15.8	15.4
Water	26.0	24.9	44.4	25.9	27.6	24.0
R.m.s. deviations						
Bond lengths (Å)	0.005	0.007	0.011	0.009	0.007	0.009
Bond angles (°)	1.03	1.05	1.19	1.04	1.08	1.06

<b>Structure</b>	<b>16</b>	<b>17</b>	<b>18</b>	<b>21</b>	<b>24</b>
<b>PDB Code</b>	<b>5O3E</b>	<b>5O3F</b>	<b>5O3G</b>	<b>5O3H</b>	<b>5O3I</b>
<b>Data Collection</b>					
Space group	P 21 21 2	P 21 21 2	P 21 21 2	P 21 21 2	P 21 21 2
Cell dimensions					
<i>a, b, c</i> (Å)	52.177, 71.95, 31.917	51.965 71.548 31.704	73.74, 52.66, 63.12	52.143, 71.837, 31.97	53.12, 72.829, 32.359
$\alpha, \beta, \gamma$ (°)	90, 90, 90	90, 90, 90	90, 90, 90	90, 90, 90	90, 90, 90
Resolution (Å)	35.98 - 1.40 (1.45 - 1.40)	42.05 - 1.75 (1.813 - 1.75)	25.41 - 1.85 (1.916 - 1.85)	35.92 - 1.40 (1.45 - 1.40)	14.31 - 1.20 (1.243 - 1.20)
<i>R</i> <sub>merge</sub>	0.1005 (0.2228)	0.1116 (0.1436)	0.07581 (0.3878)	0.06188 (0.1025)	0.1049 (0.5239)
<i>I</i> / $\sigma$ ( <i>I</i> )	15.07 (4.57)	7.72 (6.60)	9.64 (3.00)	21.35 (7.92)	9.10 (3.25)
<i>CC</i> <sub>1/2</sub>	0.998 (0.955)	0.992 (0.99)	0.997 (0.776)	0.999 (0.982)	0.994 (0.781)
Completeness (%)	99.77 (97.92)	99.66 (99.92)	95.19 (95.67)	98.72 (93.14)	99.19 (99.29)
Redundancy	9.6 (4.8)	3.9 (4.0)	3.9 (3.9)	7.5 (3.7)	5.8 (5.8)
<b>Refinement</b>					
Resolution (Å)	35.98 - 1.40 (1.45 - 1.40)	42.05 - 1.75 (1.813 - 1.75)	25.41 - 1.85 (1.916 - 1.85)	35.92 - 1.40 (1.45 - 1.40)	14.31 - 1.20 (1.243 - 1.20)
No. reflections	232876 (11299)	27589 (1075)	79692 (7845)	180745 (8305)	229769 (22505)
Unique no. of reflections	24337 (2352)	12439 (269)	20578 (2034)	24057 (2228)	39710 (3911)
<i>R</i> <sub>work</sub>	0.1315 (0.1401)	0.1721 (0.2604)	0.1888 (0.2460)	0.1477 (0.1678)	0.1557 (0.2044)
<i>R</i> <sub>free</sub>	0.1653 (0.1794)	0.2018 (0.2902)	0.2356 (0.2788)	0.1636 (0.1633)	0.1784 (0.2326)
No. atoms					
Protein	931	909	1818	932	939
Ligand/ion	41	42	66	41	45
Water	218	185	196	229	218
<i>B</i> factors					
<i>Average</i>	12.7	14.3	26.5	14.3	14.2
Protein	9.7	12.2	25.9	11.1	11.2
Ligand/ion	11.5	14.8	26.3	13.6	18.1
Water	26.0	24.7	32.0	27.5	26.2

R.m.s. deviations					
Bond lengths (Å)	0.006	0.006	0.014	0.011	0.019
Bond angles (°)	1.68	1.01	1.52	1.15	1.75

## **Materials & Methods**

### **1 – Cloning & Mutagenesis**

Plasmids pNIC28-Bsa4 KanR containing the 8 single BET bromodomain constructs BRD2 BD1 (protein start and stop positions K71-K176), BRD2 BD2 G344-D455, BRD3 BD1 P24-E144, BRD3 BD2 G306- P416, BRD4 BD1 N44-E168, BRD4 BD2 K333-E460, BRDT BD1 N21-E137 and BRDT BD2 S257-M361 were provided by the Oxford Structural Genomics Consortium (SGC) for expression with an N-terminal His6-tag and a TEV protease cleavage site (UniProt accession number, BRD2: P25440; BRD3: Q15059; BRD4: O60885). For tandem construct of BRD2, cDNA encoding both bromodomains and the linker region (G73-D455) was cloned from full-length cDNA clone purchased from DNASU Plasmid Repository at the Arizona State University into a pCri (11b) vector (based on pET15b, AmpR) for expression with an N-terminal His6-tag, a Small Ubiquitin-like Modifier (SUMO) tag, and a SUMO protease (SEN1) cleavage site. Plasmid pcDNA5-FRT/TO-GFP and cDNA clones for full length BRD2, BRD3 and BRD4 were gifts from Dr Mark Peggie from University of Dundee. Full-length cDNA of human BRD2 (M1-G801), BRD3 (M1-E726) and BRD4 (M1-F1362) were cloned into pcDNA5-FRT/TO-GFP to generate constructs for expressing corresponding protein in mammalian cell line. GFP-BRDT (pcDNA6.2/N-EmGFP-DEST)<sup>1</sup> was a gift from Kyle Miller (Addgene plasmid # 65381). NF- $\kappa$ B-RE/luc2P luciferase reporter plasmid consists of one luc2P gene, controlled by 5 copies of an NF- $\kappa$ B response element, cloned from a pGL4.32 vector into a pBABE vector. Luciferase reporter plasmid provided by Dr. Mark Peggie (Division of Signal Transduction Therapy (DSTT), MRC-PPU, University of Dundee).

Single point mutations were introduced using QuickChange II Site directed Mutagenesis Kit (Agilent). Primers were designed following the recommendations from manufacturer. The polymerase chain reaction (PCR) was performed on a 2720 Thermal Cycler (Applied Biosystems®). Upon digestion of the parental DNA strands by DpnI restriction enzyme, the PCR product was transformed into competent *E. coli* DH5 $\alpha$  cells and grown on lysogeny broth (LB) agar plates containing corresponding selection antibiotics at 37°C for 16h. Single colonies were then picked from the agar plates and grown for 12h in 10 mL of LB medium containing selection antibiotics. Extracted and purified plasmid DNA were then sequenced to confirm the presence of the desired mutation.

### **2 – Protein Expression & Purification**

BL21 *E. coli* cells were transformed with bromodomain-expressing pNIC plasmids using heat shock. Cell cultures were grown at 37°C and 200 rpm in LB media with X kanamycin. A starter culture was incubated until saturation, then diluted 100-fold in fresh media and grown until reaching an optical density of 2.0 (OD<sub>600</sub>). The temperature of the culture was decreased to 18°C, and protein expression was induced overnight with 0.4 mM IPTG. Cells were harvested the next day by centrifugation (4000 rpm for 20 minutes at 4°C, JS-4.2 rotor on a Beckman J6-MC centrifuge) and stored as pellets at -20°C.

Cell pellets were resuspended in lysis buffer (50 mM HEPES, 500 mM NaCl, 10 mM imidazole & 2 mM  $\beta$ -mercaptoethanol pH7.5) and treated with one complete protease inhibitor (Roche) tablet. Cells were lysed using a Stanstead pressure cell homogenizer and the lysate centrifuged at 20 000 rpm for 1 hour at 4°C (JA-25.50 rotor in Beckman Avanti J-25 centrifuge) and the supernatant transferred and passed through a 0.45  $\mu$ m filter.

The lysate was purified using metal ion affinity chromatography, with a His Trap 5ml Ni sepharose column (GE Healthcare) on an AKTApure™ system (GE Healthcare). The column was washed with 30 ml of lysis buffer, and the protein was eluted using 30 ml of elution buffer (50 mM HEPES, 500 mM NaCl, 250 mM imidazole and 2 mM  $\beta$ -mercaptoethanol at pH 7.5). The Ni column elution was concentrated to 2 ml using a Vivaspin 20, 10 000 MWCO (Sartorius) before further purification using size exclusion chromatography. Concentrated Ni column elution was passed through a Superdex 75 16/60 Hiload column (GE healthcare) on an AKTApure™ system, using gel filtration buffer (20 mM HEPES, 150 mM NaCl and 1 mM DTT at pH 7.5). Desired fractions were pooled, concentrated and aliquoted before being flash frozen and stored at -80°C.



### 3 – Differential Scanning Fluorimetry (DSF) / Thermal Shift

DSF experiments were performed on a BioRad CFXconnect machine, using clear 96-well plates. Protein constructs were tested at 6  $\mu$ M, with 2.5X SYPRO orange (Invitrogen), in 40  $\mu$ l of buffer (10 mM HEPES, 100 mM NaCl, pH7.5). Samples underwent a heat cycle from 20°C to 95°C, heated at a rate of 1°C every minute. Plates were read at 1 minute intervals. Each sample was tested in triplicate. Data was analyzed as recommended by Niesen et al<sup>2</sup>, using GraphPad Prism 6 and the SGC's DSF Analysis 3.02 spreadsheet.

### 4 – X-ray Crystallography

Purified BRD2 BD2 L/V protein at 8 mg/mL was mixed with excess amount of a bumped compound (2-4 mM) to form a protein-compound complex. Drops of the complex were mixed 2:1 with precipitant solution in sitting-drop vapor diffusion format. Crystallization condition of protein complexes varies with different bumped compounds, the condition ranges from 0.1 M Tris pH 7.5 - 9.0, 45 - 60 % pentaerythriol propoxylate (5/4 PO/OH), with or without 0.2 M imidazole as additive. Crystals appeared within hours and were fully grown after 2-3 d. Diffraction data were either collected at in-house Rigaku M007HF X-ray generator equipped with Varimax Cu-VHF optics using a Saturn 944HG+ CCD detector at a wavelength of 1.5418 Å or Diamond Light Source beamline I04-1 using a Pilatus 6M-F detector at a wavelength of 0.92819 Å at temperature 100K.

Indexing and integration of reflections was either performed using XDS with the XDSCUI interface<sup>3</sup> or MOSFLM<sup>4</sup>, and scaling and merging with AIMLESS<sup>5</sup> in CCP4i<sup>6</sup>. To solve the phase problem the molecular replacement method was used with the programs MOLREP<sup>7</sup> and Phaser<sup>8</sup> using search models derived from the coordinates of BRD2 BD2 WT (PDB entry 2DVV). The initial model was refined iteratively using PHENIX<sup>9, 10</sup> and COOT<sup>11</sup>. Ligand structures and restraints were generated using eLBOW<sup>12</sup>, REEL<sup>13</sup> and PRODRG<sup>14</sup>. The MOLPROBITY server<sup>15</sup> was used to validate the geometry and steric clashes in the structures. The structure models have been deposited in the protein data bank (PDB) and data collection and refinement statistics are presented in Supplementary Table X. All figures were generated using PyMOL<sup>16</sup>.

### 5 – Bio-Layer Interferometry (BLI)

All BLI experiments were carried out on a OctetRed 384 instrument (ForteBio), at 25°C and in 20 mM HEPES, 150 mM NaCl pH7.5 buffer. A histone peptide library, possessing both single and multiple lysine acetylation marks, was obtained from Alta Bioscience Ltd. Peptides were 20 residues long and were biotinylated on the C-terminal (with aminohexanoic linker). Streptavidin-coated BLI tips (ForteBio) were loaded in 100  $\mu$ l 5  $\mu$ M peptide (or 10 $\mu$ g/ml biocytin) over 10 minutes. For the assay bromodomain constructs were kept at 20  $\mu$ M in 100  $\mu$ l buffer in black 384-well plates, agitated at 1000rpm. Each assay involved exposing peptide-loaded BLI tips to buffer for 120s to determine baseline signal, 240s in protein to measure association and finally 120s in buffer to measure dissociation. Raw data was then analyzed using the ForteBio software, to account for background signal and non-specific binding.

### 6 – Isothermal Titration Calorimetry (ITC)

ITC titrations were performed on an ITC<sub>200</sub> instrument (MicroCal™, GE Healthcare). Proteins, peptides and compounds were all dissolved in ITC buffer (20 mM HEPES, 100 mM NaCl, pH7.5), with protein samples buffer-exchanged through dialysis using D-tubes (Millipore). Each ITC titrations consisted of 20 titrations: 1 initial injection of 0.4  $\mu$ l over 0.8s, followed by 19 injections of 2  $\mu$ l over 4s, at 2 minute intervals. Data was analyzed using the Microcal LLC ITC200 Origin data analysis software, using a single binding site model, to determine binding values such as Kd and enthalpy of binding.

Peptide titrations were carried out at 15°C, with 2 mM of acetylated histone peptide titrated against 50-150 µM bromodomain. Ligand titrations were performed at 30°C, with 250 µM active ligand titrated against 25 µM bromodomains, with a final DMSO concentration of 2.5%. Tandem constructs were carried out at 30°C and with 1.5% DMSO, with 150 µM compound titrated into 15 µM protein.

## 7 – AlphaLISA

In all competitive AlphaLISA assays ligand was titrated against 100 nM His-tagged bromodomain and 5 nM biotinylated JQ1 (bio-JQ1), in AlphaLISA buffer: 50 mM HEPES, 100 mM NaCl, 0.1% BSA, 0.02% CHAPS, pH7.5 (final concentration). Ligands were tested over an 11-point 3-fold serial dilution, starting at 100 µM, and giving a final DMSO concentration of 1%. Binding was detected using anti-His6 antibody-conjugated AlphaLISA acceptor beads and streptavidin-coated AlphaScreen donor beads (PerkinElmer), with a final concentration of 10 µg/ml for each bead). Titrations were prepared in light-grey 384-well Alphaplates (PerkinElmer), and read on a Pherastar FS plate reader (BMG) equipped with an AlphaLISA excitation/emission module. Data was analyzed and dose-response curves generated using GraphPad Prism 6.

Each assay well had a final volume of 25 µl. First 5 µl of 5X ligand was mixed with 10 µl of a 2.5X mix of bromodomains and Bio-JQ1 (prepared en-masse, aliquoted, flash-frozen and stored at -80°C) and incubated for 1 hour at room temperature. The assay plate was then moved to a dark room and 5 µl of 5X acceptor beads were added and incubated for 1 hour. Then (still in darkness) 5 µl of 5X donor beads were added, the plate was incubated for 1 more hour before being read. The direct titrations of Bio-JQ1 against bromodomains follows the same procedure, but in the first step of the assay 5 µl 5X Bio-JQ1 was mixed with 10 µl 5X bromodomain. Bio-JQ1 followed an 11-step 3-fold serial dilution, starting at 10 µM (final concentration).

## 8 – DMPK

Plasma Half-life:

50 µM test compound incubated in mouse BALB/c plasma (pre-warmed to 37°C and buffered to pH7.4 in ratio of 70:30 plasma:buffer). At 0, 30, 60, 120 and 180 minutes a 50 µl aliquot of incubation mixture were removed and mixed with 200µl acetonitrile, containing 50 ng/ml Donepezil as the internal standard, to stop the reaction. The samples were centrifuged to sediment any precipitated protein and the microplates sealed prior to UPLC-MS/MS analysis using a Quattro Premier XE (Waters Corporation). XLfit (IDBS) was used to calculate the exponential decay and hence the rate constant (K) using the ratio of the peak areas of the test compound to the internal standard at each time point. The half-life was calculated for each test compound using the formula:  $t_{1/2} = 0.693/K$ .

Intrinsic Clearance:

0.5 µM test compound was incubated with BAB/c female CD1 mouse liver microsomes (Xenotech LLC TM; 0.5 mg/ml 50 mM potassium phosphate buffer, pH7.4) and the reaction started with addition of excess NADPH (8 mg/ml 50 mM potassium phosphate buffer, pH7.4). At 0, 3, 6, 9, 15 and 30 minutes a 50 µl aliquot of the incubation mixture was removed and mixed with 100 µl acetonitrile to stop the reaction. Internal standard was added to all samples, which were centrifuged to sediment precipitated protein and the microplates were then sealed prior to UPLC MS/MS analysis using a Quattro Premier XE. XLfit was used to calculate the exponential decay and hence the rate constant (K), based on the ratio of the peak areas of test compound to internal standard at each time point. The rate of intrinsic clearance (CLi) was then calculated using the following formula:

$$CLi \text{ (ml/min/g liver)} = K \times V \times \text{microsomal protein yield}$$

Where V (ml/mg protein) is the incubation volume/mg protein added, and microsomal protein yield is taken as 52.5 mg protein/g liver. 0.5 µM Verapamil used as a positive control to confirm assay performance.

**PAMPA:**

PAMPA was performed using a 96-well pre-coated BD Gentest™ PAMPA plate (BD Biosciences). Each well was divided into two chambers; donor and acceptor, separated by a lipid-oil-lipid tri-layer constructed in a porous filter. The effective permeability,  $P_e$ , of the compound was measured at pH 7.4. Stock solutions (5 mM) of the compound were prepared in DMSO. The compound was then further diluted to 10  $\mu$ M in phosphate buffered saline at pH 7.4. The final DMSO concentration did not exceed 5% v/v. The compound dissolved in phosphate buffered saline was then added to the donor side of the membrane and phosphate buffered saline without compound was added to the acceptor side. The PAMPA plate was left at room temperature for 5 h. After which time, an aliquot (100  $\mu$ l) was then removed from both acceptor and donor compartments and mixed with acetonitrile (80  $\mu$ l) containing an internal standard. The samples were centrifuged (10 min, 5°C, 3270 g) to sediment precipitated protein and sealed prior to UPLC-MS/MS analysis using a Quattro Premier XE.  $P_e$  was calculated as shown in the below equation:

$$P_e \text{ (nm/sec)} = 10^7 \times -\ln [1 - C_A(t) / C_{\text{equi}}] / (A * [1/V_D + 1/V_A] * t)$$

Where:

$C_A(t)$  = peak area of compound present in acceptor well at time  $t = 18000$  sec

$C_{\text{equi}}$  =  $[C_D(t) * V_D + C_A(t) * V_A] / (V_D + V_A)$

A = filter area

$V_D$  = donor well volume

$V_A$  = acceptor well volume

t = incubation time

$C_D(t)$  = peak area of compound present in donor well at time  $t = 18000$  sec

Recovery of compound from donor and acceptor wells was calculated and data was only accepted when recovery exceeded 70 %.

## 9 – Tissue Culture

Human U2OS and HL-60 cell lines were obtained from ATCC and MV4;11 cell line was obtained from DSMZ. U2OS were kept in DMEM medium (Gibco) supplemented with 10% FBS (Gibco), 1% L-glutamate (Gibco) and 100 U/ml penicillin and streptomycin. Cells were kept in an incubator at 37°C, 5% CO<sub>2</sub>. MV4-11 and HL-60 were kept in RPMI medium (Gibco) supplemented with 10% FBS, 1% L-glutamate (Gibco) and 100 U/ml penicillin and streptomycin. All cell lines were tested for mycoplasma contamination every month using MycoAlert Mycoplasma detection kit (Lonza).

## 10 – Fluorescence Recovery after Photobleaching (FRAP)

FRAP experiments were performed in human osteosarcoma U2OS cells transfected with pcDNA5 FRT/TO plasmids encoding wild-type and mutant GFP chimeras of BET proteins. Cells were seeded into glass-bottom, 35x10mm dishes (WillCo) at ~200 000 cells in 2 ml media per dish ~66 hours before FRAP. Cells were transfected using FuGENE HD (Promega) and 1  $\mu$ g of plasmid DNA ~42 hours before FRAP. 18 hours before FRAP cells were treated with test compounds and SAHA (Sigma-Aldrich) to a final concentration of 1  $\mu$ M and 2  $\mu$ M, respectively, giving a final DMSO concentration of 0.03%.

FRAP experiments were carried out on a Deltavision Elite imaging system (GE Healthcare) running Resolve 3D (SoftWoRx) kept at 37°C and using a FITC filter set (488 nm excitation, 525 nm emission). Cells were imaged using a 60X objective lens (Olympus), with an exposure time of 0.05s and using 2x2 binning to give a 512x512 pixel image. Cells were excluded for FRAP experiments if they displayed aberrant morphology and signs of cell-death.

Cells providing a signal of <1000 fluorescence units were excluded as they were too close to the background signal for photobleaching (requiring reduction to ~50% fluorescence) to be observed. Cells fluorescing over 3500 units were also excluded due to the risk of detector saturation.

Cells were photobleached using a quantifiable laser module (QLM), set to a wavelength of 488 nm and 100% power, for 0.5s, covering an area with a  $0.5 \mu\text{m}^2$  radius. For each cell 5 images were captured pre-bleach (over 5 seconds) and 32 post-bleach, using a CoolSNAP HQ camera (Photometrics). Post-bleach imaging was usually spread over 60s and distributed to best measure a  $t_{1/2}$  of ~2s, although this was altered in some cases. FRAP experiments were analyzed in SoftWorx (GE Healthcare) using the PK analysis function, set to analyze a bleach event with  $0.5 \mu\text{m}^2$  radius. Calculated  $t_{1/2}$  values were extracted and analyzed in Prism 6 (GraphPad). Each experiment was run twice on separate days, with ~20 cells tested on each day.

### 11 – WT Cell Cytotoxicity

Compound cytotoxicity was measured using the CellTiter-Glo assay (Promega). Compounds were serially diluted in a sterile, white, clear-bottom 384-well cell culture microplate (Greiner Bio-one), at 2X concentration and a volume of 25  $\mu\text{l}$ . 25  $\mu\text{l}$  of 2X cell suspension was then added. Both cells and compounds were diluted in RPMI medium. After 48hr incubation 25  $\mu\text{l}$  of CellTiter-Glo reagent was added to each cells. Following 15 minute incubation the luminescence signal was read on a Pherastar FS. The final concentration of assay components are as follows:  $3 \times 10^5$  cells/ml, 0.05% DMSO, 5  $\mu\text{M}$  and below compound. Compounds were tested in triplicate, against the BET-dependent AML cell-lines MV4-11 and HL60.

### 12 – NF-KB Luciferase Assay

Luciferase experiments were performed in human HEK cells seeded in a 24-well plate at 100 000 cells in 500 $\mu\text{l}$  media, and transfected with pcDNA5 FRT/TO plasmids encoding WT and mutant GFP-BRD4 chimeras, and pBABE NF- $\kappa$ B-RE/luc2P reporter plasmid. Cells were transfected using Lipofectamine™ LTX (Invitrogen) with PLUS™ reagent, with each well receiving 0.5  $\mu\text{g}$  of each plasmid, 2.5  $\mu\text{l}$  LTX and 0.5  $\mu\text{l}$  PLUS reagent. The next day cells were treated with compounds, giving a final concentration of 1  $\mu\text{M}$  compound and 0.01% DMSO. 6 hours later cells were washed with PBS, lysed with passive lysis buffer (Promega) and stored at -20°C.

Luciferase activity was measured using the Promega luciferase assay. In a black 384-well plate 3 $\mu\text{l}$  of clarified lysate was mixed with 15 $\mu\text{l}$  luciferase assay reagent and after 15 minutes luminescence was measured in a Pherastar FS. Differences in cell numbers were controlled for by measuring the protein content of each lysate using the Pierce™ Coomassie (Bradford) assay. Each experiment was run twice, on separate days, with each experiment containing 3 technical replicates.

## Chemical Synthesis

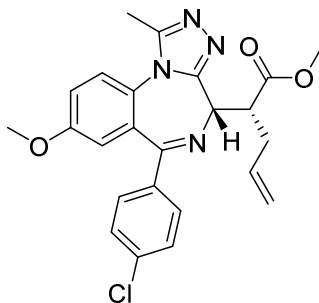
### **General information:**

NMR spectra were recorded on a Bruker 500 Ultrashield or a Bruker Ascend 400. Chemical shifts are quoted in ppm and referenced to the residual solvent signals:  $^1\text{H}$   $\delta$  = 7.26 ( $\text{CDCl}_3$ ),  $^{13}\text{C}$   $\delta$  = 77.16 ( $\text{CDCl}_3$ ). High Resolution Mass Spectra (HRMS) were recorded on a Bruker micrOTOF. All chemicals, unless otherwise stated are commercially available and used without further purification. Micro wave reactions were performed in Biotage Initiator. Flash column chromatography was performed using a Teledyne Isco Combiflash Rf or Rf200i. Prepacked columns RediSep Rf Normal Phase Disposable Columns were used. Preparative HPLC was performed on a Waters mass directed HPLC with a Waters X-Bridge C18 column (100 mm x 19 mm; 5  $\mu\text{m}$  particle size). Separation of the diastereomers was achieved with a gradient of 5 % to 95 % acetonitrile in water with 0.1 % formic acid in the aqueous phase.

Compounds **1**,<sup>2</sup> I-Bet762,<sup>2</sup> and **2**<sup>3</sup> were prepared according to literature procedures. **3**,<sup>4</sup> and **4**<sup>4</sup> were prepared according to previous work in our group.

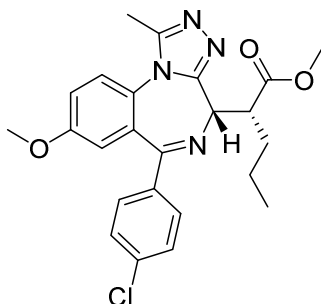
**General procedure for the alkylation in  $\alpha$ -positon:**

Compound **1** (200 mg, 487  $\mu$ mol, 1 eq.) or **2** (200 mg, 487  $\mu$ mol, 1 eq.) was dissolved in anhydrous tetrahydrofuran (5 ml in the case of **1** and 10 ml in the case of **2**). This solution was then added drop wise to a solution of Potassium hexamethyldisilazane (1.17 ml of a 0.5 M solution in toluene, 584  $\mu$ mol, 1.2 eq.) in tetrahydrofuran at -80 °C under an atmosphere of nitrogen. After 1 h at this temperature the corresponding alkyl iodide (584  $\mu$ mol, 1.2 eq.) was added drop wise. The reaction mixture was warmed to 25 °C over 18 h and a few drops of acetic acid were then added to quench the reaction. The solvent was removed and the residue purified by flash column chromatography using a linear gradient from 10 % to 60 % acetone in heptane. For isomerization the alkylated compound together with freshly prepared sodium methoxide (10 eq.) was dissolved in methanol (2 ml) and heated to 120 °C for 40 min in a microwave reactor. The reaction mixture was acidified with aqueous hydrochloric acid (1 M), diluted with water and extracted three times with dichloromethane. The combined organic phases were dried over magnesium sulfate and evaporated to dryness. Separation of the diastereoisomers was achieved as described above.

**(+)-methyl (R)-2-((S)-6-(4-chlorophenyl)-8-methoxy-1-methyl-4H-benzo[f][1,2,4]triazolo[4,3-a][1,4]diazepin-4-yl)pent-4-enoate (5).**

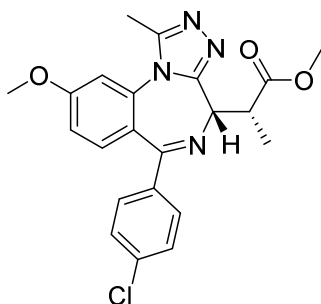
Yield: 32.3 mg (15 %);  $^1\text{H-NMR}$  ( $\text{CDCl}_3$ , 500 MHz)  $\delta$  2.40-2.46 (m, 1 H), 2.60 (s, 3 H), 2.88-2.93 (m, 1 H), 3.80 (s, 3 H), 3.81 (s, 3 H), 4.12-4.16 (m, 1 H), 4.27 (d, 1 H,  $J(\text{H,H}) = 11.0$  Hz), 4.99-5.06 (m, 2 H), 5.82-5.90 (m, 1 H), 6.87 (d, 1 H,  $J(\text{H,H}) = 2.90$  Hz), 7.21 (dd, 1 H,  $J(\text{H,H}) = 2.90$  Hz,  $J(\text{H,H}) = 8.90$  Hz), 7.30-7.33 (m, 2 H), 7.39-7.43 (m, 3 H);  $^{13}\text{C-NMR}$  ( $\text{CDCl}_3$ , 126 MHz)  $\delta$  12.1, 34.2, 47.8, 51.5, 55.8, 58.4, 115.8, 117.2, 117.9, 124.8, 126.4, 128.5, 129.9, 130.7, 134.4, 137.0, 150.4, 154.9, 158.0, 165.5, 174.7; HRMS  $m/z$  calc. for  $\text{C}_{24}\text{H}_{24}\text{ClN}_4\text{O}_3$  [ $\text{M}+\text{H}^+$ ] 451.1531, found 451.1523.

**(+)-methyl (R)-2-((S)-6-(4-chlorophenyl)-8-methoxy-1-methyl-4H-benzo[f][1,2,4]triazolo[4,3-a][1,4]diazepin-4-yl)pentanoate (6).**



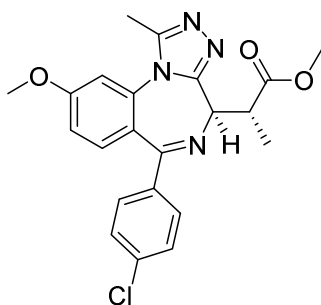
Yield: 28.6 mg (12 %);  $^1\text{H-NMR}$  (400 MHz,  $\text{CDCl}_3$ )  $\delta$  0.92 (t,  $J(\text{H,H})=7.3$  Hz, 3H), 1.35 (m, 1H), 1.53 (m, 2H), 2.06 (m, 1H), 2.59 (s, 3H), 3.80 (s, 3H), 3.83 (s, 3H), 4.05 (m, 1H), 4.22 (d,  $J(\text{H,H})=11.1$  Hz, 1H), 6.86 (d,  $J(\text{H,H})=2.9$  Hz, 1H), 7.21 (dd,  $J(\text{H,H})=8.9, 2.9$  Hz, 1H), 7.31 (m, 2H), 7.40 (m, 3H);  $^{13}\text{C-NMR}$  (100 MHz,  $\text{CDCl}_3$ )  $\delta$  12.1, 14.0, 20.6, 32.1, 48.1, 51.6, 55.8, 59.1, 115.7, 117.9, 124.8, 126.4, 128.5, 129.9, 130.7, 136.9 (2C), 150.4, 155.1, 158.0, 165.5, 175.7; HRMS  $m/z$  calc. for  $\text{C}_{24}\text{H}_{26}\text{ClN}_4\text{O}_3$   $[\text{M}+\text{H}]^+$  453.1693, found: 453.1678.

**(+)- methyl (R)-2-((S)-6-(4-chlorophenyl)-9-methoxy-1-methyl-4H-benzo[f][1,2,4]triazolo[4,3-a][1,4]diazepin-4-yl)propanoate (7).**



Yield: 35.9 mg (17 %);  $^1\text{H-NMR}$  ( $\text{CDCl}_3$ , 400 MHz)  $\delta$  1.49 (d, 3 H,  $J(\text{H,H})=6.64$  Hz), 2.64 (s, 3 H), 3.82 (s, 3 H), 3.95 (s, 3 H), 4.05-4.11 (m, 1 H), 4.23 (d, 1 H,  $J(\text{H,H})=11.04$  Hz), 6.94 (s, 1 H), 6.98 (d, 1 H,  $J(\text{H,H})=8.96$  Hz), 7.31 (d, 2 H,  $J(\text{H,H})=7.40$  Hz), 7.35-7.39 (m, 3 H);  $^{13}\text{C-NMR}$  ( $\text{CDCl}_3$ , 101 MHz)  $\delta$  12.3, 15.3, 42.4, 51.8, 55.9, 59.6, 109.4, 112.7, 121.4, 128.4, 130.8, 133.4, 134.7, 136.7, 137.4, 150.2, 154.9, 161.6, 165.7, 176.1; HRMS  $m/z$  calc. for  $\text{C}_{22}\text{H}_{22}\text{ClN}_4\text{O}_3$   $[\text{M}+\text{H}^+]$  425.1375, found 425.1381.

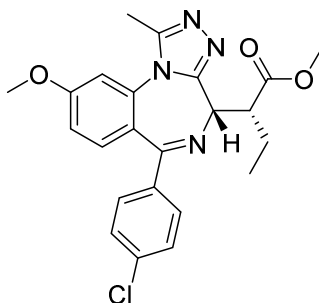
**(+)- Methyl (S\*)-2-((S\*)-6-(4-chlorophenyl)-9-methoxy-1-methyl-4H-benzo[f][1,2,4]triazolo[4,3-a][1,4]diazepin-4-yl)propanoate (S\*, S\*) 7**



$^1\text{H NMR}$  (400 MHz,  $\text{CDCl}_3$ )  $\delta$ : 1.60 (d,  $J=7.1$  Hz, 3H), 2.63 (s, 3H), 3.72 (s, 3H), 3.86- 3.92 (m, 3H), 3.94 (s, 3H), 4.27 (d,  $J=10.3$  Hz, 1H), 6.93 (d,  $J=2.4$  Hz, 1H), 6.98 (dd,  $J=2.6, 8.8$  Hz, 1H), 7.32-7.38 (m, 3H), 7.49 (d,  $J=8.1$  Hz, 2H).  $^{13}\text{C-NMR}$  (100 MHz,  $\text{CDCl}_3$ )  $\delta$ : 12.4, 15.5, 41.1, 52.0, 55.9, 57.8, 76.7, 77.0, 77.3, 109.3, 112.9, 121.4, 128.5, 130.8,

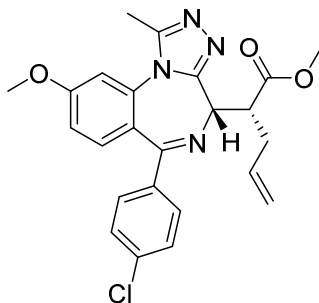
133.1, 135.1, 136.8, 137.7, 150.0, 156.1, 161.6, 166.5, 176.1; HRMS  $m/z$  calc. for  $C_{22}H_{22}ClN_4O_3$   $[M+H]^+$  425.1375, found 425.1388.

**(+)- methyl (R)-2-((S)-6-(4-chlorophenyl)-9-methoxy-1-methyl-4H-benzo[f][1,2,4]triazolo[4,3-a][1,4]diazepin-4-yl)butanoate (8).**



Yield: 25.6 mg (12 %);  $^1H$ -NMR ( $CDCl_3$ , 400 MHz)  $\delta$  1.01 (t, 3 H,  $J(H,H)$  = 7.28 Hz), 1.57-1.68 (m, 1 H), 2.12-2.21 (m, 1 H), 2.63 (s, 3 H), 3.84 (s, 3 H), 3.95 (s, 3 H), 4.00 (dd, 1 H,  $J(H,H)$  = 2.80 Hz,  $J(H,H)$  = 11.2 Hz), 4.23 (d, 1 H,  $J(H,H)$  = 10.9 Hz), 6.94 (s, 1 H), 6.98 (d, 1 H,  $J(H,H)$  = 8.48 Hz), 7.30 (d, 2 H,  $J(H,H)$  = 7.68 Hz), 7.34-7.38 (m, 3 H);  $^{13}C$ -NMR ( $CDCl_3$ , 101 MHz)  $\delta$  11.6, 12.4, 23.2, 49.7, 51.6, 55.9, 58.8, 109.4, 112.7, 121.4, 128.4, 130.8, 133.4, 134.7, 136.7, 137.4, 150.2, 155.1, 161.6, 165.8, 175.5; HRMS  $m/z$  calc. for  $C_{23}H_{24}ClN_4O_3$   $[M+H]^+$  439.1531, found 439.1513.

**(+)-methyl (R)-2-((S)-6-(4-chlorophenyl)-9-methoxy-1-methyl-4H-benzo[f][1,2,4]triazolo[4,3-a][1,4]diazepin-4-yl)pent-4-enoate (9).**

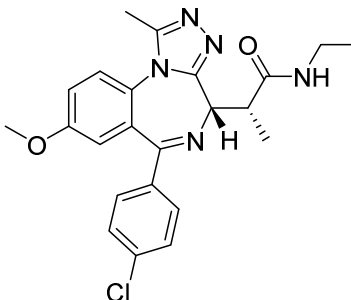


Yield: 27.3 mg (12 %);  $^1H$ -NMR ( $CDCl_3$ , 400 MHz)  $\delta$  2.38-2.46 (m, 1 H), 2.64 (s, 3 H), 2.88-2.94 (m, 1 H), 3.80 (s, 3 H), 3.95 (s, 3 H), 4.11-4.17 (m, 1 H), 4.27 (d, 1 H,  $J(H,H)$  = 10.9 Hz), 4.99-5.07 (m, 2 H), 5.82-5.92 (m, 1 H), 6.93 (d, 1 H,  $J(H,H)$  = 2.44 Hz), 6.98 (dd, 1 H,  $J(H,H)$  = 2.48 Hz,  $J(H,H)$  = 8.80 Hz), 7.29-7.32 (m, 2 H), 7.34-7.39 (m, 3 H);  $^{13}C$ -NMR ( $CDCl_3$ , 101 MHz)  $\delta$  12.4, 34.2, 47.9, 51.6, 55.9, 58.3, 109.4, 112.7, 117.2, 121.3, 128.4, 130.8, 133.4, 134.5, 134.7, 136.8, 137.3, 150.3, 154.8, 161.6, 165.9, 174.7; HRMS  $m/z$  calc. for  $C_{24}H_{24}ClN_4O_3$   $[M+H]^+$  451.1531, found 451.1540.

#### General procedure for Amide formation:

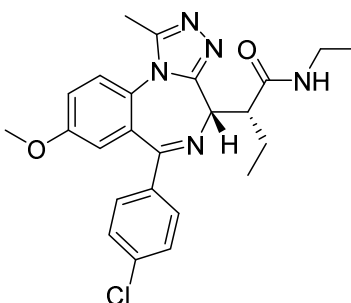
The mixture of diastereomers of the ester compounds (100  $\mu$ mol, 1 eq.) were hydrolyzed in methanol (0.5 ml) and aqueous sodium hydroxide (0.5 ml, 1 M in water) by heating to 100  $^{\circ}C$  for 30 min in a microwave oven. After quenching with aqueous hydrochloric acid (1 M) the reaction mixture was extracted three times with dichloromethane. The combined organic phases were dried over magnesium sulfate and evaporated to dryness. To this end, the obtained free carboxylic acid was dissolved in dichloromethane, the corresponding amine (150  $\mu$ mol, 1.5 eq.), HATU (57.0 mg, 150  $\mu$ mol, 1.5 eq.) and *N,N*-diisopropylethylamine (69.9  $\mu$ l, 400  $\mu$ mol, 4 eq.) were added and the reaction mixture stirred at 25  $^{\circ}C$  for 2 h. The solvent was removed and the residue subject to flash column chromatography before the diastereomers were separated as described above.

**(+/-) (R)-2-((S)-6-(4-chlorophenyl)-8-methoxy-1-methyl-4H-benzo[f][1,2,4]triazolo[4,3-a][1,4]diazepin-4-yl)-N-ethylpropanamide (16).**



Yield: 13.2 mg (30 %);  $^1\text{H-NMR}$  ( $\text{CDCl}_3$ , 500 MHz)  $\delta$  1.25 (t, 3 H,  $J(\text{H,H})=7.25$  Hz), 1.44 (d, 3 H,  $J(\text{H,H})=6.75$  Hz), 2.59 (s, 3 H), 3.33-3.50 (m, 2 H), 3.63-3.69 (m, 1 H), 3.79 (s, 3 H), 4.24 (d, 1 H,  $J(\text{H,H})=9.80$  Hz), 6.25 (t, 1 H,  $J(\text{H,H})=5.49$  Hz), 6.85 (d, 1 H,  $J(\text{H,H})=2.90$  Hz), 7.20 (dd, 1 H,  $J(\text{H,H})=2.90$  Hz,  $J(\text{H,H})=8.90$  Hz), 7.29-7.32 (m, 2 H), 7.39 (d, 1 H,  $J(\text{H,H})=8.85$  Hz), 7.43-7.46 (m, 2 H);  $^{13}\text{C-NMR}$  ( $\text{CDCl}_3$ , 126 MHz)  $\delta$  12.1, 15.0, 15.6, 34.4, 43.6, 55.8, 59.7, 115.6, 118.1, 124.8, 126.4, 128.4, 130.0, 136.9, 137.1, 150.3, 155.6, 158.0, 165.5, 174.4; HRMS  $m/z$  calc. for  $\text{C}_{23}\text{H}_{25}\text{ClN}_5\text{O}_2$  [ $\text{M}+\text{H}^+$ ] 438.1691, found 438.1675.

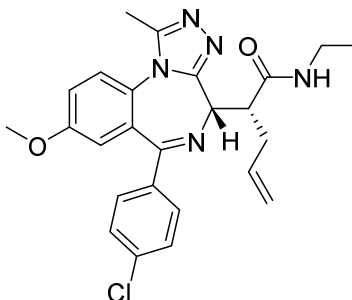
**(+/-) (R)-2-((S)-6-(4-chlorophenyl)-8-methoxy-1-methyl-4H-benzo[f][1,2,4]triazolo[4,3-a][1,4]diazepin-4-yl)-N-ethylbutanamide (17).**



Yield: 11.7 mg (26 %);  $^1\text{H-NMR}$  ( $\text{CDCl}_3$ , 500 MHz)  $\delta$  1.03 (t, 3 H,  $J(\text{H,H})=7.35$  Hz), 1.27 (t, 3 H,  $J(\text{H,H})=7.25$  Hz), 1.64-1.74 (m, 1 H), 2.01-2.09 (m, 1 H), 2.59 (s, 3 H), 3.42-3.49 (m, 3 H), 3.79 (s, 3 H), 4.23 (d, 1 H,  $J(\text{H,H})=10.0$  Hz), 6.17 (s, 1 H), 6.85 (d, 1 H,  $J(\text{H,H})=2.85$  Hz), 7.20 (dd, 1 H,  $J(\text{H,H})=2.90$  Hz,  $J(\text{H,H})=10.4$  Hz), 7.30-7.21 (m, 2 H), 7.38 (d, 1 H,  $J(\text{H,H})=8.90$  Hz), 7.42-7.45 (m, 2 H);  $^{13}\text{C-NMR}$  ( $\text{CDCl}_3$ , 126 MHz)  $\delta$  11.9, 12.1, 15.2, 22.9, 34.4, 51.3, 55.8, 59.0, 115.6, 118.1, 124.8, 126.5, 128.4, 130.0, 130.8, 136.9, 137.1, 150.3, 155.7, 158.0, 165.4, 173.5; HRMS  $m/z$  calc. for  $\text{C}_{24}\text{H}_{26}\text{ClN}_5\text{O}_2$  [ $\text{M}+\text{H}^+$ ] 452.1848, found 452.1839.

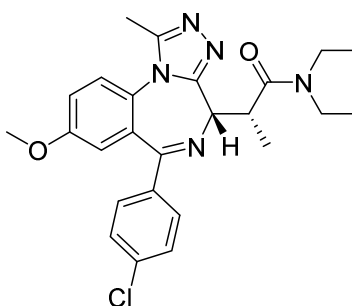
**(+/-) (R)-2-((S)-6-(4-chlorophenyl)-8-methoxy-1-methyl-4H-benzo[f][1,2,4]triazolo[4,3-a][1,4]diazepin-4-yl)-N-ethylpent-4-enamide (18).**





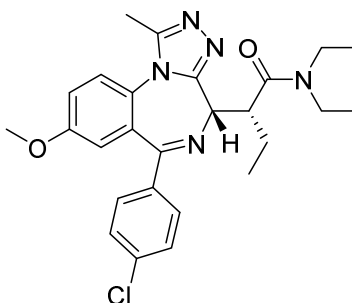
Yield: 14.7 mg (32 %);  $^1\text{H-NMR}$  ( $\text{CDCl}_3$ , 400 MHz)  $\delta$  1.19 (t, 3 H,  $J(\text{H,H})=7.20$  Hz), 2.48-2.56 (m, 1 H), 2.62 (s, 3 H), 2.70-2.76 (m, 1 H), 3.32-3.44 (m, 2 H), 3.52-3.58 (m, 1 H), 3.80 (s, 3 H), 4.32 (d, 1 H,  $J(\text{H,H})=8.48$  Hz), 5.02 (d, 1 H,  $J(\text{H,H})=10.3$  Hz), 5.10 (d, 1 H,  $J(\text{H,H})=17.0$  Hz), 5.82-5.92 (m, 1 H), 6.60 (s, 1 H), 6.86 (d, 1 H,  $J(\text{H,H})=2.84$  Hz), 7.23 (dd, 1 H,  $J(\text{H,H})=2.84$  Hz,  $J(\text{H,H})=8.96$  Hz), 7.33-7.35 (m, 2 H), 7.44-7.48 (m, 3 H);  $^{13}\text{C-NMR}$  ( $\text{CDCl}_3$ , 101 MHz)  $\delta$  11.8, 14.9, 34.4, 48.5, 55.9, 57.7, 116.1, 117.5, 118.1, 125.2, 125.6, 128.5, 129.9, 130.9, 134.8, 136.8, 137.2, 150.8, 155.3, 158.4, 166.4, 172.9; HRMS  $m/z$  calc. for  $\text{C}_{25}\text{H}_{27}\text{ClN}_5\text{O}_2$  [ $\text{M}+\text{H}^+$ ] 464.1848, found 464.1840.

**(+)- (R)-2-((S)-6-(4-chlorophenyl)-8-methoxy-1-methyl-4H-benzo[f][1,2,4]triazolo[4,3-a][1,4]diazepin-4-yl)-N,N-diethylpropanamide (19)**



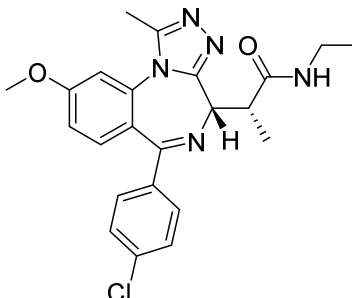
Yield: 17.3 mg (37 %);  $^1\text{H-NMR}$  ( $\text{CDCl}_3$ , 400 MHz)  $\delta$  1.24 (t, 3 H,  $J(\text{H,H})=7.24$  Hz), 1.33 (t, 3 H,  $J(\text{H,H})=6.92$  Hz), 1.41 (d, 3 H,  $J(\text{H,H})=6.64$  Hz), 2.65 (s, 3 H), 3.37-3.45 (m, 1 H), 3.50-3.74 (m, 3 H), 3.80 (s, 3 H), 4.21-4.29 (m, 1 H), 4.40 (d, 1 H,  $J(\text{H,H})=10.6$  Hz), 6.88 (s, 1 H), 7.21-7.29 (m, 1 H), 7.30 (d, 2 H), 7.41-7.46 (m, 3 H);  $^{13}\text{C-NMR}$  ( $\text{CDCl}_3$ , 101 MHz)  $\delta$  11.8, 13.4, 15.0, 15.6, 38.0, 40.7, 42.5, 55.9, 60.4, 115.7, 118.1, 125.0, 125.8, 128.3, 130.0, 130.8, 136.9, 137.0, 150.7, 155.8, 158.3, 165.1, 174.3; HRMS  $m/z$  calc. for  $\text{C}_{25}\text{H}_{29}\text{ClN}_5\text{O}_2$  [ $\text{M}+\text{H}^+$ ] 466.2004, found 466.1997.

**(+)- (R)-2-((S)-6-(4-chlorophenyl)-8-methoxy-1-methyl-4H-benzo[f][1,2,4]triazolo[4,3-a][1,4]diazepin-4-yl)-N,N-diethylbutanamide (20)**



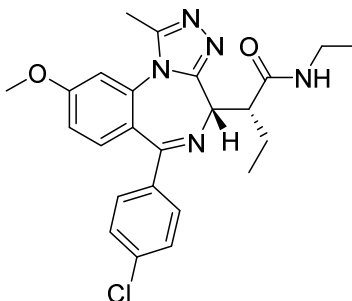
Yield: 15.8 mg (33 %);  $^1\text{H-NMR}$  ( $\text{CDCl}_3$ , 400 MHz)  $\delta$  1.00 (t, 3 H,  $J(\text{H,H})=7.28$  Hz), 1.26 (t, 3 H,  $J(\text{H,H})=7.00$  Hz), 1.33 (t, 3 H,  $J(\text{H,H})=6.84$  Hz), 1.65-1.74 (m, 1 H), 2.04-2.11 (m, 1 H), 2.62 (s, 3 H), 3.50-3.76 (m, 4 H), 3.80 (s, 3 H), 4.11-4.23 (m, 1 H), 4.31 (d, 1 H,  $J(\text{H,H})=10.5$  Hz), 6.86 (s, 1 H), 7.19-7.22 (m, 1 H), 7.29 (d, 2 H,  $J(\text{H,H})=7.64$  Hz), 7.40-7.43 (m, 3 H);  $^{13}\text{C-NMR}$  ( $\text{CDCl}_3$ , 101 MHz)  $\delta$  11.6, 11.9, 13.4, 14.8, 40.8, 42.5, 44.4, 55.9, 59.9, 115.7, 118.1, 124.9, 126.0, 128.3, 129.9, 130.8, 136.8, 137.1, 150.6, 155.9, 158.2, 165.2, 173.5; HRMS  $m/z$  calc. for  $\text{C}_{26}\text{H}_{31}\text{ClN}_5\text{O}_2$  [ $\text{M}+\text{H}^+$ ] 480.2161, found 480.2171.

(+)-(R)-2-((S)-6-(4-chlorophenyl)-9-methoxy-1-methyl-4H-benzo[f][1,2,4]triazolo[4,3-a][1,4]diazepin-4-yl)-N-ethylpropanamide (21).



Yield: 12.6 mg (29 %);  $^1\text{H-NMR}$  ( $\text{CDCl}_3$ , 400 MHz)  $\delta$  1.24 (t, 3 H,  $J(\text{H,H})=7.20$  Hz), 1.44 (d, 3 H,  $J(\text{H,H})=6.56$  Hz), 2.62 (s, 3 H), 3.32-3.50 (m, 2 H), 3.62-3.70 (m, 1 H), 3.93 (s, 3 H), 4.23 (d, 1 H,  $J(\text{H,H})=9.64$  Hz), 6.28 (s, 1 H), 6.93-6.97 (m, 2 H), 7.28-7.34 (m, 3 H), 7.40 (d, 2 H,  $J(\text{H,H})=7.62$  Hz);  $^{13}\text{C-NMR}$  ( $\text{CDCl}_3$ , 101 MHz)  $\delta$  12.3, 15.0, 15.6, 34.4, 43.6, 55.9, 59.6, 109.4, 112.7, 121.4, 128.3, 130.8, 133.4, 134.7, 136.7, 137.5, 150.2, 155.5, 161.5, 165.8, 174.4; HRMS  $m/z$  calc. for  $\text{C}_{23}\text{H}_{25}\text{ClN}_5\text{O}_2$  [ $\text{M}+\text{H}^+$ ] 438.1691, found 438.1684.

(+)-(R)-2-((S)-6-(4-chlorophenyl)-9-methoxy-1-methyl-4H-benzo[f][1,2,4]triazolo[4,3-a][1,4]diazepin-4-yl)-N-ethylbutanamide (22)

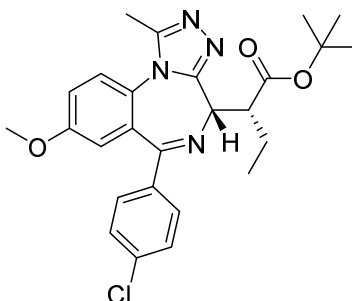


Yield: 9.5 mg (21 %);  $^1\text{H-NMR}$  ( $\text{CDCl}_3$ , 400 MHz)  $\delta$  1.03 (t, 3 H,  $J(\text{H,H})=7.24$  Hz), 1.24 (t, 3 H,  $J(\text{H,H})=7.24$  Hz), 1.70-1.78 (m, 1 H), 1.96-2.06 (m, 1 H), 2.64 (s, 3 H), 3.41-3.48 (m, 3 H), 3.94 (s, 3 H), 4.26 (d, 1 H,  $J(\text{H,H})=9.32$  Hz), 6.43 (s, 1 H), 6.97-6.99 (m, 2 H), 7.31-7.34 (m, 3 H), 7.42 (d, 2 H,  $J(\text{H,H})=7.94$  Hz);  $^{13}\text{C-NMR}$  ( $\text{CDCl}_3$ , 101 MHz)  $\delta$  11.9, 12.2, 15.0, 23.2, 34.4, 50.9, 56.0, 58.4, 109.4, 113.3, 121.2, 128.4, 130.9, 133.5, 134.4, 137.0, 137.3, 150.5, 155.5, 161.8, 173.7; HRMS  $m/z$  calc. for  $\text{C}_{24}\text{H}_{27}\text{ClN}_5\text{O}_2$  [ $\text{M}+\text{H}^+$ ] 452.1848, found 452.1855.

#### General procedure for *tert*-butyl ester formation:

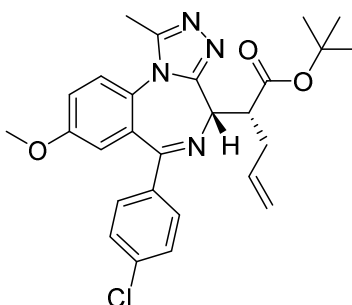
The mixture of diastereoisomers of the alkylated methyl-esters (100  $\mu\text{mol}$ , 1 eq.) were hydrolyzed in methanol (0.5 ml) and aqueous sodium hydroxide (0.5 ml, 1 M in water) by heating to 100  $^\circ\text{C}$  for 30 min in a microwave reactor. After quenching with aqueous hydrochloric acid (1 M) the reaction mixture was extracted three times with dichloromethane. The combined organic phases were dried over magnesium sulfate and evaporated to dryness. The crude was dissolved in anhydrous dichloromethane and *tert*-butyl trichloroacetimidate (200  $\mu\text{mol}$ , 2 eq.) was added. After addition of boron trifluoride-diethyl ether complex (5  $\mu\text{mol}$ , 0.05 eq.) the reaction mixture was stirred at 25  $^\circ\text{C}$  for 18 h. The solvent was removed and the residue subject to flash column chromatography before the diastereoisomers were separated as described above.

**tert-butyl (R)-2-((S)-6-(4-chlorophenyl)-8-methoxy-1-methyl-4H-benzo[f][1,2,4]triazolo[4,3-a][1,4]diazepin-4-yl)butanoate (23).**



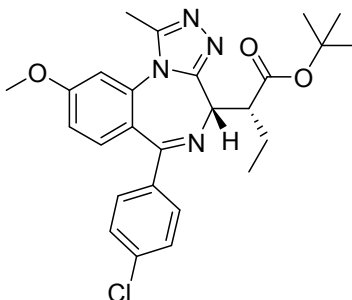
Yield: 3.21 mg (7 %);  $^1\text{H-NMR}$  ( $\text{CDCl}_3$ , 400 MHz)  $\delta$  1.04 (t, 3 H,  $J(\text{H,H})=7.40$ ), 1.56 (s, 9 H), 1.58-1.63 (m, 1 H), 2.11-2.18 (m, 1 H), 2.59 (s, 3 H), 3.81 (s, 3 H), 3.84-3.90 (m, 1 H), 4.19 (d, 1 H,  $J(\text{H,H})=11.1$ ), 6.88 (d, 1 H,  $J(\text{H,H})=2.7$ ), 7.20 (dd, 1 H,  $J(\text{H,H})=2.9$ ,  $J(\text{H,H})=8.98$ ), 7.30-7.32 (m, 2H), 7.38-7.40 (m, 1 H), 7.46-7.48 (m, 2 H);  $^{13}\text{C-NMR}$  ( $\text{CDCl}_3$ , 101 MHz)  $\delta$  11.6, 12.3, 23.5, 28.5, 50.2, 56.0, 59.1, 80.7, 115.7, 118.0, 124.9, 126.6, 128.5, 128.8, 130.2, 130.9, 137.0, 137.2, 150.4, 155.5, 158.1, 165.2, 174.2; HRMS  $m/z$  calc. for  $\text{C}_{26}\text{H}_{30}\text{ClN}_4\text{O}_3$  [ $\text{M}+\text{H}^+$ ] 481.2001, found 481.2009.

**tert-butyl (R)-2-((S)-6-(4-chlorophenyl)-8-methoxy-1-methyl-4H-benzo[f][1,2,4]triazolo[4,3-a][1,4]diazepin-4-yl)pent-4-enoate (24).**



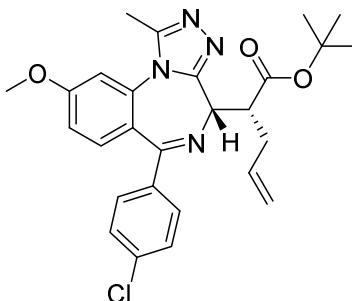
Yield: 5.20 mg (11 %);  $^1\text{H-NMR}$  ( $\text{CDCl}_3$ , 400 MHz)  $\delta$  1.52 (s, 9 H), 2.35-2.43 (m, 1 H), 2.60 (s, 3 H), 2.85-2.90 (m, 1 H), 3.81 (s, 3 H), 3.99 (dt, 1 H,  $J(\text{H,H})=3.7$ ,  $J(\text{H,H})=10.5$ ), 4.22 (d, 1 H,  $J(\text{H,H})=11.0$ ), 4.98-5.05 (m, 2 H), 5.83-5.93 (m, 1 H), 6.88 (d, 1 H,  $J(\text{H,H})=2.8$ ), 7.20 (dd, 1 H,  $J(\text{H,H})=2.8$ ,  $J(\text{H,H})=8.8$ ), 7.30-7.32 (m, 2 H), 7.38-7.40 (m, 1 H), 7.46-7.48 (m, 2 H);  $^{13}\text{C-NMR}$  ( $\text{CDCl}_3$ , 101 MHz)  $\delta$  12.3, 28.4, 34.7, 48.3, 56.0, 58.6, 81.0, 115.8, 117.2, 118.0, 124.9, 126.6, 128.6, 130.1, 130.9, 134.7, 137.0, 137.1, 150.4, 155.2, 158.1, 165.3, 173.4; HRMS  $m/z$  calc. for  $\text{C}_{27}\text{H}_{30}\text{ClN}_4\text{O}_3$  [ $\text{M}+\text{H}^+$ ] 493.2001, found 493.2021.

**tert-butyl (R)-2-((S)-6-(4-chlorophenyl)-9-methoxy-1-methyl-4H-benzo[f][1,2,4]triazolo[4,3-a][1,4]diazepin-4-yl)butanoate (25)**



$^1\text{H}$  NMR (400 MHz,  $\text{CDCl}_3$ ) 1.04 (t,  $J=7.6$  Hz, 3H), 1.55-1.63 (m, 11H), 2.11-2.18 (m, 1H), 2.62 (s, 3H), 3.81-3.87 (m, 1H), 3.95 (s, 3H), 4.18 (d,  $J=11.1$  Hz, 1H), 6.93 (d,  $J=2.2$  Hz, 1H), 6.98 (dd,  $J=2.5, 8.7$  Hz, 1H), 7.30 (d,  $J=8.5$  Hz, 2H), 7.36 (d,  $J=8.7$  Hz, 1H), 7.43 (d,  $J=8.7$  Hz, 2H).  $^{13}\text{C}$ -NMR ( $\text{CDCl}_3$ , 500 MHz) 11.5, 12.4, 23.4, 28.3, 50.2, 55.9, 58.9, 80.6, 109.4, 112.7, 121.5, 128.3, 130.9, 133.3, 134.8, 136.7, 137.5, 150.1, 155.3, 161.5, 165.4, 174.0; HRMS  $m/z$  calc. for  $\text{C}_{26}\text{H}_{30}\text{ClN}_4\text{O}_3$  [ $\text{M}+\text{H}^+$ ] 481.2006, found 481.2015

**tert-butyl (R)-2-((S)-6-(4-chlorophenyl)-9-methoxy-1-methyl-4H-benzo[f][1,2,4]triazolo[4,3-a][1,4]diazepin-4-yl)pent-4-enoate (26)**



$^1\text{H}$  NMR ( $\text{CDCl}_3$ , 500 MHz) 1.52 (s, 9H), 2.36-2.43 (m, 1H), 2.64 (s, 3H), 2.86-2.91 (m, 1H), 3.95 (s, 3H), 3.96-4.02 (m, 1H), 4.22 (d,  $J=11.0$  Hz, 1H), 4.98-5.07 (m, 2H), 5.85-5.94 (m, 1H), 6.93 (d,  $J=2.4$  Hz, 1H), 6.98 (dd,  $J=2.5, 8.8$  Hz, 1H), 7.30 (d,  $J=8.4$  Hz, 2H), 7.37 (d,  $J=8.7$  Hz, 1H), 7.43 (d,  $J=8.7$  Hz, 2H).  $^{13}\text{C}$ -NMR ( $\text{CDCl}_3$ , 500 MHz) 12.4, 28.3, 34.6, 48.3, 55.9, 58.4, 80.8, 109.4, 112.7, 117.0, 121.5, 128.4, 130.9, 133.3, 134.7, 134.8, 136.7, 137.5, 150.1, 155.1, 161.5, 165.5, 173.2; HRMS  $m/z$  calc. for  $\text{C}_{27}\text{H}_{30}\text{ClN}_4\text{O}_3$  [ $\text{M}+\text{H}^+$ ] 493.2006, found 493.2025

### Chiral HPLC separation of compound 7

Racemate 7 was dissolved to 20 mg/mL in ethanol and was then purified by HPLC. Combined fractions of each of UD5\_1 and UD5\_2 were then evaporated to near dryness using a rotary evaporator, transferred into final vessels with DCM, which was removed under a stream of nitrogen at 40°C before being stored in a vacuum oven at 40°C and 5mbar for 16 hours to afford UD5\_1 and UD5\_2 as off white glasses.

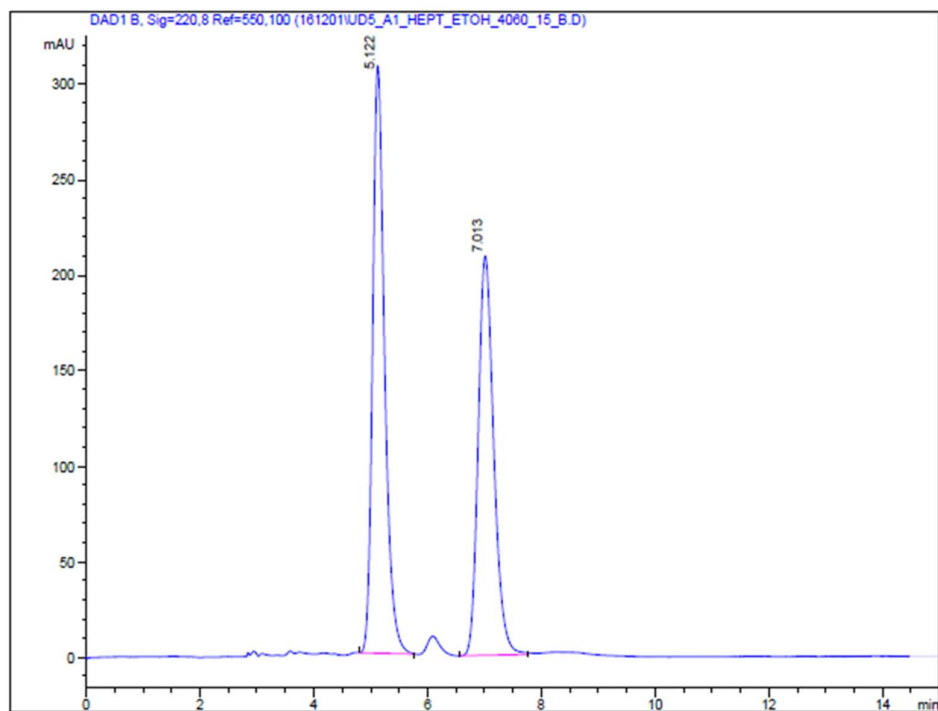
Column Details Lux A1 (21.2mm x 250mm, 5 $\mu\text{m}$ )

Column Temperature Ambient

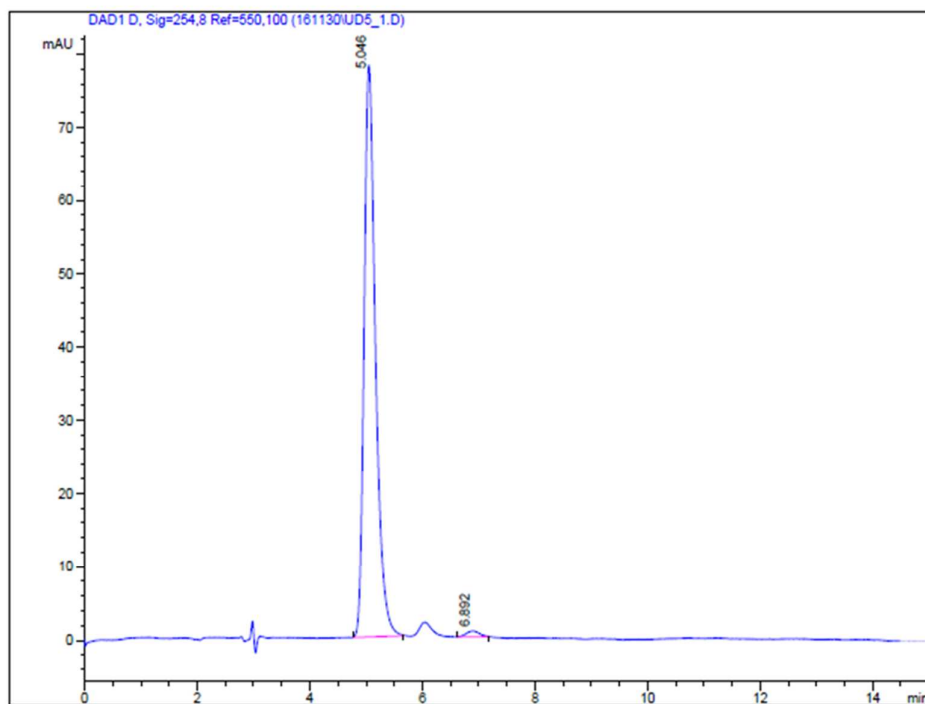
Flow Rate 21 mL/min

Detector Wavelength 220 nm

Injection Volume 1000  $\mu\text{L}$  (20 mg)

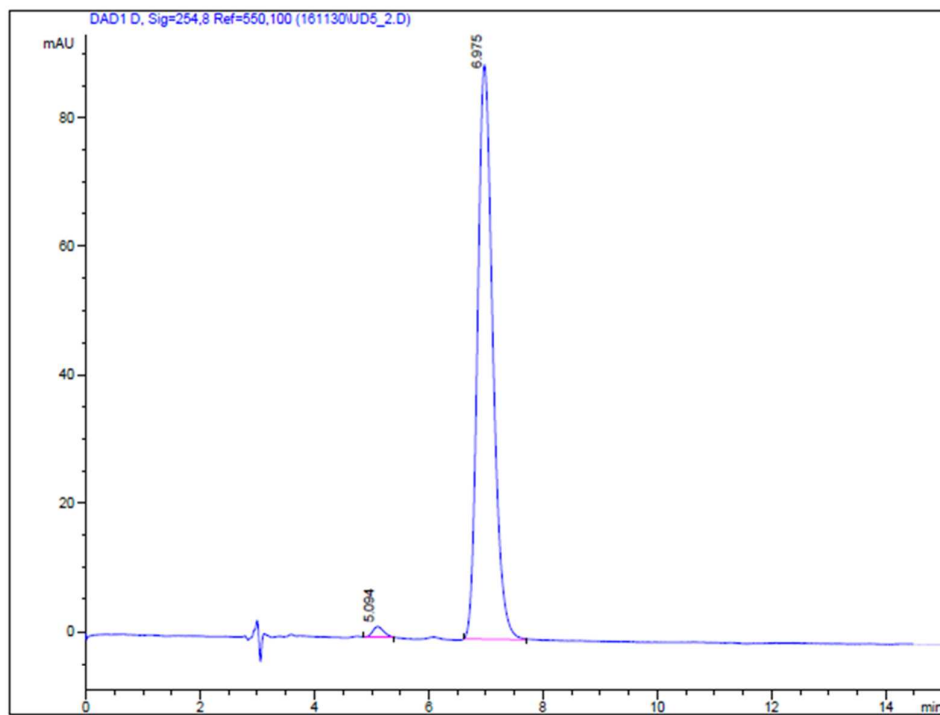
Isocratic Conditions 4:6 HEPT:EtOH (0.1% v/v NH<sub>3</sub>)A

#	Meas. R	Height	Width	Area	Area %	Symmetr
1	5.122	307.488	0.243	4.484e3	53.076	0.730
2	7.013	208.429	0.294	3.965e3	46.924	0.789



#	Meas. R	Height	Width	Area	Area %	Symmetr
1	5.046	78.080	0.234	1.094e3	98.786	0.692
2	6.892	0.828	0.271	13.447	1.214	0.986

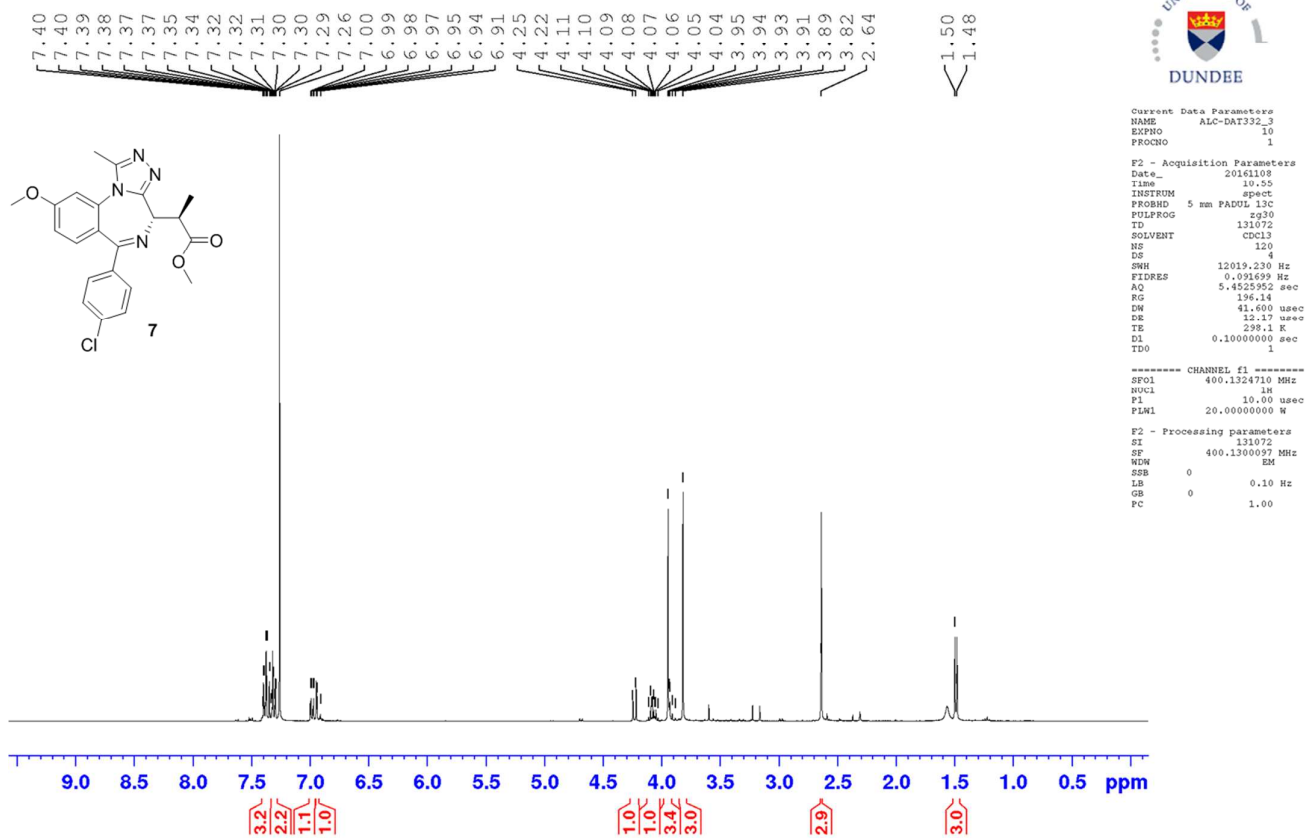
B)

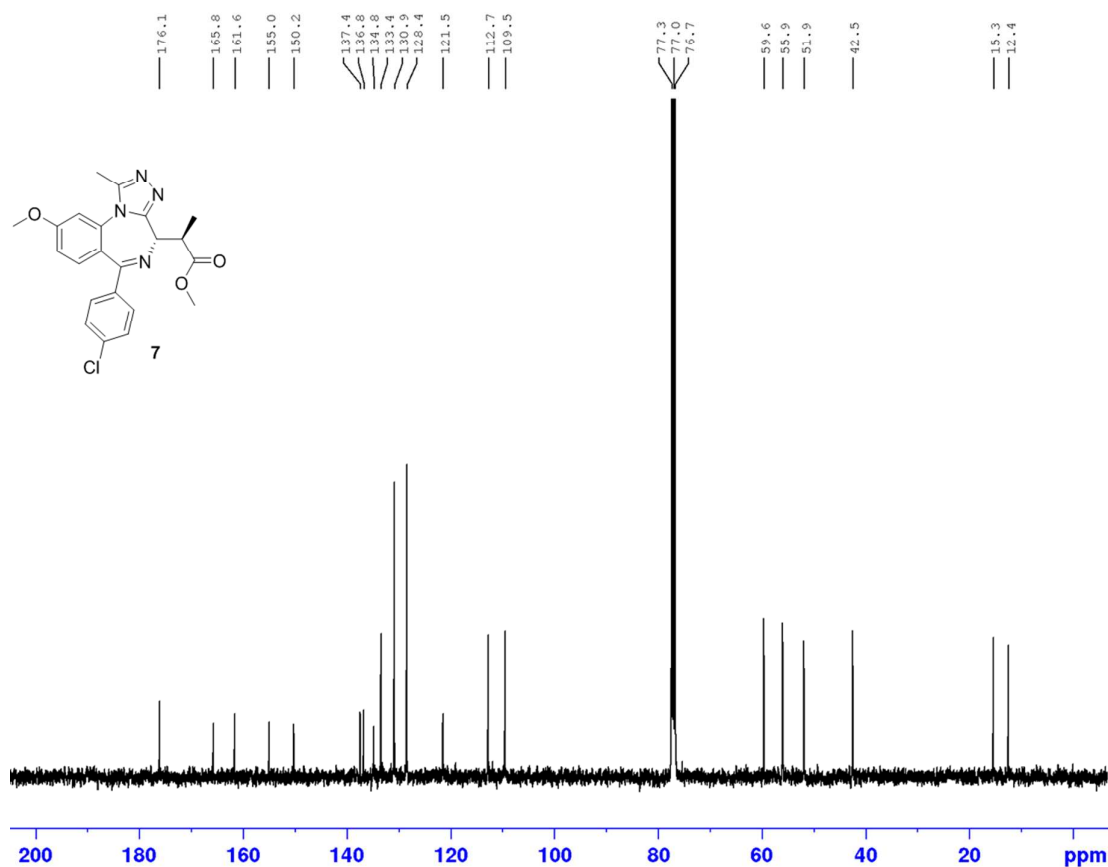


#	Meas. R	Height	Width	Area	Area %	Symmetr
1	5.094	1.621	0.227	22.051	1.314	0.650
2	6.975	88.925	0.297	1.657e3	98.686	0.793

C)

HPLC traces of A) 7 racemate (7), B) (2R, 3S)-7, C) (2S,3R)-7





Current Data Parameters  
NAME ALC-DAT32\_3  
EXPNO 11  
PROCNO 1

F2 - Acquisition Parameters  
Date\_ 20161109  
Time 1.25  
INSTRUM spect  
PROBHD 5 mm PABUL 13C  
PULPROG udeft  
TD 17996  
SOLVENT CDCl3  
NS 6000  
DS 0  
SWH 25000.000 Hz  
FIDRES 1.389198 Hz  
AQ 0.3599200 sec  
RG 196.14  
DW 20.000 usec  
DE 8.66 usec  
TE 298.1 K  
D1 3.0000000 sec  
D11 0.0300000 sec  
D12 0.0000200 sec  
D20 200.0000000 sec  
TD0 1

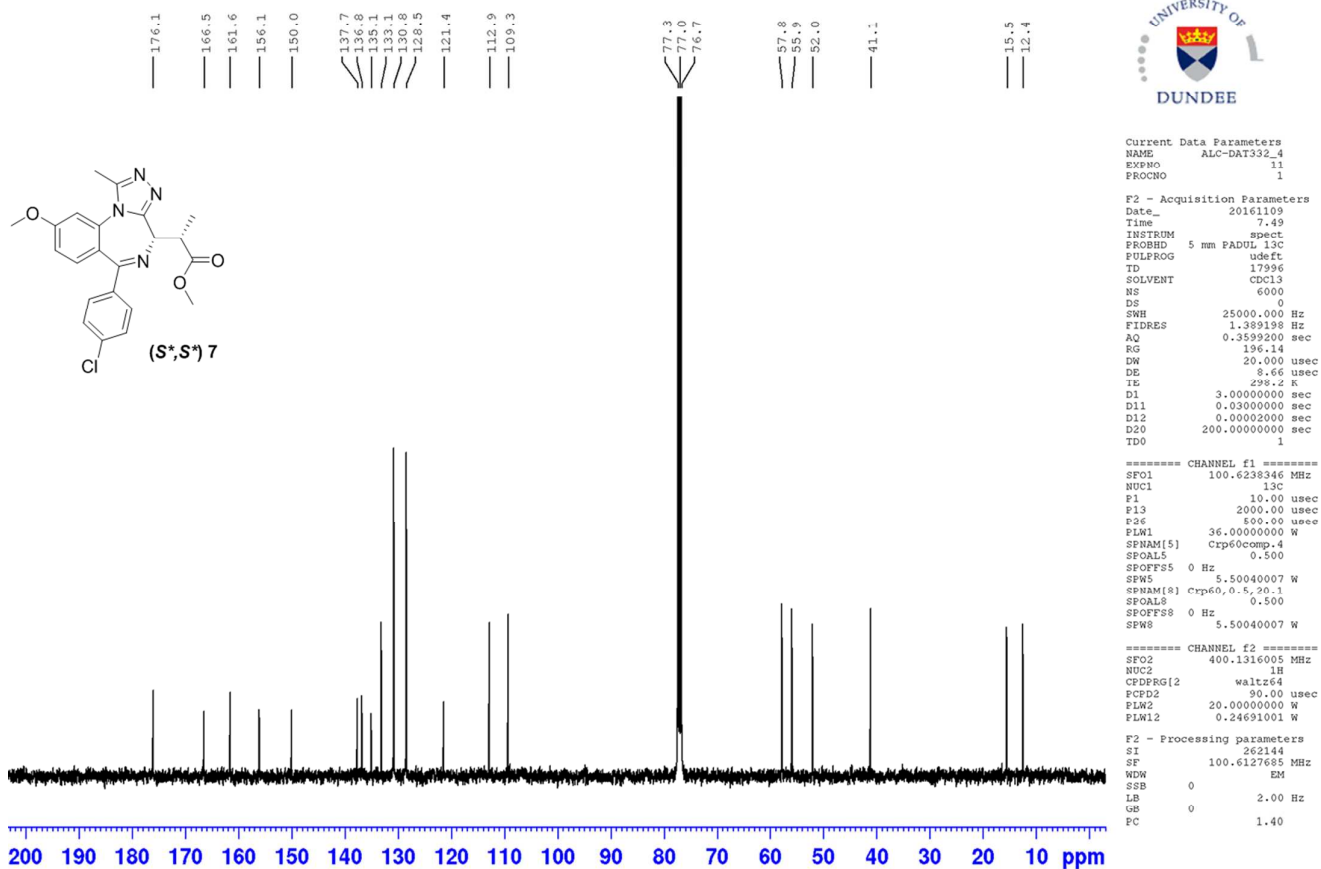
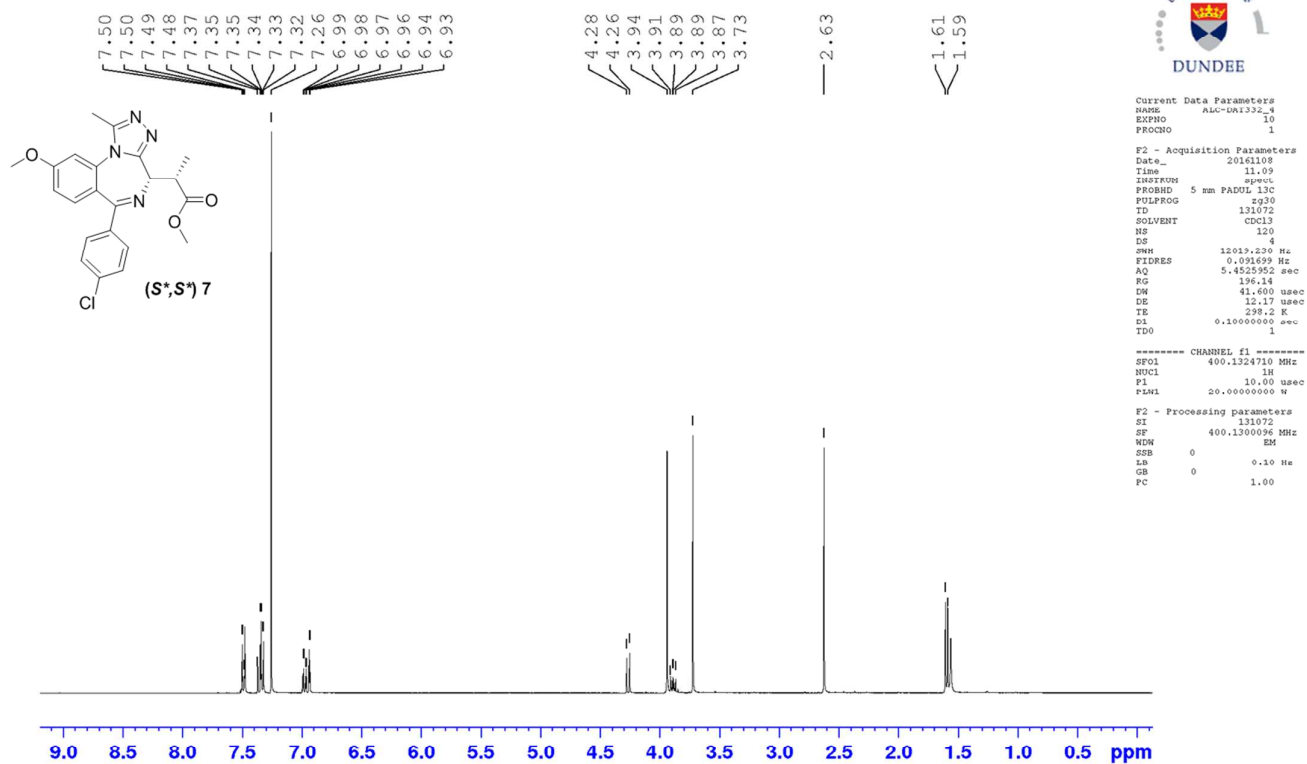
===== CHANNEL f1 =====  
SFO1 100.6230346 MHz  
NUC1 13C  
P1 10.00 usec  
PL1 2000.00 usec  
P2 500.00 usec  
PL2 36.00000000 W  
SFOFF5 0 Hz  
SFOFF8 0 Hz  
SFW5 5.50040007 W  
SFW8 5.50040007 W

===== CHANNEL f2 =====  
SFO2 400.1316005 MHz  
NUC2 1H  
CFDPRG[2] waltz64  
PCPD2 90.00 usec  
PLW2 20.00000000 W  
PLW12 0.24691001 W

F2 - Processing parameters  
SI 262144  
SF 100.6127695 MHz  
WDW EM  
SSB 0  
LB 2.00 Hz  
GB 0  
PC 1.40

<sup>1</sup>H and <sup>13</sup>C NMR spectra of 7 *S*\**R*\* diastereomer





$^1\text{H}$  and  $^{13}\text{C}$  NMR spectra of 7 S\*S\* diastereomer

### Supplemental References

1. F. Gong, L. Y. Chiu, B. Cox, F. Aymard, T. Clouaire, J. W. Leung, M. Cammarata, M. Perez, P. Agarwal, J. S. Brodbelt, G. Legube and K. M. Miller, *Genes Dev*, 2015, 29, 197-211.
2. F. H. Niesen, H. Berglund and M. Vedadi, *Nat Protoc*, 2007, 2, 2212-2221.
3. W. Kabsch, *Acta Crystallogr D Biol Crystallogr*, 2010, 66, 125-132.
4. T. G. Battye, L. Kontogiannis, O. Johnson, H. R. Powell and A. G. Leslie, *Acta Crystallogr D Biol Crystallogr*, 2011, 67, 271-281.
5. P. R. Evans and G. N. Murshudov, *Acta Crystallogr D Biol Crystallogr*, 2013, 69, 1204-1214.
6. M. D. Winn, C. C. Ballard, K. D. Cowtan, E. J. Dodson, P. Emsley, P. R. Evans, R. M. Keegan, E. B. Krissinel, A. G. Leslie, A. McCoy, S. J. McNicholas, G. N. Murshudov, N. S. Pannu, E. A. Potterton, H. R. Powell, R. J. Read, A. Vagin and K. S. Wilson, *Acta Crystallogr D Biol Crystallogr*, 2011, 67, 235-242.
7. A. Vagin and A. Teplyakov, *Acta Crystallogr D Biol Crystallogr*, 2010, 66, 22-25.
8. A. J. McCoy, R. W. Grosse-Kunstleve, P. D. Adams, M. D. Winn, L. C. Storoni and R. J. Read, *J Appl Crystallogr*, 2007, 40, 658-674.
9. P. V. Afonine, R. W. Grosse-Kunstleve, N. Echols, J. J. Headd, N. W. Moriarty, M. Mustyakimov, T. C. Terwilliger, A. Urzhumtsev, P. H. Zwart and P. D. Adams, *Acta Crystallogr D Biol Crystallogr*, 2012, 68, 352-367.
10. P. D. Adams, P. V. Afonine, G. Bunkoczi, V. B. Chen, I. W. Davis, N. Echols, J. J. Headd, L. W. Hung, G. J. Kapral, R. W. Grosse-Kunstleve, A. J. McCoy, N. W. Moriarty, R. Oeffner, R. J. Read, D. C. Richardson, J. S. Richardson, T. C. Terwilliger and P. H. Zwart, *Acta Crystallogr D Biol Crystallogr*, 2010, 66, 213-221.
11. P. Emsley, B. Lohkamp, W. G. Scott and K. Cowtan, *Acta Crystallogr D Biol Crystallogr*, 2010, 66, 486-501.
12. N. W. Moriarty, R. W. Grosse-Kunstleve and P. D. Adams, *Acta Crystallogr D Biol Crystallogr*, 2009, 65, 1074-1080.
13. N. W. Moriarty, E. J. Draizen and P. D. Adams, *Acta Crystallogr D Struct Biol*, 2017, 73, 123-130.
14. A. W. Schuttelkopf and D. M. van Aalten, *Acta Crystallogr D Biol Crystallogr*, 2004, 60, 1355-1363.
15. V. B. Chen, W. B. Arendall, 3rd, J. J. Headd, D. A. Keedy, R. M. Immormino, G. J. Kapral, L. W. Murray, J. S. Richardson and D. C. Richardson, *Acta Crystallogr D Biol Crystallogr*, 2010, 66, 12-21.
16. The PyMol Molecular Graphics System Schrodinger, LLC,